Analytical Approaches to Non–Linear Cosmological Structure Formation

Katrine Skovbo

PhD Dissertation

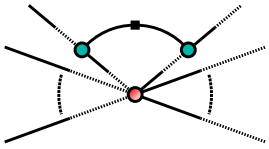

Department of Physics and Astronomy
Faculty of Science
Aarhus University
Denmark

Analytical Approaches to Non–Linear Cosmological Structure Formation

A Dissertation
Presented to the Faculty of Science
of Aarhus University
in Partial Fulfilment of the Requirements for
the PhD Degree

By Katrine Skovbo
July 2011

Abstract

The theory of cosmological structure formation deals with the evolution from an almost homogeneous distribution of matter in the early universe to the appearance of the structures we see today. The proces is dominated by the clustering properties of dark matter that form a collisionless fluid that evolves under the influence of gravity. It can be simulated numerically in N–body simulations or modeled analytically with the help of cosmological perturbation theory. A comparison between the two approaches offers a consistency check on the overall understanding of the non–linear clustering and on the approximations used. With data on the large scale structure of the universe coming from galaxy surveys such as the Sloan Digital Sky Survey we are also starting to be able to more precisely distinguish between models.

The work presented in this thesis focuses on the analytical description of structure formation. The framework of cosmological perturbation theory has been developed in many new directions in the past 10 years, all aiming to go beyond the order by order inclusion of corrections in standard perturbation theory. I have used a renormalization group formalism that resums a class of diagrams to all orders obtaining a result that is well–behaved on all scales. The resummation scheme improves on standard perturbation theory by allowing for a more accurate sampling of the baryon acoustic oscillation scales.

With the renormalization group approach as a starting point I have developed the notation and theory needed to deal with multi–point propagators both in the case of Gaussian and non-Gaussian initial conditions. My results in the large–k regime are in agreement with results obtained using other resummation schemes, and I have generalized the calculations to include a new class of multi–point propagators that arises naturally in the renormalization group framework.

Resumé (Summary in Danish)

Teorien om kosmologisk strukturdannelse undersøger udviklingen fra en næsten homogen fordeling af stof i det tidlige univers op til dannelsen af de strukturer, vi ser i dag. Processen er domineret af mørkt stof, der kun interagerer via tyngdekraften, og som gradvist samler sig i områder med større tæthed end gennemsnittet. Udviklingen kan simuleres numerisk i N–body simulationer eller modelleres analytisk ved hjælp af kosmologisk perturbationsteori. En sammenligning mellem de to fremgangsmåder kan give en idé om hvorvidt den overordnede teori og de approksimationer, der bliver brugt, er konsistente. Med data, der måler strukturen i universet på store skalaer ved at bestemme positionen af en stor mængde galakser, er det også blevet muligt mere præcist at skelne mellem forskellige modeller.

Arbejdet, som jeg præsenterer i denne afhandling, har fokuseret på den analytiske beskrivelse af strukturdannelse. Kosmologisk perturbationsteori er over de sidste 10 år blevet udviklet i mange nye retninger, der alle forsøger at gå videre end den gradvise inklusion af loop diagrammer i standard perturbations teori. Jeg har benyttet en renormaliseringsgruppe formalisme, der summerer en klasse af diagrammer til alle ordener, så resultatet giver mening på alle skalaer. Metoden giver en mere præcis modellering af de bayoniske akustiske oscillationer end standard perturbationsteori.

Med renormaliseringsgruppe formalismen som udgangspunkt har jeg udviklet den notation og teori, der er nødvendig for at undersøge multi–punkt propagatorer både med Gaussiske og ikke-Gaussiske begyndelsesbetingelser. Mine resultater for store k–værdier er i overensstemmelse med tidligere resultater, der benytter andre resummeringsmetoder, og jeg har generaliseret udregningerne til en ny klasse af multi–punkt propagatorer, der opstår naturligt i renormaliseringsgruppe formalismen.

Contents

Preface

The theory of structure formation traces the evolution of the matter density through the matter dominated part of the history of the universe back to the very early universe where the initial conditions were set up. The matter dominated epoch has lasted for about 9.6 Gyr and so a good understanding of the processes at work will provide information about a substantial part of the history of the universe. It is also essential to be able to predict the evolution of the initial density perturbations to distinguish between models of the early universe and rule out models that do not evolve into a density profile that matches the present one.

As the matter collapses to structures such as galaxies and clusters of galaxies the perturbations enter the non–linear regime where it is difficult to predict the evolution analytically. The most accurate approach to non–linear structure formation is N–body simulations, where a gas of millions of particles is simulated to undergo gravitational collapse. The results show very good agreement with data from galaxy surveys, but simulating the evolution does not give very good insight into the physics at work, so there is also a need for developing the analytical approaches to include non–linear clustering.

There has been considerable progress in reaching this goal since the realization that many concepts from quantum field theory can be adjusted to deal with many–body problems such as the cosmological one. For many years perturbation theory has been the preferred approach, but the regime where perturbation theory gives good results is small because the size of the loop corrections quickly grow very large, i.e. the transition from the perturbative regime to the non–perturbative regime is very fast. The overall result is only reasonable because large negative contributions cancel large positive contributions, but stopping the summation at any finite order will only provide useful results in the weakly non–linear regime.

In recent years there has been some interest in applying renormalization group theory to structure formation. This approach corresponds to summing some perturbative contributions to all orders and has a nice diagrammatical interpretation that can be exploited to gain some intuition for the couplings present between the different scales. Also the resummation to all orders makes sure that the result is well–behaved further into the non–linear regime than standard perturbation theory.

My work has been focused on an analytical approach using renormalization group theory

that relies heavily on the quantum field theoretical framework that has inspired the renewed interest in perturbation theory. In Chapter 1 I will present the underlying cosmological framework of structure formation. Chapter 2 will be a short introduction to the relevant aspects of quantum field theory. In Chapter 3 I will address the renormalization group approach to structure formation and develop the theory and notation needed in Chapter 4, where I will present my work on obtaining an analytical result for the resummation of multi–point propagators in the large–k limit. Finally Chapter 5 will be concerned with the future use of the renormalization group formalism and the results from Chapter 4.

Throughout this thesis I will use units with the speed of light set to 1.

Chapter 1

Structure Formation

The structures we see in the universe today have grown from a nearly homogeneous distribution of matter in the early universe. In the standard model of cosmology the early distribution of matter was set up after an epoch of very rapid expansion controlled by a scalar field, the inflaton. After inflation the inflaton decayed into the ordinary particles we know today and the still unknown particles that make up the dark matter. The resulting distribution of matter and energy is the starting point for structure formation.

From then on the small deviations from a homogeneous distribution have evolved under the influence of gravity. The densest regions have collapsed into galaxies and clusters of galaxies while the underdense regions have become even emptier during the continuous expansion of the universe. The growth of the perturbations depends on what kind of energy the universe consists of and how quickly the space is expanding.

In this chapter I will present the basics of standard cosmology relevant for structure formation. I will describe how the expansion is related to the energy content and how the growth of structures is affected by this. I will also discuss how the initial conditions were set up by inflation and how the early evolution has left an imprint in the matter distribution in the form of the baryon acoustic oscillations.

1.1 Homogeneity and Isotropy

It is generally assumed in cosmology that the particular spot in the universe where we live is not unique. If we could take the earth and move everyone and everything on it to another solar system in another galaxy in a different cluster of galaxies, the general laws of physics and cosmology that we would deduce from there should be similar to what we have concluded from our present position. This idea is called the cosmological principle and it can be translated into the dual requirements of homogeneity and isotropy on large scales. Large in this context means on scales that are larger than the size of superclusters, i.e. $r > 100\,\mathrm{Mpc}$.

Homogeneity implies that the average density in a sphere with a radius that is bigger than $\sim 100\,\mathrm{Mpc}$ should be the same no matter where it is centered. This average density of the universe is roughly $\rho_{\mathrm{ave,b}} \approx 0.4 \times 10^{-30}\,\mathrm{g\,cm^{-3}}$ of baryonic matter [5], which means that the universe is largely empty compared to our neighbourhood (the solar system has an average density of $\rho \sim 10^{-5}\mathrm{kg\,m^{-3}}$). The average of the total energy density including dark matter, dark energy and radiation is not much bigger $\rho_{\mathrm{ave,tot}} \approx 9 \times 10^{-30}\,\mathrm{g\,cm^{-3}}$.

The assumption of isotropy means that there is no preferred direction on large scales. On scales smaller than the super clusters there are obvious anisotropies, the Earth is moving around the Sun, the Sun is moving around the center of the Milky Way, the Milky Way is moving towards the Virgo cluster and so on. Draw a large enough sphere though and there will be no preferred direction. The best illustration of this is the cosmic microwave background (CMB).

The CMB is a residue from the early universe when the temperature was high enough for the baryonic matter to be ionized. At these temperatures the photons could not propagate far between interactions with the free electrons, so they were kept in equilibrium at the common temperature of the photon–baryon fluid. In such an equilibrium system the photons have the same energy distribution as a blackbody and the spectrum depends only on the temperature. When the universe expanded and cooled below the ionization temperature the photons decoupled. This happened when the universe was about $380,000$ years old, and the photons have been traveling almost unhindered through the expanding universe for the subsequent $13.75\,\mathrm{Gyr}$. The expansion has caused the temperature to drop considerably to $T = 2.726\,\mathrm{K}$ as measured by FIRAS [2], but the spectrum remains that of a perfect blackbody.

A measurement of the temperature of the CMB over the whole sky needs to be corrected for the dipole induced by the local velocity of the Milky Way towards the Virgo cluster and other foreground sources. After this is done what is left is a remarkably isotropic sky map. The variations in temperature of different patches of the sky is only of the order $\Delta T/T \sim 1 \times 10^{-5}$. The fact that opposite patches of the sky have the same temperature at such a high precision lends support to the theory of inflation where the uniformity arises naturally. I will return to this in Section 1.7. The small anisotropies that are present are the starting point for structure formation as described in Section 1.8.

1.2 The Expanding Universe

The assumptions of homogeneity and isotropy still allow for an expanding universe if it is space itself that is expanding. This means that no matter where you are situated, everything that is far enough away from you to not be gravitationally bound to your local cluster of galaxies will be receding from you.

We can quantify the expansion rate of the universe by measuring how fast distant galaxies are moving away from us. This is typically done by measuring the redshift of the galaxies by comparing how absorption or emission lines have shifted with respect to their position at emission

$$z = \frac{\lambda_{\mathrm{ob}} - \lambda_{\mathrm{em}}}{\lambda_{\mathrm{em}}} \tag{1.1}$$

where λ_{em} is the wavelength at emission, as measured in laboratories on earth, and λ_{ob} is the wavelength we measure when we observe the sources. For distant galaxies the wavelengths are stretched as the radiation moves through the expanding space, so z will be a positive number that quantifies how much space has expanded during the transit time of the light.

Apart from the shifts caused by the expansion of space there are also shifts in the spectra due to the peculiar velocities of the galaxies, but by observing a large enough amount of galaxies these Doppler shifts should average to zero. They do however cause scattering in a plot of redshift as a function of distance. For small z such a plot can help us determine the current rate of expansion, but to do that we need a way to measure cosmological distances.

First we need a coordinate system to describe positions. We can take the expansion into account by using comoving coordinates (r, θ, ϕ), where the radius r follows the expansion so that it is constant over time. The physical distance to a point at a given time in a flat universe will then be given by a scale factor, that keeps track of the expansion, times the comoving radius $d_{\text{p}}(t) = a(t)r$. The time variable t is called cosmic time and is the time measured by an observer that is stationary with respect to the CMB. The scale factor is normalized to 1 at the present time $a(t_0) = 1$ and is related to the redshift as

$$a = \frac{1}{1+z} \tag{1.2}$$

That is, a galaxy that is observed to have a redshift z emitted the light we are observing when the universe was smaller by a factor of a given by equation (1.2). Because the universe has been expanding ever since the Big Bang, the parameters a and z can be used unambiguously as time parameters.

Another time parameter that we will be using extensively is the conformal time τ. It is defined as the total comoving distance that light could have traveled since $t = 0$. As light travels with velocity $c = 1$ we have $a\mathrm{d}r/\mathrm{d}t = 1$, and we can write

$$\tau = \int_0^t \mathrm{d}r = \int_0^t \frac{\mathrm{d}t'}{a(t')} \tag{1.3}$$

Because nothing can move faster than light, it is in fact the greatest distance over which information can be shared at a given time.

The physical distance cannot be measured directly, but we can use the concept of standard candles to define another distance measure, the luminosity distance. Standard candles are astronomical objects that have a well known luminosity, L, no matter when in cosmic time they emitted the radiation. Type Ia supernovae constitute such a class of objects. Their luminosity has a well known relation to the shape of their light curve, which is believed to be unchanged over time and they are bright enough to be observed over great distances. Knowing the inherent luminosity of the supernovae, L, the luminosity distance is defined as

$$d_{\text{L}} = \left(\frac{L}{4\pi f}\right)^{1/2} \tag{1.4}$$

where f is the flux of light that we measure.

In a flat universe (I will come back to this in Section 1.3) and for small z the luminosity distance can be approximated by

$$d_{\mathrm{L}} \approx \frac{z}{H_0}\left(1 + \frac{1-q_0}{2}z\right) \tag{1.5}$$

where H_0 is the Hubble parameter and q_0 is the deceleration parameter, both at the present time. These two parameters describe the overall evolution of the universe and are related to the scale factor.

The Hubble parameter keeps track of how fast the scale factor is changing and is defined as

$$H(t) = \frac{\dot{a}}{a} \tag{1.6}$$

where the dot denotes differentiation with respect to cosmic time. The present value of the Hubble parameter is parametrized by a dimensionless number h, $H_0 = 100h\,\mathrm{km\,s^{-1}\,Mpc^{-1}}$. The value of h determined from observations of type Ia supernovae is 0.738 ± 2.4 [3].

The deceleration parameter is defined as

$$q_0 = -\left(\frac{\ddot{a}a}{\dot{a}^2}\right)_{t=t_0} \tag{1.7}$$

Observations of type Ia supernovae [4] and measurements of the CMB [5] and baryon acoustic oscillations [6] agree that the expansion is accelerating so that $q_0 < 0$. I will come back to this in Section 1.4.

1.3 The Einstein Equation

The evolution of the universe is controlled by the amount of energy that is present in the form of radiation, matter and dark energy. According to general relativity the presence of energy causes space–time to curve which in turn affects a redistribution of energy. In this section and Section 1.4 I will describe the overall evolution of the universe where we assume that the energy is uniformly distributed in space. In this way we get the background evolution in which the small perturbations evolve as we will see in Section 1.5.

It is the same key equation that controls both the background evolution and the growth of perturbations namely the Einstein equation

$$G_{\mu\nu} = 8\pi G T_{\mu\nu} \tag{1.8}$$

Here $G_{\mu\nu}$ is the Einstein tensor which is related to the geometry of space–time, G is Newton's constant and $T_{\mu\nu}$ is the energy–momentum tensor that describes the distribution of energy and the properties of the contents of the universe. The Einstein equation relates the geometrical properties of space–time to the energy present.

The geometry of space–time is conveniently described by use of a metric that specifies how infinitesimal distances are measured in the given geometry. The distance between two

nearby points is called $\mathrm{d}s$ and it is invariant under a change of variables. We use the metric to relate $\mathrm{d}s$ to the specific coordinate system we are using

$$\mathrm{d}s^2 = \sum_{\mu,\nu=0}^{3} g_{\mu\nu}\mathrm{d}x^\mu \mathrm{d}x^\nu = g_{\mu\nu}\mathrm{d}x^\mu \mathrm{d}x^\nu \tag{1.9}$$

where $g_{\mu\nu}$ denotes the metric. We will suppress the $\sum$ sign as in the last expression above, but the sum is implicit whenever there are repeated indices. The indices $1, 2, 3$ correspond to the three spatial dimensions while the index 0 corresponds to time.

In an expanding, homogeneous and isotropic universe the only parameters we need to describe the geometry are the scale factor a, the curvature constant κ and the current radius of curvature R_0. The curvature constant specifies if space is positively curved (closed), $\kappa = 1$, flat, $\kappa = 0$, or negatively curved (open), $\kappa = -1$. The metric that describes such universes is called the Friedmann–Robertson–Walker (FRW) metric. If we are using cosmic time t and spherical comoving coordinates r, θ, ϕ the invariant distance takes the form

$$\mathrm{d}s^2 = -\mathrm{d}t^2 + a(t)^2\left(\mathrm{d}r^2 + S_\kappa(r)^2\mathrm{d}\Omega^2\right) \tag{1.10}$$

where $\mathrm{d}\Omega^2 = \mathrm{d}\theta^2 + \sin^2\theta\mathrm{d}\phi^2$ and

$$S_\kappa(r) = \begin{cases} R_0 \sin(r/R_0) & ,\kappa = +1 \\ r & ,\kappa = 0 \\ R_0 \sinh(r/R_0) & ,\kappa = -1 \end{cases} \tag{1.11}$$

We will primarily be interested in a spatially flat universe where we see from equations (1.10) and (1.11) that the metric is given by

$$g^\mu{}_\nu = \begin{pmatrix} -1 & 0 & 0 & 0 \\ 0 & a^2 & 0 & 0 \\ 0 & 0 & a^2 r^2 & 0 \\ 0 & 0 & 0 & a^2 r^2 \sin^2\theta \end{pmatrix} \tag{1.12}$$

In Section 1.5 we will add small corrections to this metric to describe perturbations in the spatial curvature. The Einstein tensor $G_{\mu\nu}$ is a function of the metric and its derivatives, so when we have specified the metric we know the left hand side of the Einstein equation.

In the case of a uniformly distributed energy density the energy–momentum tensor $T_{\mu\nu}$ assumes a very simple form

$$T^\mu{}_\nu = \begin{pmatrix} -\rho & 0 & 0 & 0 \\ 0 & P & 0 & 0 \\ 0 & 0 & P & 0 \\ 0 & 0 & 0 & P \end{pmatrix} \tag{1.13}$$

where ρ is the energy density and P is the pressure of the fluid under consideration. Calculating G_{00} from the metric, the time-time component of the Einstein equation yields the

Friedmann equation

$$\left(\frac{\dot{a}}{a}\right)^2 = H^2 = \frac{8\pi G}{3}\rho(t) - \frac{\kappa}{R_0^2 a^2} \tag{1.14}$$

From this we see that we can define a critical density that corresponds to a flat universe, $\kappa = 0$

$$\rho_{\rm cr} = \frac{3H_0^2}{8\pi G} = 1.88\, h^2 \times 10^{-29} {\rm g\,cm^{-3}} \tag{1.15}$$

The measurements of the cosmic microwave background radiation by the WMAP spacecraft imply that ρ is very close to the critical density of the universe. The best fit value to the data from WMAP, large scale structure and supernova measurements is $\Omega_0 = \frac{\rho}{\rho_{\rm cr}} = 1.0023^{+0.0056}_{-0.0054}$ [5]. From now on I will assume a flat universe and set $\kappa = 0$.

1.4 Background Evolution

We can derive another important cosmological equation from the requirement of conservation of the energy–momentum tensor. In an expanding universe described by the FRW metric this means that the covariant derivative of $T_{\mu\nu}$ should vanish. The covariant derivative corrects for effects induced by the non–Euclidean geometry we are working in so it depends on the metric and the final result will therefore include the scale factor. What we end up with is the fluid equation

$$\frac{\partial \rho}{\partial t} + 3\frac{\dot{a}}{a}(\rho + P) = 0 \tag{1.16}$$

relating the energy density and pressure to the scale factor.

The total energy density is a sum of the contributions from the different components of the universe. Each component has an equation of state that relates the pressure of the substance to its density. The equation of state can be written in a simple form parametrized by the dimensionless parameter w

$$P = w\rho \tag{1.17}$$

If the different components do not interact, each component will satisfy the fluid equation separately and we can determine the evolution of the corresponding energy density as a function of the scale factor. This is a good first approximation, though interactions between for instance baryons and photons result in non negligible effects such as the baryon acoustic oscillations discussed in Section 1.10.

Using equation (1.17) the fluid equation can be solved for constant w to give

$$\rho(a) = \rho_0 a^{-3(1+w)} \tag{1.18}$$

where ρ_0 denotes the present value of the energy density. This gives the evolution of non relativistic matter with negligible pressure, $w = 0$, radiation with $w = \frac{1}{3}$ and a cosmological constant that has negative pressure and $w = -1$

$$\rho_{\rm m} = \frac{\rho_{\rm m,0}}{a^3} \quad , \quad \rho_{\rm r} = \frac{\rho_{\rm r,0}}{a^4} \quad \text{and} \quad \rho_\Lambda = \text{const.} \tag{1.19}$$

We see that the radiation density falls off more rapidly with the expansion than the matter density while the cosmological constant is obviously kept constant. This explains how we can have radiation as the dominant energy content in the early universe and matter as the dominant content later on, though the cosmological constant if it is present will eventually completely dominate the energy density.

In a flat universe and with equation (1.18) we can solve the Friedmann equation to give a as a function of time

$$a(t) \propto t^{2/(3+3w)} \tag{1.20}$$

except in the case $w = -1$ where the scale factor will increase exponentially with time. We can approximate the universe as being dominated in turn by the three components in equation (1.19) with short transition periods in between.

We are not only interested in the rate at which the universe is expanding, but also in determining whether the expansion is speeding up or slowing down as measured by the deceleration parameter q_0. To examine how the energy content affects this parameter we can take the time derivative of equation (1.14) and combine with equation (1.16) arriving at the acceleration equation

$$\frac{\ddot{a}}{a} = -\frac{4\pi G}{3}(\rho + 3P) \tag{1.21}$$

From this it can be seen that both matter and radiation that have $w > -\frac{1}{3}$ contributes to a deceleration of the expansion while a cosmological constant speeds it up. In fact any component that has $w < -\frac{1}{3}$ will accelerate the expansion and they are all referred to as dark energy. Some dark energy candidates have an equation of state parameter that varies with time, but the current data is well fitted by having dark energy in the form of a cosmological constant.

The current energy content in the universe is usually presented as fractions of the critical density $\Omega_0 = \rho/\rho_{\text{cr}}$. The current standard model is a flat universe dominated by a cosmological constant, $\Omega_{\Lambda,0} = 0.728$, with the contribution from matter shared between baryons and cold dark matter as $\Omega_{b,0} = 0.0456$ and $\Omega_{c,0} = 0.227$ [5]. This means that we are currently in the transition period between being dominated by matter and dark energy and the expansion of the universe is accelerating. The deceleration parameter in a universe dominated by a cosmological constant and matter is given by $q_0 = \frac{1}{2}\Omega_{m,0} - \Omega_{\Lambda,0} = -0.59$.

Today radiation makes up only a negligible contribution that can be calculated from the temperature of the microwave background radiation, $T_{\text{CMB}} = 2.726\,\text{K}$. The energy density of blackbody radiation is proportional to T^4 giving $\rho_{\text{CMB}} = 4.61 \times 10^{-34}\,\text{g}\,\text{cm}^{-3}$ so that $\Omega_{\text{CMB}} = 4.9 \times 10^{-5}$. There will also be a background of neutrinos that contributes to the total radiation density. This contribution depends on the number of neutrino species and the mass of the neutrinos which is not yet known. With three massless neutrinos it will be $\Omega_\nu = 3.08 \times 10^{-5}$ [7], while it will depend on the total mass $M_\nu = \sum m_\nu$ as $\Omega_\nu = \frac{M_\nu}{51.2\,\text{eV}}$ [7]. The current limits on the total mass is $0.05\,\text{eV} < M_\nu < 0.58\,\text{eV}$. The lower bound is a consequence of neutrino oscillations [8] while the upper bound comes from cosmological considerations [5].

The density perturbations will only grow appreciably in the matter dominated era which lasted from $z \sim 3232$ [5] to

$$z = \frac{1}{a_{\Lambda\mathrm{m}}} - 1 = \left(\frac{\Omega_{\Lambda,0}}{\Omega_{\mathrm{m},0}}\right)^{1/3} - 1 \approx 0.39 \tag{1.22}$$

where $a_{\Lambda\mathrm{m}}$ is the scale factor when the energy densities of Λ and matter were equal. Matter domination lasted for about 9.6 Gyr with the current age of the universe being $t \approx 13.75$ Gyr.

1.5 Perturbations

In the previous sections we have been working in a homogeneous universe, but now we want to relate perturbations in the energy densities to perturbations in the metric. Metric perturbations can be classified as scalar, vector or tensor perturbations according to how they transform under a change of coordinates. It can be shown that the three classes of perturbations are decoupled from each other so that they evolve independently with time. Most inflationary models set up a combination of scalar and tensor perturbations as initial conditions for the evolution of the universe, but only scalar perturbations affect the matter density, so in this section I will focus on these. I will return to the initial conditions in Section 1.8.

The Einstein equation is a differential equation (remember that $G_{\mu\nu}$ depends on the metric and its derivatives), so there is a gauge freedom when choosing how to parametrize the perturbed metric. It is similar to electrodynamics where a constant term can be added to the vector potential A_μ without causing a change in the resulting electric and magnetic fields. Here we will be working in the conformal Newtonian gauge where the scalar perturbations can be described by the Newtonian gravitational potential Ψ and a perturbation to the spatial curvature Φ. The metric is

$$\begin{aligned} g_{00}(\mathbf{x},\tau) &= -1 - 2\Psi(\mathbf{x},\tau) \\ g_{0i}(\mathbf{x},\tau) &= 0 \\ g_{ij}(\mathbf{x},\tau) &= a^2\delta_{ij}\left(1 + 2\Phi(\mathbf{x},\tau)\right) \end{aligned} \tag{1.23}$$

where the indices i and j run over the spatial indices 1 to 3, $\mathbf{x}$ is the comoving position and τ is conformal time.

To describe all the features of structure formation we will need to know how the perturbations to the metric affect each component of the energy perturbations and the other way around. The starting point for these considerations is the Boltzmann equation that describes changes in the distribution of states in phase space $f(\tau, \mathbf{x}, \mathbf{p})$ due to interactions. If we are dealing with a collisionless substance such as dark matter, the distribution function does not change with time, but because of the change in the geometry of space–time, the partial derivatives with respect to τ, $\mathbf{x}$ and $\mathbf{p}$ will change. When dealing with photons and baryons there will be additional terms from interactions. In general we can write

$$\frac{\mathrm{d}f}{\mathrm{d}\tau} = \frac{\partial f}{\partial \tau} + \frac{\partial f}{\partial x^i}\frac{\mathrm{d}x^i}{\mathrm{d}\tau} + \frac{\partial f}{\partial p^i}\frac{\mathrm{d}p^i}{\mathrm{d}\tau} = C[f] \tag{1.24}$$

where $C[f]$ represents all collision terms and we use conformal time as our time parameter.

Structure formation is governed by dark matter, firstly because it dominates the matter density and secondly because it decouples from radiation much earlier than the baryons do. This means that the dark matter will already have formed gravitational structures when the baryons start to cluster and the main features of clustering can be determined by following the evolution of dark matter. Thus the most important equation for structure formation can be obtained from the Boltzmann equation for a gas of collisionless matter. The initial conditions for this equation will be set up by inflation and the early evolution is affected by the coupling of baryons and radiation before the CMB was released. In Sections 1.8 and 1.10 I will come back to the early evolution.

We will now set $C[f] = 0$ and consider how to express the partial derivatives in the Boltzmann equation in terms of known quantities. On scales smaller than the Hubble radius we can neglect relativistic effects and use Newtonian gravity to describe the evolution, provided we correct for the expansion of space. We will typically set the initial conditions at a redshift of $z \sim 50$ when the scales we are interested in are well inside the horizon.

First off we note that $\frac{\mathrm{d}\mathbf{x}}{\mathrm{d}\tau} = \mathbf{u}$ is the peculiar velocity (that is the velocity relative to the comoving grid) of the particles. The momentum will then be given by

$$\mathbf{p} = am\frac{\mathrm{d}\mathbf{x}}{\mathrm{d}\tau} \tag{1.25}$$

where m is the mass of the particle. Any change in momentum over time is caused by gradients in the cosmological gravitational potential

$$\frac{\mathrm{d}\mathbf{p}}{\mathrm{d}\tau} = -am\nabla\Psi \tag{1.26}$$

where Ψ is defined to be sourced by the density fluctuations δ instead of the density field ρ. This is what we would expect from equation (1.23) where the Newtonian potential Ψ is defined as a perturbation to a homogeneous background. The density perturbations δ are defined as deviations from the average density

$$\int \mathrm{d}^3\mathbf{p}\; f(\tau, \mathbf{x}, \mathbf{p}) \equiv \rho(\mathbf{x}, \tau) \equiv \bar{\rho}(\tau)\left(1 + \delta(\mathbf{x}, \tau)\right) \tag{1.27}$$

where $\bar{\rho}$ denotes the average density. The first equality defines the density field as the zeroth order moment of the distribution function.

The Poisson equation for Ψ then reads

$$\nabla^2\Psi = \frac{3}{2}\Omega_{\mathrm{m}}(\tau)\mathcal{H}^2(\tau)\delta(\mathbf{x}, \tau) \tag{1.28}$$

with $\mathcal{H} = \frac{\mathrm{d}\log a}{\mathrm{d}\tau} = aH$ the conformal Hubble parameter. For most of this work we can assume an Einstein–de Sitter background that has $\Omega_{\mathrm{m}} = 1$, $\Omega_\Lambda = 0$ and consequently $a \propto \tau^2$ and $\mathcal{H} = 2\tau^{-1}$. Later on we will allow for other background cosmologies by reinterpreting the time parameter but keeping (1.28) in the Einstein–de Sitter form.

Inserting equations (1.25) and (1.26) in the Boltzmann equation we end up with the Vlasov equation governing the evolution of dark matter

$$\frac{\partial f}{\partial \tau} + \frac{\mathbf{p}}{am} \cdot \nabla f - am \nabla \Psi \cdot \nabla_{\mathbf{p}} f = 0 \tag{1.29}$$

where $\nabla_{\mathbf{p}}$ denotes derivatives with respect to $\mathbf{p}$. This is the main equation we will have to solve to determine the growth of structures.

It is a lot easier to recognize the physics hidden in the Vlasov equation if we take moments of the distribution function as was done in equation (1.27) for the zeroth order case. The next two order moments are

$$\int \mathrm{d}^3\mathbf{p} \, \frac{\mathbf{p}}{am} f(\tau, \mathbf{x}, \mathbf{p}) \equiv \rho(\mathbf{x}, \tau)\mathbf{v}(\mathbf{x}, \tau) \tag{1.30}$$

$$\int \mathrm{d}^3\mathbf{p} \, \frac{p_i p_j}{a^2 m^2} f(\tau, \mathbf{x}, \mathbf{p}) \equiv \rho(\mathbf{x}, \tau) v_i(\mathbf{x}, \tau) v_j(\mathbf{x}, \tau) + \sigma_{ij}(\mathbf{x}, \tau) \tag{1.31}$$

where we have defined the peculiar velocity field $\mathbf{v}$ and the stress tensor σ_{ij}.

The stress tensor provides us with a natural truncation of the hierarchy of equations that result from taking moments of the Vlasov equation. It measures the deviation from a single coherent flow of the dark matter particles in the gas and will be approximately zero for cold dark matter except in the highly non–linear regime where our treatment will already have broken down due to other limitations. If we wish to include warm dark matter (e.g. neutrinos) this assumption breaks down, but here we will restrict our attention to cold dark matter. Thus we set $\sigma_{ij} = 0$ and take the zeroth and first order moments of the Vlasov equation giving

$$\begin{aligned} \frac{\partial \delta}{\partial \tau} + \nabla \cdot [(1+\delta)\mathbf{v}] &= 0 \\ \frac{\partial \mathbf{v}}{\partial \tau} + \mathcal{H}\mathbf{v} + (\mathbf{v} \cdot \nabla)\mathbf{v} &= -\nabla \Psi \end{aligned} \tag{1.32}$$

These are the continuity and the Euler equation respectively representing conservation of mass and momentum in the dark matter gas. Together with the Poisson equation they constitute a closed set of differential equations in the two fields δ and $\mathbf{v}$.

1.6 Linear Treatment

In the linear treatment we keep only terms that are first order in the perturbations δ, $\mathbf{v}$ and Ψ reducing the continuity and Euler equations to

$$\frac{\partial \delta}{\partial \tau} + \nabla \cdot \mathbf{v} = 0 \quad \text{and} \quad \frac{\partial \mathbf{v}}{\partial \tau} + \mathcal{H}\mathbf{v} = -\nabla \Psi \tag{1.33}$$

The velocity field can be described by its divergence $\theta(\mathbf{x}, \tau) = \nabla \cdot \mathbf{v}(\mathbf{x}, \tau)$ and its vorticity $\mathbf{w}(\mathbf{x}, \tau) = \nabla \times \mathbf{v}(\mathbf{x}, \tau)$. Taking the curl of the second equation above yields

$$\frac{\partial \mathbf{w}}{\partial \tau} + \frac{\mathrm{d} \log a}{\mathrm{d}\tau} \mathbf{w} = 0 \quad \Rightarrow \quad \mathbf{w} \propto a^{-1} \tag{1.34}$$

where we see that any vorticity that would be present in the early universe decays quickly as the universe expands and no new contributions to $\mathbf{w}$ will be generated in the linear evolution. In the non–linear case the term $(\mathbf{v}\cdot\nabla)\,\mathbf{v}$ in the Euler equation could complicate things, but if the initial vorticity is zero new contributions will still not be generated. We will therefore assume that we can describe the velocity field completely by its divergence and set the vorticity to zero. This leaves us with

$$\frac{\partial\delta}{\partial\tau}+\theta=0 \tag{1.35}$$

$$\frac{\partial\theta}{\partial\tau}+\mathcal{H}\theta+\frac{3}{2}\Omega_m\mathcal{H}^2\delta=0 \tag{1.36}$$

In the linear treatment the dependence on Ω_m is essential so we will keep this factor in the equations.

We can eliminate the velocity divergence and introduce the linear growth factor $D(\tau)$ through $\delta(\mathbf{x},\tau)=D(\tau)\delta(\mathbf{x},\tau_i)$ where τ_i denotes some initial time, obtaining

$$\frac{\mathrm{d}^2D}{\mathrm{d}\tau^2}+\mathcal{H}\frac{\mathrm{d}D}{\mathrm{d}\tau}=\frac{3}{2}\Omega_m\mathcal{H}^2D \tag{1.37}$$

This second–order differential equation has two independent solutions, which in the Einstein–de Sitter case can easily be found to be

$$D\propto\tau^n\propto a^{n/2}\quad,\quad n=2,-3 \tag{1.38}$$

giving for the density fluctuations and velocity divergence

$$\begin{aligned}\delta(\mathbf{x},\tau)&=\delta(\mathbf{x},\tau_i)\left(\frac{a(\tau)}{a(\tau_i)}\right)^{n/2}\\ \theta(\mathbf{x},\tau)&=-\frac{\partial\delta(\mathbf{x},\tau)}{\partial\tau}=-\frac{n}{\tau}\delta(\mathbf{x},\tau)=-\frac{1}{2}\mathcal{H}n\delta(\mathbf{x},\tau)\end{aligned} \tag{1.39}$$

In the growing mode ($n=2$) the density fluctuations are proportional to the scale factor.

It can be shown that in the radiation dominated period, when the gravitational potential was sourced by radiation instead of matter, the matter perturbations grew logarithmically with the scale factor. After matter-radiation equality at $z_\mathrm{rm}\approx 3232$ the dark matter perturbations started growing proportionally to a while the tight coupling between baryons and photons delayed the clustering of the baryons. When they finally decoupled at $z_\mathrm{dec}\approx 1088$ the dark matter perturbations had already grown by a factor of

$$\frac{a_\mathrm{dec}}{a_\mathrm{rm}}\sim\frac{z_\mathrm{rm}}{z_\mathrm{dec}}\sim 3 \tag{1.40}$$

creating gravitational wells that the baryons could fall into.

In the more general case where we allow for radiation and a cosmological constant we will only be interested in the growing mode D^+. Equation (1.37) can be integrated to give

$$D^+(a)=\frac{5\Omega_\mathrm{m}}{2}\frac{H(a)}{H_0}\int_0^a\frac{\mathrm{d}a'}{\left(a'H(a')/H_0\right)^3} \tag{1.41}$$

with $H(a)$ given by

$$H(a) = H_0\sqrt{\frac{\Omega_{\mathrm{r},0}}{a^4} + \frac{\Omega_{\mathrm{m},0}}{a^3} + \Omega_{\Lambda,0} + \frac{1-\Omega_{\mathrm{r},0}-\Omega_{\mathrm{m},0}-\Omega_{\Lambda,0}}{a^2}} \tag{1.42}$$

where the last term accounts for the possibility of curved space.

The growing modes of the density fluctuations and the velocity divergence are related through

$$\theta(\mathbf{x},\tau) = -\frac{\mathrm{d}\ln D^+}{\mathrm{d}\tau}\delta(\mathbf{x},\tau) = -\mathcal{H}\frac{\mathrm{d}\ln D^+}{\mathrm{d}\ln a}\delta(\mathbf{x},\tau) = -\mathcal{H}f\delta(\mathbf{x},\tau) \tag{1.43}$$

where we have defined the dimensionless linear growth rate f. As seen from equation (1.39) in the matter dominated era we have $f \sim 1$.

1.7 Inflation

Inflation is a period in the early universe where the scale factor grew exponentially with time just as it does at late times if the cosmological constant is the dominant energy content. Such a rapid expansion will erase any structures that were present before it started, creating the almost homogeneous universe we observe. There are two main issues in standard cosmology that inflation also provides a nice solution to the flatness problem and the horizon problem.

The flatness problem deals with the question why the universe is so close to being flat at the present time. Any deviation from flat space in the early universe would have been enhanced through the radiation and matter dominated periods, so if the universe has $\Omega \approx 1$ today, the deviation from one at early times would have been extremely small. At the present day we have $|1-\Omega_0| \leq 0.008$. We can use the Friedmann equation to trace this back to the Planck time $t_\mathrm{P} = 5\times10^{-44}\,\mathrm{s}$ where we get $|1-\Omega_\mathrm{P}| \leq 1\times10^{-60}$. Thus without inflation the initial energy density at the Planck time would have to be extremely fine tuned to the critical density. An exponential expansion rate on the other hand makes the deviation of Ω from one fall off exponentially with time so that a period of inflation can make any curvature in the initial universe disappear if it lasts for long enough.

In Section 1.1 I noted that the CMB has the same temperature if we look in opposite directions in the sky. We would not expect this to be the case if the universe had only gone through the matter and radiation dominated eras because the two opposite patches would never have been in causal contact. The conformal time defined in equation (1.3) represents the particle horizon, where areas within this distance of each other could have had time to interact since $t = 0$. At the time of last scattering when the photons of the CMB started free streaming this horizon was only $\sim 100\,\mathrm{Mpc}$ corresponding to an angular separation on todays sky of $\sim 1°$. Inflation would solve this problem by ensuring that the two opposite patches we can see from here were in fact very close together initially. The exponential expansion forces them far from each other and only now are they reentering the horizon.

To achieve the exponential expansion required to solve the above problems, inflation should be caused by a component similar to dark energy that has an equation of state parameter $w < -\frac{1}{3}$. This can be realized by a scalar field ϕ that is trapped in a false vacuum so that

its potential energy is bigger that its kinetic energy. The energy density and pressure of a homogeneous scalar field is given by

$$\begin{aligned} \rho_\phi &= \frac{1}{2}\left(\frac{\mathrm{d}\phi}{\mathrm{d}t}\right)^2 + V(\phi) \\ P_\phi &= \frac{1}{2}\left(\frac{\mathrm{d}\phi}{\mathrm{d}t}\right)^2 - V(\phi) \end{aligned} \tag{1.44}$$

where $V(\phi)$ is the potential of the field. If the field has very low kinetic energy compared to potential energy we see that $w_\phi = P_\phi/\rho_\phi \sim -1$ as required.

The false vacuum also provides us with a neat way to end inflation if the field can evolve into the true vacuum state over time. The scalar field is generically referred to as the inflaton field. After inflation when the inflaton field has settled into the true vacuum state it will decay into the dark and ordinary matter that make up the universe today.

During inflation the Hubble parameter is very close to being constant ($w = -1$ corresponds to $H = \text{const}$) and the scale factor grows as $a = e^{Ht}$. This gives a very large contribution to the conformal time given by the integral

$$\tau_{\text{inf}} = \int_{t_{\text{in}}}^{t_{\text{end}}} \mathrm{d}t\; e^{-Ht} \approx -\frac{1}{H}\left(\frac{1}{a_{\text{end}}} - \frac{1}{a_{\text{in}}}\right) \approx \frac{1}{a_{\text{in}}H} \tag{1.45}$$

where a_{in} is the initial scale factor and a_{end} is the scale factor at the end of inflation. For inflation to solve the above issues we will have to have at least $a_{\text{end}} \sim 10^{28} a_{\text{in}}$ and a_{in} will be $< 10^{-56}$. Such a large early contribution to the conformal time makes it an impractical measure of time so we will redefine τ by subtracting the inflationary contribution. As a consequence τ will be negative during inflation, $\tau \approx -\frac{1}{aH}$. The factor $\frac{1}{aH}$ is the comoving Hubble radius defining the maximum scale over which there can be a causal connection. Regions separated by more than this are receding from each other at a rate faster than the speed of light.

1.8 Power Spectrum from Inflation

The early variations in density are caused by quantum fluctuations in the inflaton field and make up small perturbations on an otherwise homogeneous background. The inflaton field can be written as a homogeneous part that may vary with time but is independent of $\mathbf{x}$, and a perturbation that describes the fluctuations around the mean value

$$\phi\left(\mathbf{x}, \tau\right) = \phi^{(0)}\left(\tau\right) + \delta\phi\left(\mathbf{x}, \tau\right) \tag{1.46}$$

The homogeneous part is responsible for the exponential expansion during inflation while the perturbations give rise to the inhomogeneities that make up the initial fluctuations in the average density.

As the inflaton field is evolving it is setting up the inhomogeneities so we can assume that the geometry of the background space–time is described by the unperturbed Friedmann–Robertson–Walker metric. The fluctuations $\delta\phi$ will then have to be translated into metric

perturbations that will finally result in fluctuations in the matter density. As long as the assumption of $\sigma_{ij} = 0$ holds, the two functions Φ and Ψ that describe the metric perturbations will be related simply by $\Phi + \Psi = 0$ so it will be sufficient to relate the fluctuations in ϕ to the Newtonian potential Ψ.

It is most convenient to work in Fourier space when dealing with the statistics of clustering and here we will concentrate on the two–point function, the power spectrum, which is generally defined through

$$\left\langle \Psi(\mathbf{k},\tau)\Psi(\mathbf{k}',\tau)\right\rangle \equiv (2\pi)^3 P_\Psi(k)\,\delta^3\left(\mathbf{k}-\mathbf{k}'\right) \tag{1.47}$$

The matter power spectrum is the Fourier transform of the two–point correlation function $\xi(x) = \langle\delta(\mathbf{x})\delta(\mathbf{x}+\mathbf{x}')\rangle$. The fluctuations from most standard single field inflation models constitute a Gaussian random field where the power spectrum is the only non–zero initial correlation function and different k–modes do not correlate. Any presence of initial non–Gaussianities will constrain the plausible models for inflation.

The energy–momentum tensor for a scalar field like the inflaton is given by

$$T^\mu_{\ \nu} = g^{\mu\alpha}\frac{\partial\phi}{\partial x^\alpha}\frac{\partial\phi}{\partial x^\nu} - g^\mu_{\ \nu}\left(\frac{1}{2}g^{\alpha\beta}\frac{\partial\phi}{\partial x^\alpha}\frac{\partial\phi}{\partial x^\beta} + V(\phi)\right) \tag{1.48}$$

where a summation over the indices α and β is implied. In the case of a homogeneous field in a smoothly expanding background $T^\mu_{\ \nu}$ reduces to a diagonal matrix as in equation (1.13) with the density and pressure given in equation (1.44). When we include the perturbations $\delta\phi$ there will also be non–diagonal entries in $T^\mu_{\ \nu}$. Assuming that the perturbations are small $\delta\phi \ll 1$ and neglecting second order terms, conservation of the energy–momentum tensor leads to an evolution equation for the perturbations

$$\frac{\mathrm{d}^2\delta\phi(\mathbf{k},\tau)}{\mathrm{d}\tau^2} + 2aH\frac{\mathrm{d}\delta\phi(\mathbf{k},\tau)}{\mathrm{d}\tau} + k^2\delta\phi(\mathbf{k},\tau) = 0 \tag{1.49}$$

A general solution of this can be found to be

$$\delta\phi = \frac{e^{ik/(aH)}}{a\sqrt{2k}}\left(1+\frac{iaH}{k}\right) \tag{1.50}$$

where we have used $\tau = -\frac{1}{aH}$.

The scales we are interested in are large compared to the comoving Hubble horizon at the time of inflation so we will take the limit $k \gg aH$ giving

$$\delta\phi = \frac{iH}{\sqrt{2k^3}} \tag{1.51}$$

This shows that the perturbations are frozen at a constant value while they are outside the horizon. As the Fourier modes reenter the horizon the energy fluctuations will result in metric perturbations. The relation between the primordial Newtonian potential and $\delta\phi$ at horizon crossing can be shown to be [7]

$$\Psi_p = \frac{2}{3}aH\frac{\delta\phi}{\mathrm{d}\phi^{(0)}/\mathrm{d}\tau}\bigg|_{aH=k} \tag{1.52}$$

so that the power spectrum for Ψ_p becomes

$$P_{\Psi_p}(k) = \frac{2}{9k^3}\left(\frac{aH^2}{\mathrm{d}\phi^{(0)}/\mathrm{d}\tau}\right)^2\Bigg|_{aH=k} \tag{1.53}$$

If the power spectrum is proportional to k^{-3} it is called a scale-free spectrum. Most inflationary models predict that the primordial power spectrum should be close to scale free so equation (1.53) is often written as a power law in k in the form

$$P_{\Psi_p}(k) = A_\mathrm{s}\frac{k^{n_\mathrm{s}-1}}{k^3} \tag{1.54}$$

where n_s is the scalar spectral index and A_s is the initial scalar amplitude. This parametrization is defined so that $n_\mathrm{s} = 1$ corresponds to a scale free spectrum. Currently the experimental values are $n_\mathrm{s} = 0.963 \pm 0.012$ and $A_\mathrm{s} = (2.441^{+0.088}_{-0.092}) \times 10^{-9}$ [5]. The power spectrum is usually normalized at the present time using the root mean square matter fluctuation at a scale of $8h^{-1}$Mpc denoted σ_8 to quantify the amplitude of the power spectrum. This parameter squared is proportional to the initial amplitude of scalar fluctuations, though the constant of proportionality depends on other cosmological parameters. The experimental value is $\sigma_8 = 0.809 \pm 0.024$ [5].

To relate the metric perturbations given in equation (1.52) to the matter perturbations at later times we need to consider the evolution from the end of inflation into the matter dominated era. The initial fluctuations gradually reenter the horizon while the universe is also changing from being radiation dominated to being matter dominated so the details of the transition will depend on the momentum of the mode. This dependence is described by the transfer function $T(k)$. After horizon crossing the evolution will be described by the Vlasov equation and in the linear regime by the linear growth factor $D^+(a)$. Putting these factors together we can evolve Ψ from its primordial value Ψ_p via

$$\Psi(\mathbf{k}, a) = \frac{9}{10}\Psi_p(\mathbf{k})T(k)\frac{D^+(a)}{a} \tag{1.55}$$

where the factors of $9/10$ and a^{-1} are due to convention.

The gravitational potential is related to the density fluctuations through the Poisson equation which in Fourier space reads

$$k^2\Psi(\mathbf{k}, \tau) = -\frac{3}{2}\Omega_\mathrm{m}\mathcal{H}^2\delta(\mathbf{k}, \tau) \tag{1.56}$$

This finally relates the linear matter power spectrum to the primordial power spectrum in equation (1.54)

$$P_\mathrm{m}(k, a) = \frac{9}{25}\frac{k^4}{\Omega_m^2 a^2\mathcal{H}^4}T^2(k)D^{+2}(a)P_\Psi(k) \tag{1.57}$$

The transfer function and the linear power spectrum above can be obtained numerically from software such as CAMB [12], CMBFAST [13] and CLASS [14]. The calculations involve

the linearized Boltzmann equations for the different species including the coupling between radiation and baryonic matter that set up the baryon acoustic oscillations (see Section 1.10). In figure 1.1 I plot the linear matter power spectrum at $z = 0$ as calculated by CAMB in a ΛCDM model with the parameters $\Omega_\Lambda = 0.728$, $\Omega_\mathrm{b} = 0.0456$, $\Omega_\mathrm{c} = 0.227$, $h = 0.738$, $n = 1$. The small fluctuations seen at $k \sim 0.1$ are the baryon acoustic oscillations.

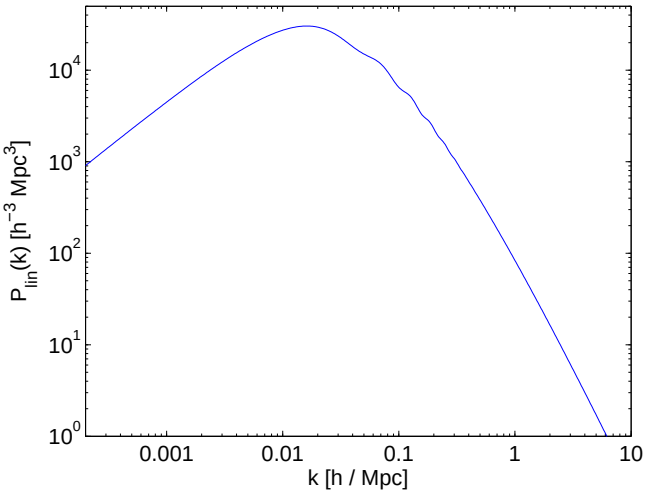

Figure 1.1: The linear matter power spectrum at $z = 0$ with the current best fit parameters in a ΛCDM model.

1.9 Non–Gaussianities

There are two distinct kinds of non–Gaussianities that play a role in the theory of structure formation. Firstly non–Gaussianities will be generated during the non–linear evolution even if the initial conditions are Gaussian, and secondly there could be primordial non–Gaussianities in the initial distributions. If we want to constrain the possible models of the very early universe it is important to be able to distinguish between the two and to separate out the primordial contribution.

To quantify non–Gaussianities we use the ensemble averages

$$\begin{aligned} \langle \Phi(\mathbf{k}_1)\Phi(\mathbf{k}_2)\Phi(\mathbf{k}_3)\rangle &= \delta_D(\mathbf{k}_1+\mathbf{k}_2+\mathbf{k}_3)B_\Phi(\mathbf{k}_1,\mathbf{k}_2,\mathbf{k}_3) \\ \langle \Phi(\mathbf{k}_1)\Phi(\mathbf{k}_2)\Phi(\mathbf{k}_3)\Phi(\mathbf{k}_4)\rangle &= \delta_D(\mathbf{k}_1+\mathbf{k}_2+\mathbf{k}_3+\mathbf{k}_4)T_\Phi(\mathbf{k}_1,\mathbf{k}_2,\mathbf{k}_3,\mathbf{k}_4) \\ &\vdots \end{aligned} \tag{1.58}$$

where B_Φ is the bispectrum, T_Φ the trispectrum and so on for higher order statistics. In a cosmology with Gaussian initial conditions the evolution of these quantities can be followed using cosmological perturbation theory. At lowest order this results in spectra that are nearly independent of the background cosmology [9], but higher order corrections modify this simple

result. The first loop corrections to the bispectrum have been calculated in [15] extending the range of validity into the weakly non–linear regime. Unfortunately the numerical calculations of the perturbative corrections quickly become very time consuming, so alternatives to standard perturbation theory are needed. In [44] a resummation scheme was introduced that show promising results and my work presented in Chapter 4 has been focused on extending the formalism presented there.

The presence of initial non–Gaussianities will also modify the gravitationally induced spectra and often they will leave imprints that are qualitatively different from the Gaussian case. Cosmological perturbation theory is complicated by the initial higher order spectra though, because the power spectrum receives one–loop corrections from the bispectrum, the bispectrum from the trispectrum and so on. The non–linear evolution of the power spectrum and bispectrum has been modeled in [16] using the time renormalization group approach to perturbation theory and in [43] and [45] initial non–Gaussianities have been incorporated into other resummation formalisms. In Chapter 4 I will show how their results generalize in the renormalization group formalism.

In the conformal Newtonian gauge the primordial non–Gaussianities can be parametrized as deviations from a Gaussian distribution in the curvature potential Φ. The deviations are often assumed to be determined locally so that Φ is given by

$$\Phi(\mathbf{x}) = \phi(\mathbf{x}) + f_{\mathrm{NL}}^{\mathrm{loc}}\phi^2(\mathbf{x}) + g_{\mathrm{NL}}^{\mathrm{loc}}\phi^3(\mathbf{x}) \tag{1.59}$$

where ϕ is a Gaussian random field and the dimensionless non–linearity parameters $f_{\mathrm{NL}}^{\mathrm{loc}}$ and $g_{\mathrm{NL}}^{\mathrm{loc}}$ measure the deviations from Gaussianity. The leading term in the bispectrum will be given by

$$B_{\Phi}^{\mathrm{loc}}(\mathbf{k}_1, \mathbf{k}_2, \mathbf{k}_3) = 2f_{\mathrm{NL}}^{\mathrm{loc}}\left(P_\phi(k_1)P_\phi(k_2) + (2\mathrm{perm.})\right) \tag{1.60}$$

while the trispectrum also includes terms involving $g_{\mathrm{NL}}^{\mathrm{loc}}$

$$\begin{aligned} T_\Phi(\mathbf{k}_1, \mathbf{k}_2, \mathbf{k}_3, \mathbf{k}_4) = {} & 4\left(f_{\mathrm{NL}}^{\mathrm{loc}}\right)^2\Big(P_\phi(k_1)P_\phi(k_2)\left[P_\Phi(|\mathbf{k}_1+\mathbf{k}_3|) + P_\Phi(|\mathbf{k}_1+\mathbf{k}_4|)\right] + (5\mathrm{perm.})\Big) \\ & + 6g_{\mathrm{NL}}^{\mathrm{loc}}\big(P_\phi(k_1)P_\phi(k_2)P_\phi(k_3) + (3\mathrm{perm.})\big) \end{aligned} \tag{1.61}$$

The parameter $f_{\mathrm{NL}}^{\mathrm{loc}}$ can be constrained by measurements of the bispectrum in the CMB and the large scale structure. The current combined constraints are $-5 < f_{\mathrm{NL}}^{\mathrm{loc}} < 59$ [17].

1.10 Baryon Acoustic Oscillations

The baryon acoustic oscillations (BAO) are the most distinctive feature in the matter power spectrum at the scales where perturbation theory and renormalization group theory takes over from linear theory and so they act as the best reference point to compare different approaches. Here I will give a short qualitative description of how they arise.

In the very early universe when the temperature is still high enough for hydrogen to be ionized, radiation and baryons are tightly coupled and can be approximated as a single fluid.

The evolution of this fluid is determined by the gravitational attraction of the baryons to the overdensities of dark matter that have already begun to grow, and by the pressure of the radiation that tends to expand the fluid. As long as a specific scale is outside the horizon it will not evolve, but when it enters the horizon it will begin to oscillate until recombination when the radiation is no longer energetic enough to keep hydrogen ionized. The small–scale modes that enter the horizon early on will have undergone many oscillations before recombination while the largest modes will enter the horizon after recombination and keep their initial amplitude with no oscillations.

The power spectrum measures both overdensities and underdensities, so the first peak in the spectrum corresponds to the mode that entered the horizon and just oscillated for one quarter of a cycle to a maximal overdensity while the mode at the second peak oscillated for three quarters of a cycle to a minimal density. The frequency of the oscillations and therefore the position of the peaks in the power spectrum is determined by the sound speed in the fluid which in turn is determined by the ratio of the radiation and baryon densities. On small scales the oscillations will be damped due to the scattering of the photons on the electrons that smoothes out any initial perturbations. All in all the BAO will be most prominent in the wavenumber range $k \approx 0.05 - 0.3h\mathrm{Mpc}^{-1}$.

The BAO are most clearly observed in the CMB power spectrum because the photons have traveled almost undisturbed to us from the last scattering surface. In figure 1.2 the temperature anisotropy power spectrum as measured by WMAP is shown. The curve is calculated using the best fit parameters after the WMAP 7–year data release. The damping at small scales is seen at multipole moments $l \gtrsim 1000$.

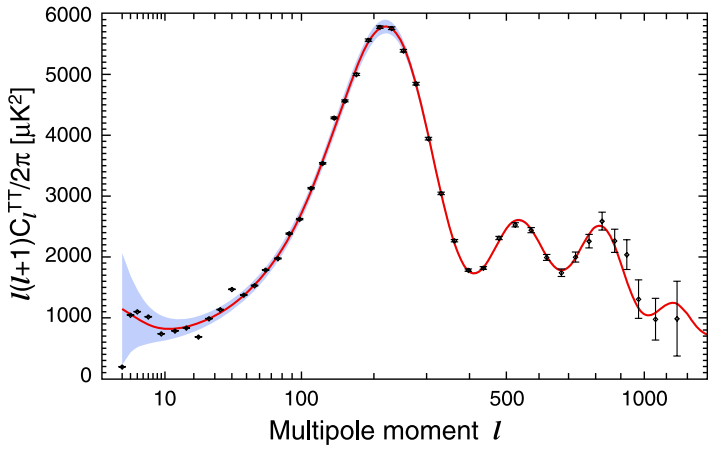

Figure 1.2: The CMB temperature anisotropy power spectrum as measured by WMAP. The figure is taken from [18]

The BAO will also leave an imprint on the matter power spectrum though the amplitude will be suppressed due to the dominant dark matter that does not oscillate. A comparison of the amplitude of fluctuations in figure 1.1 and figure 1.2 illustrates how large this suppression is. If the position and amplitude of the oscillations can be predicted as a function of z the BAO scale can be used as a standard distance through the evolution of the universe much in

the same way as type Ia supernovae are used as standard candles. Thus it is important to extend the validity of analytical approaches to the scales relevant to the BAO. Unfortunately the scales of interest are mostly in the non–linear regime at the present time, so the linear treatment in Section 1.6 is not sufficient when comparing the results with data from galaxy surveys.

Chapter 2

Quantum Field Theory

As quantum field theory has developed its own tools to deal with perturbation theory and diverging contributions to cross sections, it has become clear that these tools can also be used in certain parts of classical physics when dealing with many–body problems in statistical physics and cosmology. In this chapter I will introduce the theory that will be relevant for deducing the renormalization group equation for the cosmological evolution of large–scale structure.

2.1 The Variational Principle

One way of describing the dynamics of classical mechanics is through the use of the variational principle. This principle states that an object moving in a potential V from one point x_A to another x_B will take the path that minimizes the action S. The action is defined as the time integration of the Lagrangian L

$$S = \int_{t_A}^{t_B} \mathrm{d}t \; L\left(r(t), \dot{r}(t)\right) \tag{2.1}$$

where $r(t)$ is the position of the object and $\dot{r}(t)$ its velocity. In simple systems the Lagrangian is the kinetic energy minus the potential energy $L = T - V = \frac{1}{2}m\dot{r}^2 - V(r)$.

A small variation of the path $r(t) \to r(t) + \delta r(t)$ leads to a variation of the action given by

$$\delta S = \int_{t_A}^{t_B} \mathrm{d}t \; \left(\frac{\partial L}{\partial r}\delta r(t) + \frac{\partial L}{\partial \dot{r}}\delta\dot{r}(t)\right) = \int_{t_A}^{t_B} \mathrm{d}t \; \left(\frac{\partial L}{\partial r} - \frac{\mathrm{d}}{\mathrm{d}t}\left(\frac{\partial L}{\partial \dot{r}}\right)\right)\delta r(t) \tag{2.2}$$

where we have performed a partial integration of the last term and used $\delta r(t_A) = \delta r(t_B) = 0$ because the initial and final positions are kept fixed. To minimize the action we set $\delta S = 0$

and requiring this to be true for any variation δr we get the Euler–Lagrange equation in one dimension

$$\frac{\partial L}{\partial r} - \frac{\mathrm{d}}{\mathrm{d}t}\left(\frac{\partial L}{\partial \dot{r}}\right) = 0 \tag{2.3}$$

The Euler–Lagrange equation defines the equation of motion of the object under consideration. In the simple case of $L = \frac{1}{2}m\dot{r}^2 - V(r)$ we get $-\frac{\mathrm{d}V}{\mathrm{d}r} = m\ddot{r}$ or $F = ma$ in the presence of a conservative force field. Thus the variational principle can reproduce the known behaviour of classical conservative systems.

When dealing with quantum field theories the particles are described by fields $\phi = \phi(\mathbf{x}, t)$ and we define a Lagrangian density $\mathcal{L} = \mathcal{L}(\phi, \partial_\mu \phi)$ where μ runs from zero to three denoting derivatives with respect to time and position. The action will now be an integration over both time and position

$$S[\phi] = \int \mathrm{d}^4x \, \mathcal{L}(\phi, \partial_\mu \phi) = \int \mathrm{d}t \, L[\phi(t), \dot{\phi}(t)] \tag{2.4}$$

where $L[\phi(t), \dot{\phi}(t)]$ is the Lagrangian functional given by integrating out the spatial dependency of the Lagrangian density. The Euler–Lagrange equation obtained from this action is

$$\frac{\partial \mathcal{L}}{\partial \phi} = \partial_\mu \frac{\partial \mathcal{L}}{\partial(\partial_\mu \phi)} \tag{2.5}$$

equivalent to equation (2.3), but now in four dimensions. If the system involves more than one field there will be a set of separate Euler–Lagrange equation obtained from varying one field at a time and keeping the others fixed.

2.2 Generating Functionals

The variational principle defines the classical evolution of a field configuration at an initial time $\phi(\mathbf{x}, t_A)$ into a different configuration at a later time $\phi(\mathbf{x}, t_B)$. In quantum field theories we have to take quantum fluctuations into account so we can only assign probabilities to each final distribution. We can take advantage of the fact that the action varies slowly around the classical solution with $\delta S = 0$ and define the probability as a path integral

$$P[\phi(t_B); \phi(t_A)] = \mathcal{N} \int \mathcal{D}''\phi \, e^{iS} = \mathcal{N} \int \mathcal{D}''\phi \, e^{i \int \mathrm{d}^4x \, \mathcal{L}(\phi, \partial_\mu \phi)} \tag{2.6}$$

where the integration is over every possible intermediate configuration and the primes indicate that the initial and final configuration are kept fixed. We will not be concerned with the normalization constant $\mathcal{N}$ as it will not be part of our final results, so we set it to 1 from now on. The contribution to the integration in (2.6) will only be significant where the action varies slowly because the phases of the exponential will cancel out elsewhere. This reflects the nature of quantum fluctuations away from the classical solution.

Starting from the probability measure in equation (2.6) we can define a generating functional $Z[J]$ by adding a source J for the field and integrating over the initial and final states

$$Z[J] \equiv \int \mathcal{D}\phi e^{i\int \mathrm{d}^4x\,[\mathcal{L}+J(x)\phi(x)]} \tag{2.7}$$

The generating functional can be used to generate correlation functions by taking functional derivatives with respect to the source J

$$\frac{\delta Z}{\delta J(x_a)} = \int \mathcal{D}\phi\; i\phi(x_a) e^{i\int \mathrm{d}^4x\,[\mathcal{L}+J(x)\phi(x)]} \tag{2.8}$$

or setting J to zero to recover the physical situation

$$\left.\frac{\delta Z}{\delta J(x)}\right|_{J=0} = i\int \mathcal{D}\phi\;\phi(x)e^{iS} = i\langle\phi(x)\rangle\, Z[J=0] \tag{2.9}$$

The expectation value $\langle\phi(x)\rangle$ is the classical solution to the equation of motion given by

$$\phi_{\mathrm{cl}}(x) = \langle\phi(x)\rangle = -i\left.\frac{\delta \log Z}{\delta J(x)}\right|_{J=0} = \left.\frac{\delta W}{\delta J(x)}\right|_{J=0} \tag{2.10}$$

where we have defined $W = -i\log Z$, the generator of connected Green's functions.

Connected n–point functions can be obtained by taking n derivatives of W with respect to the source. For the two-point function we get

$$\begin{aligned}
\left.\frac{\delta^2 W}{\delta J(x_1)\delta J(x_2)}\right|_{J=0} =& \left.\frac{\delta}{\delta J(x_1)}\left(\frac{1}{Z}\int \mathcal{D}\phi\;\phi(x_2)e^{i\int \mathrm{d}^4x\,[\mathcal{L}+J\phi]}\right)\right|_{J=0} \\
=& \frac{i}{Z[J=0]}\int \mathcal{D}\phi\;\phi(x_1)\phi(x_2)e^{i\int \mathrm{d}^4x\,\mathcal{L}} \\
&- \frac{i}{Z[J=0]^2}\int \mathcal{D}\phi\;\phi(x_1)e^{i\int \mathrm{d}^4x\,\mathcal{L}}\int \mathcal{D}\phi\;\phi(x_2)e^{i\int \mathrm{d}^4x\,\mathcal{L}} \\
=& i\langle\phi(x_1)\phi(x_2)\rangle - i\langle\phi(x_1)\rangle\langle\phi(x_2)\rangle = i\langle\phi(x_1)\phi(x_2)\rangle_{\mathrm{conn}}
\end{aligned} \tag{2.11}$$

In general we will have

$$\left.\frac{\delta^n W}{\delta J(x_1)\cdots\delta J(x_n)}\right|_{J=0} = (i)^{n-1}\langle\phi(x_1)\cdots\phi(x_n)\rangle_{\mathrm{conn}} \tag{2.12}$$

In a system with interactions we can split the Lagrangian density into a free part and an interacting part $\mathcal{L} = \mathcal{L}_0 + \mathcal{L}_{\mathrm{int}}$. The free part can usually be written as a quadratic term in the form $\mathcal{L}_0 = -\frac{1}{2}\phi\cdot\Delta^{-1}\cdot\phi$ and we can perform the Gaussian integration of the free part of Z

$$Z_0[J] = \int \mathcal{D}\phi \exp\left(i\int \mathrm{d}^4x\;\left[-\frac{1}{2}\phi\cdot\Delta^{-1}\cdot\phi + J\phi\right]\right) = \exp\left(i\int \mathrm{d}^4x\;\frac{1}{2}J\cdot\Delta\cdot J\right) \tag{2.13}$$

This expression can be used to rewrite Z by explicitly calculating Δ in the free limit and plugging the inverse back into the full generating functional.

We can also obtain Z from Z_0 by taking functional derivatives. If the interacting part of $\mathcal{L}$ can be written as a function of the field, $\mathcal{L}_{\text{int}} = V(\phi(x))$, then according to Wick's theorem Z will be given by

$$Z[J] = \exp\left\{ i \int d^4x \, V\left(\frac{-i\delta}{\delta J(x)} \right) \right\} Z_0[J] \tag{2.14}$$

By expanding the exponential we can get a perturbative expression order by order in the interaction terms that make up $V(\phi(x))$.

We can read off the Feynman rules for a given theory from equation (2.14). Connected Green's functions that relate the field at one point in space and time to the field at another point are also called propagators and they are represented as lines in Feynman diagrams. The interaction terms from $V(\phi(x))$ are represented as vertices merging two or more lines.

When drawing Feynman diagrams we distinguish between unconnected diagrams, connected diagrams and one–particle irreducible (1PI) diagrams. When using W as the generating functional we get all the possible diagrams minus the unconnected ones as was seen in equation (2.11). The correlation functions that we are interested in are represented by the connected diagrams so W will be a key object in the theory.

The 1PI diagrams are diagrams that cannot be split in two by cutting just one propagator line. In general a contribution to the correlation functions can be written in terms of 1PI diagrams connected by full propagators, so we will also be interested in the generator of 1PI diagrams which is defined as the Legendre transform of W

$$\Gamma[\phi_{\text{cl}}] \equiv W[J] - \int d^4x J(x)\phi_{\text{cl}}(x) \tag{2.15}$$

Taking the Legendre transform changes variables from J to ϕ_{cl} and differentiating Γ with respect to ϕ_{cl} gives the source field J

$$\frac{\delta\Gamma}{\delta\phi_{\text{cl}}(x)} = -J(x) \tag{2.16}$$

If we take the derivative of this equation with respect to $J(y)$ we get

$$\begin{aligned} -\delta(x-y) = \frac{\delta}{\delta J(y)} \frac{\delta\Gamma}{\delta\phi_{\text{cl}}(x)} &= \int \mathrm{d}^4z \, \frac{\delta\phi_{\text{cl}}(z)}{\delta J(y)} \frac{\delta^2\Gamma}{\delta\phi_{\text{cl}}(z)\delta\phi_{\text{cl}}(x)} \\ &= \int \mathrm{d}^4z \, \frac{\delta^2 W}{\delta J(y)\delta J(z)} \frac{\delta^2\Gamma}{\delta\phi_{\text{cl}}(z)\delta\phi_{\text{cl}}(x)} \end{aligned} \tag{2.17}$$

showing that the second derivatives of W and Γ constitute inverse matrices to each other except for a minus sign.

The 1PI corrections to the two–point propagator are usually referred to as the self–energy because it corresponds to loop diagrams with both legs connected to the same propagator, e.g. an electron emitting a virtual photon and reabsorbing it. The relation in equation (2.17) can be used to write the two–point correlation functions in terms of propagators and the self–energy as we will see in Chapter 3.

2.3 Renormalization Group Theory

In quantum field theory we are usually interested in calculating observable quantities such as scattering amplitudes between particles. Perturbation theory takes the form of a series of loop corrections to the tree level expressions for the quantities obtained by expanding the exponential in equation (2.14). In many cases the loop corrections display ultraviolet divergences when the integration over loop momenta are performed. This problem can be solved by introducing a cut–off for large momenta in the integrations, with the unwanted consequence that the result will depend on the cut–off scale. We are not interested in theories that depend on an artificial cut–off, so instead the dependency can be incorporated into the strength of coupling constants and mass terms present in the theory. The resulting running of the parameters means that the strength of the couplings and the mass of the particles will depend on which energy scale we choose to renormalize the theory at.

The renormalization group equations are differential equations that keep track of how the coupling constants and mass terms varies with the cut–off scale. They are often written as

$$\frac{d\lambda}{d(\ln \Lambda)} = \beta(\lambda) \tag{2.18}$$

where λ is a running parameter, Λ is the cut–off and β is the β–function of a given theory. The specific form of the β–function is not relevant here. It can be derived from the requirement that the scattering amplitudes remain constant when the cut–off is varied.

In the case of cosmological perturbation theory we will not be interested in absorbing the cut–off dependence into coupling constants and mass terms, so the analogy to the renormalization group flow of equation (2.18) is not complete. Instead we will be using the cut–off as a way of gradually including more and more loop corrections to the observable quantities and letting the cut–off go to infinity we can in principle recover the full theory with all loop corrections included. In practice we will construct renormalization group equations for the observable quantities directly and integrate these equations to obtain the result in the limit where the cut–off goes to infinity. This will correspond to including more and more non–linearities in the calculations. As we will see in Chapter 3 we will need to make approximations to the right hand side of the differential equations by restricting the calculation to a certain class of Feynman diagrams, but the integration still corresponds to resumming perturbation theory to all orders.

Chapter 3

Renormalization Group Formalism

We will now return to the subject of structure formation and go beyond the linear treatment of the process. Higher order corrections to the linear behaviour was first considered using a perturbative approach in [21]–[24]. The similarities to quantum field theory allow for a diagrammatical interpretation of the perturbative series using Feynman diagrams to gain intuition about the underlying theory. The results improve on linear theory, but the non–linear couplings are strong so the regime where standard perturbation theory is applicable is small. In particular at $z = 0$ one–loop perturbation theory breaks down on the scales of $k \sim 0.1\ h\ \mathrm{Mpc}^{-1}$ where the BAO are prominent. Also the computation of higher order loop corrections is numerically challenging and has only been done up to two–loop order [25]. It is well known that the perturbative series contains cancellations between large positive and negative contributions at intermediate and small scales so that terminating the expansion at a given order does not yield meaningful results at these scales. A thorough review of cosmological perturbation theory is given in [9].

The analogy between cosmological perturbation theory and quantum field theory was used in [26] to introduce a field theoretical interpretation of the processes at work in structure formation. This interpretation has been developed into a renormalized perturbation theory in [27] and [28] where the perturbative series has been resummed to all orders at small scales. In [29] and [30] the analogy to quantum field theory was further developed into a path integral representation of the equations governing structure formation and in [31] a renormalization group approach to solving differential equations perturbatively was applied. A different renormalization group approach using a cut–off at small scales was employed in [32] and [33] and developed into the time renormalization group (time–RG) formalism in [34] where time is the parameter controlling the cut–off scale.

The time–RG formalism makes very few references back to the field theoretical inspirations leading up to it when a numerical solution of the differential equations is computed, so it is a very straightforward approach compared to the others. To gain analytical insights in the

evolution it does however follow the approach of [33] closely as seen in [35]. Other schemes that avoid references to field theory are the closure theory inspired by the statistical theory of turbulence introduced in [36] and solved numerically in [37] and Lagrangian perturbation theory as presented in [38]. The validity of some of these approaches has been tested and compared against each other in [39] and N–body simulations in [25].

In my work I have followed the formalism of renormalization group (RG) theory as applied by [33] where the equation of motion is given a path integral representation and subsequently solved by a method resembling the renormalization group differential equations of quantum field theory. The result includes a class of Feynman diagrams summed to all orders so that the irregular behaviour at small scales encountered in standard perturbation theory is avoided.

In this chapter I will first present the framework of standard perturbation theory and the diagrammatical interpretation in the context of a path integral formulation of the equation of motion. Then I present the RG formalism of [33]. Sections 3.6 and 3.7 contain my work on developing the notation and theory needed to deal with multi–point propagators in Chapter 4.

3.1 The Equation of Motion

We begin by returning to the continuity and Euler equations (1.32). We argued in Section 1.6 that we can use the velocity divergence θ in stead of the peculiar velocity field $\mathbf{v}$ so we will take the divergence of the Euler equation as we did in the linear treatment. Transforming to Fourier space we get

$$\begin{aligned} &\frac{\partial\delta(\mathbf{k},\tau)}{\partial\tau} + \theta(\mathbf{k},\tau) + \int \mathrm{d}^3\mathbf{q}\mathrm{d}^3\mathbf{p}\; \delta_D(\mathbf{k}-\mathbf{q}-\mathbf{p})\alpha(\mathbf{q},\mathbf{p})\theta(\mathbf{q},\tau)\delta(\mathbf{p},\tau) = 0 \\ &\frac{\partial\theta(\mathbf{k},\tau)}{\partial\tau} + \mathcal{H}\theta(\mathbf{k},\tau) + \frac{3}{2}\mathcal{H}^2\delta(\mathbf{k},\tau) \\ &\qquad\qquad + \int \mathrm{d}^3\mathbf{q}\mathrm{d}^3\mathbf{p}\; \delta_D(\mathbf{k}-\mathbf{q}-\mathbf{p})\beta(\mathbf{q},\mathbf{p})\theta(\mathbf{q},\tau)\theta(\mathbf{p},\tau) = 0 \end{aligned} \tag{3.1}$$

with the two momentum factors given by

$$\alpha(\mathbf{q},\mathbf{p}) = \frac{(\mathbf{q}+\mathbf{p})\cdot\mathbf{q}}{q^2} \quad \text{and} \quad \beta(\mathbf{q},\mathbf{p}) = \frac{(\mathbf{q}+\mathbf{p})^2\mathbf{q}\cdot\mathbf{p}}{2q^2p^2} \tag{3.2}$$

These factors carry the non–linearity of the equations by coupling different modes of the density and velocity perturbations. Setting them to zero gives the linear limit discussed in Section 1.6, but we have now gone back to the Einstein–de Sitter case with $\Omega_\mathrm{m} = 1$.

To write these equations in a form that resembles the notation used in field theory we define a two–component field

$$\phi_a(\mathbf{k},\eta) = \begin{pmatrix} \phi_1(\mathbf{k},\eta) \\ \phi_2(\mathbf{k},\eta) \end{pmatrix} \equiv e^{-\eta} \begin{pmatrix} \delta(\mathbf{k},\eta) \\ -\theta(\mathbf{k},\eta)/\mathcal{H} \end{pmatrix} \tag{3.3}$$

where we have defined a new time variable as the logarithm of the scale factor $\eta = \ln(a/a_i)$ with a_i corresponding to the scale factor at some initial time when the evolution of all relevant scales was still in the linear regime. We see that the linearly growing mode in (1.39) corresponds to ϕ_a being constant and the decaying mode has $\phi_a \propto e^{-\frac{5}{2}\eta}$.

With this field the equations (3.1) can be combined to yield a more compact equation of motion for the dark matter fluid where repeated indices (running from 1 to 2) and momenta are being summed and integrated over respectively

$$\left(\delta_{ab}\partial_\eta + \Omega_{ab}\right)\phi_b(\mathbf{k},\eta) = e^{\eta}\gamma_{abc}(\mathbf{k},-\mathbf{p},-\mathbf{q})\phi_b(\mathbf{p},\eta)\phi_c(\mathbf{q},\eta) \tag{3.4}$$

with

$$\Omega_{ab} = \begin{pmatrix} 1 & -1 \\ -3/2 & 3/2 \end{pmatrix} \tag{3.5}$$

and the non–zero entries in the vertex factor are given by

$$\begin{aligned} \gamma_{121}(\mathbf{k},\mathbf{p},\mathbf{q}) = \gamma_{112}(\mathbf{k},\mathbf{q},\mathbf{p}) &= \frac{1}{2}\delta_D(\mathbf{k}+\mathbf{p}+\mathbf{q})\alpha(\mathbf{p},\mathbf{q}) \\ \gamma_{222}(\mathbf{k},\mathbf{p},\mathbf{q}) &= \delta_D(\mathbf{k}+\mathbf{p}+\mathbf{q})\beta(\mathbf{p},\mathbf{q}) \end{aligned} \tag{3.6}$$

Equation (3.4) is the equation of motion for the gas of dark matter particles that we wish to explore using the formalism introduced in Chapter 2.

Before doing this we will return to the linear treatment and solve for the linear propagator of the system, that is the operator that evolves the linear solution ϕ_a^0 forward in time or the Green's function of the linearized system

$$\phi_a^0(\mathbf{k},\eta_a) = g_{ab}(\eta_a,\eta_b)\phi_b^0(\mathbf{k},\eta_b) \quad \text{for} \quad \eta_a > \eta_b \tag{3.7}$$

By putting this expression into equation (3.4) with $\gamma_{abc} = 0$ we see that the linear propagator satisfies the equation

$$\left(\delta_{ab}\partial_{\eta_a} + \Omega_{ab}\right) g_{ab}(\eta_a,\eta_b) = \delta_{ac}\delta_D(\eta_a - \eta_b) \tag{3.8}$$

which can be solved to give

$$g_{ab}(\eta_a,\eta_b) = \frac{1}{5}\left(\begin{bmatrix} 3 & 2 \\ 3 & 2 \end{bmatrix} + \begin{bmatrix} 2 & -2 \\ -3 & 3 \end{bmatrix} e^{-\frac{5}{2}(\eta_a-\eta_b)}\right)\theta(\eta_a - \eta_b) \tag{3.9}$$

where the step function θ ensures causality. The last matrix term with the decaying exponential factor controls the linearly decaying mode while the first term controls the linearly growing mode. By selecting appropriate initial conditions we can follow the evolution of each mode choosing ϕ_a proportional to $u_a = \binom{1}{1}$ for the growing mode and $v_a = \binom{1}{-3/2}$ for the decaying mode. Due to the factor of $e^{-\eta}$ in the definition of the two–component field in equation (3.3) the first term in the linear propagator reduces to a time independent matrix in contrast to the growing mode of the linear propagator of [28] that grows as e^{η}.

3.2 Background Cosmologies

In an Einstein–de Sitter background cosmology the time variable η is equal to the logarithm of the linear growth factor, $\eta = \ln(D^+/D_i^+)$, since $D^+ \propto a$. This is not the case in more general background cosmologies with dark energy. If however we make a redefinition of the field ϕ_a as

$$\phi_a(\mathbf{k},\eta) \to e^{-\eta} \begin{pmatrix} \delta(\mathbf{k},\eta) \\ -\theta(\mathbf{k},\eta)/(\mathcal{H}f) \end{pmatrix} = \begin{pmatrix} \phi_1'(\mathbf{k},\eta) \\ \phi_2'(\mathbf{k},\eta) \end{pmatrix} \tag{3.10}$$

where f was defined in Section 1.6 and the time variable $\eta \to \ln(D^+/D_i^+)$, we can show that the equation of motion remains in the form of (3.4).

We can rewrite the time derivatives with respect to τ using

$$\frac{\mathrm{d}}{\mathrm{d}\tau} = \frac{\mathrm{d}\eta}{\mathrm{d}\tau}\frac{\mathrm{d}}{\mathrm{d}\eta} = \frac{\mathrm{d}\ln D^+}{\mathrm{d}\tau}\frac{\mathrm{d}}{\mathrm{d}\eta} = \frac{\mathrm{d}\ln D^+}{\mathrm{d}\ln a}\frac{1}{a}\frac{\mathrm{d}a}{\mathrm{d}\tau}\frac{\mathrm{d}}{\mathrm{d}\eta} = \mathcal{H}f\frac{\mathrm{d}}{\mathrm{d}\eta} \tag{3.11}$$

The first equation in (3.1) then becomes

$$\mathcal{H}f\left(\frac{\mathrm{d}}{\mathrm{d}\eta}\left(\phi_1' e^{\eta}\right) - e^{\eta}\phi_2' - e^{2\eta}\int \mathrm{d}^3\mathbf{q}\mathrm{d}^3\mathbf{p}\;\delta_D(\mathbf{k}-\mathbf{q}-\mathbf{p})\alpha(\mathbf{q},\mathbf{p})\phi_2'\phi_1'\right) = 0 \tag{3.12}$$

or

$$\frac{\mathrm{d}}{\mathrm{d}\eta}\phi_1' + \phi_1' - \phi_2' - e^{\eta}\int \mathrm{d}^3\mathbf{q}\mathrm{d}^3\mathbf{p}\;\delta_D(\mathbf{k}-\mathbf{q}-\mathbf{p})\alpha(\mathbf{q},\mathbf{p})\phi_2'\phi_1' = 0 \tag{3.13}$$

where I have suppressed the arguments of the ϕ'–functions. We see that there is no change as compared to the $a = 1$ component of equation (3.4). The second equation in (3.1) becomes

$$\begin{aligned} -\mathcal{H}^2 f^2\Bigg(\frac{1}{\mathcal{H}f}\frac{\mathrm{d}}{\mathrm{d}\eta}\left(\mathcal{H}f e^{\eta}\phi_2'\right) + \frac{e^{\eta}\phi_2'}{f} - \frac{3\Omega_\mathrm{m}}{2f^2}e^{\eta}\phi_1' \\ - e^{2\eta}\int \mathrm{d}^3\mathbf{q}\mathrm{d}^3\mathbf{p}\;\delta_D(\mathbf{k}-\mathbf{q}-\mathbf{p})\beta(\mathbf{q},\mathbf{p})\phi_2'\phi_2'\Bigg) = 0 \end{aligned} \tag{3.14}$$

We can use the evolution equation for the growth factor equation (1.37) to rewrite the first term in the parentheses so that

$$\begin{aligned} \frac{1}{\mathcal{H}f}\frac{\mathrm{d}}{\mathrm{d}\eta}\left(\mathcal{H}f\right) &= \frac{1}{\mathcal{H}^2 f^2}\frac{\mathrm{d}}{\mathrm{d}\tau}\left(\frac{\mathrm{d}\ln D^+}{\mathrm{d}\tau}\right) = \frac{1}{\mathcal{H}^2 f^2}\left[\frac{1}{D^+}\frac{\mathrm{d}^2 D^+}{\mathrm{d}\tau^2} - \frac{1}{D^{+2}}\left(\frac{\mathrm{d}D^+}{\mathrm{d}\tau}\right)^2\right] \\ &= \frac{1}{\mathcal{H}^2 f^2}\left[\frac{3}{2}\Omega_\mathrm{m}\mathcal{H}^2 - \mathcal{H}^2 f - \mathcal{H}^2 f^2\right] = \frac{3}{2}\frac{\Omega_\mathrm{m}}{f^2} - \frac{1}{f} - 1 \end{aligned} \tag{3.15}$$

Equation (3.14) then reduces to

$$\frac{\mathrm{d}}{\mathrm{d}\eta}\phi_2' + \frac{3\Omega_\mathrm{m}}{2f^2}\phi_2' - \frac{3\Omega_\mathrm{m}}{2f^2}\phi_1' - e^{\eta}\int \mathrm{d}^3\mathbf{q}\mathrm{d}^3\mathbf{p}\;\delta_D(\mathbf{k}-\mathbf{q}-\mathbf{p})\beta(\mathbf{q},\mathbf{p})\phi_2'\phi_2' = 0 \tag{3.16}$$

where we see that the overall effect of the redefinitions of ϕ_a and η is to replace the matrix in equation (3.5) with

$$\Omega'_{ab} = \begin{pmatrix} 1 & -1 \\ -3\Omega_{\rm m}/(2f^2) & 3\Omega_{\rm m}/(2f^2) \end{pmatrix} \tag{3.17}$$

The factor $\Omega_{\rm m}/f^2$ is time dependent but if we try to solve for the linear propagator in equation (3.8) we can still get an explicit expression for the growing part

$$g^+_{ab} = \frac{1}{3 + 2f^2/\Omega_{\rm m}} \begin{pmatrix} 3 & 2f^2/\Omega_{\rm m} \\ 3 & 2f^2/\Omega_{\rm m} \end{pmatrix} \theta(\eta_a - \eta_b) \tag{3.18}$$

showing that the growing mode $u_a = \left(\begin{smallmatrix} 1 \\ 1 \end{smallmatrix}\right)$ is still constant in time. The evolution of the decaying mode on the other hand will depend on the factor $\Omega_{\rm m}/f^2$, but in the matter dominated period, $\Omega_{\rm m}/f^2 \approx 1$, we recover the Einstein–de Sitter case. Thus for most of the history of the universe the Einstein–de Sitter assumption is well justified, and in the late evolution when dark energy starts to dominate, most of the changes are encoded in the linear growth factor D^+. As long as D^+ is scale independent we will therefore use the reinterpretation of the time variable $\eta = \ln\left(D^+/D^+_i\right)$ to include more general background cosmologies, specifically the standard ΛCDM case. Any change in background cosmology will then simply result in a reevaluation of η, but with the original equation of motion (3.4) to describe the dynamics.

3.3 Standard Perturbation Theory

The assumption of cosmological perturbation theory is that the full solution to equation (3.4) can be expanded as a perturbative series around the linear solution ϕ^0_a. If we only consider the growing mode we can write

$$\phi_a(\mathbf{k}, \eta) = \sum_{n=1}^{\infty} e^{(n-1)\eta} \psi^{(n)}_a(\mathbf{k}) \tag{3.19}$$

where we see that the linear solution ($n = 1$) is constant in time as we saw in Section 3.1, i.e. $\psi^{(1)}_a(\mathbf{k})$ is the growing part of $\phi^0_a(\mathbf{k}, \eta)$ proportional to u_a. Substituting equation (3.19) into equation (3.4) gives

$$\sum_{n=1}^{\infty} \left((n-1)\delta_{ab} + \Omega_{ab}\right) e^{(n-1)\eta} \psi^{(n)}_b(\mathbf{k}) = e^{\eta} \gamma_{abc}\left(\mathbf{k}, \mathbf{k}_1, \mathbf{k}_2\right) \sum_{m=1}^{\infty} \sum_{l=1}^{\infty} e^{(l+m-1)\eta} \psi^{(m)}_b(\mathbf{k}_1) \psi^{(l)}_c(\mathbf{k}_2) \tag{3.20}$$

Equating equal powers of e^{η} we get a set of recursion relations for $\psi^{(n)}_a$

$$\left((n-1)\delta_{ab} + \Omega_{ab}\right) \psi^{(n)}_a(\mathbf{k}) = \gamma_{abc}\left(\mathbf{k}, \mathbf{k}_1, \mathbf{k}_2\right) \sum_{m=1}^{n-1} \psi^{(m)}_b(\mathbf{k}_1) \psi^{(n-m)}_c(\mathbf{k}_2) \tag{3.21}$$

For $n > 1$ we can identify $\sigma_{ab}^{-1}(n) = (n-1)\delta_{ab} + \Omega_{ab}$ so that the inverse is

$$\sigma_{ab}(n) = \frac{1}{(2n+3)(n-1)} \begin{pmatrix} 2n+1 & 2 \\ 3 & 2n \end{pmatrix} \tag{3.22}$$

and equation (3.21) simplifies to

$$\psi_a^{(n)}(\mathbf{k}) = \sigma_{ab}(n)\gamma_{bcd}\left(\mathbf{k}, \mathbf{k}_1, \mathbf{k}_2\right) \sum_{m=1}^{n-1} \psi_c^{(m)}(\mathbf{k}_1)\psi_d^{(n-m)}(\mathbf{k}_2) \tag{3.23}$$

These recursion relations show that each order in the perturbation series includes an extra factor of $\sigma_{ab}(n)\gamma_{bcd}$ expressing the non–linear couplings of Fourier modes. The vertex factors α and β in equation (3.2) can become very large so the higher order terms $\psi_a^{(n)}$ can grow bigger than $\psi_a^{(1)}$ signaling the breakdown of perturbation theory.

With growing mode initial conditions we have $\psi_a^{(1)}(\mathbf{k}) = u_a\delta^0(\mathbf{k})$ where δ^0 is the initial matter density perturbation and $\psi_a^{(2)}$ reduces to

$$\begin{aligned} \psi_a^{(2)}(\mathbf{k}) &= \sigma_{ab}(2)\gamma_{bcd}\left(\mathbf{k}, \mathbf{k}_1, \mathbf{k}_2\right) u_c u_d \delta^0(\mathbf{k}_1)\delta^0(\mathbf{k}_2) \\ &= \int \mathrm{d}^3\mathbf{k}_1 \mathrm{d}^3\mathbf{k}_2\, \delta_D(\mathbf{k}+\mathbf{k}_1+\mathbf{k}_2) \begin{pmatrix} F_2(\mathbf{k}_1, \mathbf{k}_2) \\ G_2(\mathbf{k}_1, \mathbf{k}_2) \end{pmatrix} \delta^0(\mathbf{k}_1)\delta^0(\mathbf{k}_2) \end{aligned} \tag{3.24}$$

where I have introduced the integration kernels F_2 and G_2

$$\begin{aligned} F_2(\mathbf{k}_1, \mathbf{k}_2) &= \frac{5}{7} + \frac{1}{2}\frac{\mathbf{k}_1\cdot\mathbf{k}_2}{k_1 k_2}\left(\frac{k_1}{k_2} + \frac{k_2}{k_1}\right) + \frac{2}{7}\frac{(\mathbf{k}_1\cdot\mathbf{k}_2)^2}{k_1^2 k_2^2} \\ G_2(\mathbf{k}_1, \mathbf{k}_2) &= \frac{3}{7} + \frac{1}{2}\frac{\mathbf{k}_1\cdot\mathbf{k}_2}{k_1 k_2}\left(\frac{k_1}{k_2} + \frac{k_2}{k_1}\right) + \frac{4}{7}\frac{(\mathbf{k}_1\cdot\mathbf{k}_2)^2}{k_1^2 k_2^2} \end{aligned} \tag{3.25}$$

In general the nth order contribution to the perturbation series can be written in terms of the initial density perturbations and integration kernels F_n and G_n

$$\psi_a^{(n)}(\mathbf{k}) = \int \mathrm{d}^3\mathbf{k}_1 \cdots \mathrm{d}^3\mathbf{k}_n\, \delta_D(\mathbf{k} + \textstyle\sum \mathbf{k}_i) \begin{pmatrix} F_n(\mathbf{k}_1, \cdots, \mathbf{k}_n) \\ G_n(\mathbf{k}_1, \cdots, \mathbf{k}_n) \end{pmatrix} \delta^0(\mathbf{k}_1)\cdots\delta^0(\mathbf{k}_n) \tag{3.26}$$

where the integration kernels are given by a set of recursion relations that can be derived from equation (3.23) (see [9]).

The observable statistics (power spectrum, bispectrum etc.) at the time η can be calculated by taking ensemble averages of the field $\phi_a(\mathbf{k}, \eta)$. This gives a perturbative series for each statistic that can be expressed in terms of integrals over the initial statistics multiplied by the integration kernels F_n and G_n. The integrals quickly become too extensive to be calculated numerically putting a limit to how far standard perturbation theory can be explored.

With our definition of the two–component field in equation (3.3) the linear matter power spectrum $P_{11}^{\mathrm{L}}(k)$ will be constant in time because we have separated out the linear growth factor e^{η}. If the initial conditions are Gaussian the next contribution to the matter power spectrum will be two one–loop expressions

$$P_{11}^{1-\mathrm{loop}}(k, \eta) = P_{11}^{(2,2)}(k, \eta) + P_{11}^{(1,3)}(k, \eta) \tag{3.27}$$

given by

$$P_{11}^{(2,2)}(k,\eta) = e^{2\eta}\langle\psi_1^{(2)}(\mathbf{k})\psi_1^{(2)}(\mathbf{k}')\rangle = 2e^{2\eta}\int \mathrm{d}^3\mathbf{q}\ [F_2(\mathbf{k}-\mathbf{q},\mathbf{q})]^2\, P_{11}^L(|\mathbf{k}-\mathbf{q}|)P_{11}^L(q)$$
$$= \frac{2\pi k^3 e^{2\eta}}{98}\int_0^\infty \mathrm{d}r\ P_{11}^L(kr)\int_{-1}^1 \mathrm{d}x\ P_{11}^L\left(k\sqrt{1+r^2-2rx}\right)\frac{\left(3r+7x-10rx^2\right)^2}{\left(1+r^2-2rx\right)^2} \tag{3.28}$$

and

$$P_{11}^{(1,3)}(k,\eta) = e^{2\eta}\langle\psi_1^{(2)}(\mathbf{k})\psi_1^{(2)}(\mathbf{k}')\rangle = 6e^{2\eta}\int \mathrm{d}^3\mathbf{q}\ F_3(\mathbf{k},\mathbf{q},-\mathbf{q})P_{11}^L(k)P_{11}^L(q)$$
$$= \frac{2\pi k^3 e^{2\eta}}{252}P_{11}^L(k)\int_0^\infty \mathrm{d}r\ P_{11}^L(kr)\left(\frac{12}{r^2}-158+100r^2-42r^4\right.$$
$$\left.+\frac{3}{r^2}\left(1-r^2\right)^3\left(2+7r^2\right)\log\left|\frac{1-r}{1+r}\right|\right) \tag{3.29}$$

In Sections 3.10 and 3.9 we will recognize these two results as corrections to the self–energy Φ defined in equation (3.51) and the propagator respectively.

3.4 Path Integral Formulation

To apply the machinery of Chapter 2 to the cosmological dynamics presented in Section 3.1 we need to define an action that gives the equation of motion (3.4) at its extrema. To do this we will introduce an auxiliary doublet field χ_a making sure that the equation of motion obtained for this field is satisfied by $\chi_a = 0$. These requirements are met by the action

$$S[\phi_a,\chi_a] = \int \mathrm{d}\eta\ L(\phi_a,\partial_\eta\phi_a,\chi_a) = \int \mathrm{d}\eta\ \left[\chi_a(-\mathbf{k},\eta)(\delta_{ab}\partial_\eta+\Omega_{ab})\phi_b(\mathbf{k},\eta)\right.$$
$$\left.-e^\eta\gamma_{abc}(-\mathbf{k},-\mathbf{p},-\mathbf{q})\chi_a(\mathbf{k},\eta)\phi_b(\mathbf{p},\eta)\phi_c(\mathbf{q},\eta)\right] \tag{3.30}$$

Because the Lagrangian does not depend on the derivatives of χ_a the Euler–Lagrange equation obtained by varying S with respect to χ_a is simply $\frac{\partial L}{\partial\chi_a} = 0$ yielding equation (3.4) for the evolution of ϕ_a. The equation of motion for χ_a is obtained by varying S with respect to ϕ_a giving

$$\chi_a\left(\Omega_{ab}-2e^\eta\gamma_{abc}\phi_c\right) = \partial_\eta\left(\chi_a\delta_{ab}\right) = \partial_\eta\chi_b \tag{3.31}$$

which is satisfied by $\chi_a = 0$ as required. We can use equation (3.8) to make the substitution $\delta_{ab}\partial_\eta+\Omega_{ab}\to g_{ab}^{-1}$ in equation (3.30).

The density and velocity divergence fields of structure formation are classical fields so the evolution is completely determined by the equation of motion with no additional quantum fluctuations. The probability of ending up with a certain final field configuration given an initial field $\phi_a(0)$ will then be a delta function

$$P[\phi_a(\eta_f);\phi_a(0)] = \delta\left[\phi_a(\eta_f)-\bar{\phi}_a[\eta_f;\phi_a(0)]\right] = \int \mathcal{D}''\phi_a\mathcal{D}\chi_b e^{iS} \tag{3.32}$$

where $\bar{\phi}_a$ denotes the solution of the equation of motion at the final time η_f. The path integral representation is such that the integration over χ_b gives the delta function and the integration over ϕ_a fixes the initial and final field configurations.

Instead of specifying an initial field we will deal with a distribution of initial conditions and specify the statistical properties of this distribution. In the path integral formalism we will define a weight function W that specifies the initial statistics

$$\begin{aligned} W[\phi_a(0); C's] = \exp\Bigg(& -\frac{1}{2}\phi_a(\mathbf{k},0)C_{ab}(k)\phi_b(-\mathbf{k},0) \\ & -\frac{i}{6}C_{abc}\left(\mathbf{k}_1,\mathbf{k}_2,\mathbf{k}_3\right)\phi_a(\mathbf{k}_1,0)\phi_b(\mathbf{k}_2,0)\phi_c(\mathbf{k}_3,0)+\cdots\Bigg) \end{aligned} \tag{3.33}$$

so that the generating functional Z becomes

$$Z[J_a,K_b;C's] = \int \mathcal{D}\phi_a\mathcal{D}\chi_b\, W[\phi_a(0);C's]\exp\left(iS + i\int \mathrm{d}\eta\ \left(J_a\phi_a + K_b\chi_b\right)\right) \tag{3.34}$$

where we have added sources for both the ϕ_a– and χ_b–fields. The correlation functions C_i are related to the initial power spectrum, bispectrum and higher order statistics. Here I will go through the details using Gaussian initial conditions so that only the power spectrum is non–zero. The general case of initial non–Gaussianities has been treated in [43].

For Gaussian initial conditions only C_{ab} is non–zero and it is the inverse of the initial power spectrum so that the weight function will be given by

$$W[\phi_a(0);P^0_{ab}] = \exp\left(-\tfrac{1}{2}\phi_a(\mathbf{k},0)\left(P^0\right)^{-1}_{ab}(k)\phi_b(-\mathbf{k},0)\right) \tag{3.35}$$

where $P^0_{ab}(k) = w_a w_b P^0(k)$ is a matrix with the entries $P^0_{\delta\delta}$, $P^0_{\delta(\theta/\mathcal{H})}$, $P^0_{(\theta/\mathcal{H})\delta}$ and $P^0_{(\theta/\mathcal{H})(\theta/\mathcal{H})}$ and w_a is a combination of u_a and v_a giving the initial composition of growing and decaying modes. Choosing the growing mode only, $w_a = u_a = \binom{1}{1}$, and taking $P^0(k)$ as the matter power spectrum from the CAMB code at some initial redshift where everything is still linear corresponds to setting all four initial power spectra equal to the linear matter power spectrum at the initial time.

In this definition of the power spectrum we have not included the factor of $(2\pi)^3$ in equation (1.47) so when using the output power spectrum from CAMB as initial condition we will have to divide by this factor. Also we have to remember the factor of $e^{-\eta}$ in equation (3.3) when we compare our results with other approaches. Thus to get the properly normalized power spectra we will have to multiply our result with $e^{2\eta}$ because of the presence of ϕ^2 in the correlation functions.

Inserting (3.35) in (3.34) we get the generating functional Z with the free (linear) part Z_0 given by

$$\begin{aligned} Z_0[J_a,K_b;P^0] = \int \mathcal{D}\phi_a\mathcal{D}\chi_b \exp\Bigg(& -\frac{1}{2}\phi_a(\mathbf{k},0)\left(P^0\right)^{-1}_{ab}(k)\phi_b(-\mathbf{k},0) \\ & + i\int \mathrm{d}\eta_a\mathrm{d}\eta_b\ \chi_a(-\mathbf{k},\eta_a)g^{-1}_{ab}(\eta_a,\eta_b)\phi_b(\mathbf{k},\eta_b) \\ & + i\int \mathrm{d}\eta\ \left(J_a(\mathbf{k},\eta)\phi_a(\mathbf{k},\eta) + K_b(\mathbf{k},\eta)\chi_b(\mathbf{k},\eta)\right)\Bigg) \end{aligned} \tag{3.36}$$

The integration over χ_b will give a delta function in ϕ_a of the form

$$\delta_D\left(g_{ab}^{-1}\phi_b + K_a\right) \quad \Rightarrow \quad \left(\delta_{ab}\partial_\eta + \Omega_{ab}\right)\phi_b(\eta) = -K_a(\eta) \tag{3.37}$$

which is just the linear equation of motion sourced by K_a. The solution can be written in terms of the linearly evolved field ϕ_a^0 as

$$\tilde{\phi}_a(\eta_a) = \phi_a^0(\eta_a) - \int \mathrm{d}\eta_b \; g_{ab}(\eta_a, \eta_b) K_b(\eta_b) \tag{3.38}$$

Performing the integration over ϕ_a then yields

$$Z_0[J_a, K_b; P^0] = \int \mathrm{d}\phi_a(0) \; \exp\left(-\frac{1}{2}\phi_a(\mathbf{k}, 0)\left(P^0\right)_{ab}^{-1}(k)\phi_b(-\mathbf{k}, 0) + i\int \mathrm{d}\eta \; J_a\tilde{\phi}_a\right) \tag{3.39}$$

and finally the integration over the initial configuration $\phi_a(0)$ is just a Gaussian integration resulting in

$$\begin{aligned} Z_0[J_a, K_b; P^0] = \exp\Bigg(-\int \mathrm{d}\eta_a \mathrm{d}\eta_b \; \Bigg[& \frac{1}{2} J_a(\mathbf{k}, \eta_a) P_{ab}^{\mathrm{L}}(k; \eta_a, \eta_b) J_b(-\mathbf{k}, \eta_b) \\ & + i J_a(\mathbf{k}, \eta_a) g_{ab}(\eta_a, \eta_b) K_b(-\mathbf{k}, \eta_b) \Bigg] \Bigg) \end{aligned} \tag{3.40}$$

where we see that differentiating twice with respect to J gives the linearly evolved power spectrum, $P_{ab}^{\mathrm{L}}(k; \eta_a, \eta_b) = g_{ac}(\eta_a, 0) g_{bd}(\eta_b, 0) P_{cd}^0(k)$, and differentiating once with respect to J and once with respect to K gives the linear propagator. These two objects along with the vertex constitute the fundamental parts of the Feynman diagrams we will consider. They will be represented by the diagrams in figure 3.1, where solid lines represent ϕ and dashed lines represent χ.

We can rewrite the full generating functional Z following the procedure outlined in Section 2.2 where from equation (3.40) we see that

$$\Delta = \begin{pmatrix} iP_{ab}^L & -g_{ab} \\ -g_{ba} & 0 \end{pmatrix} \tag{3.41}$$

giving for the inverse

$$\Delta^{-1} = \begin{pmatrix} 0 & -g_{ba}^{-1} \\ -g_{ab}^{-1} & -i\delta(\eta_a)\delta(\eta_b)P_{ab}^0 \end{pmatrix} \tag{3.42}$$

and substituting this back into the full expression for Z gives

$$\begin{aligned} Z[J_a, K_b; P^0] = \int \mathcal{D}\phi_a \mathcal{D}\chi_b \exp\Bigg(& -\frac{1}{2}\int \mathrm{d}\eta_a \mathrm{d}\eta_b \; \chi_a P_{ab}^0 \delta(\eta_a)\delta(\eta_b)\chi_b \\ & + i\int \mathrm{d}\eta \left[\chi_a g_{ab}^{-1}\phi_b - e^\eta \gamma_{abc}\chi_a\phi_b\phi_c + J_a\phi_a + K_b\chi_b\right] \Bigg) \end{aligned} \tag{3.43}$$

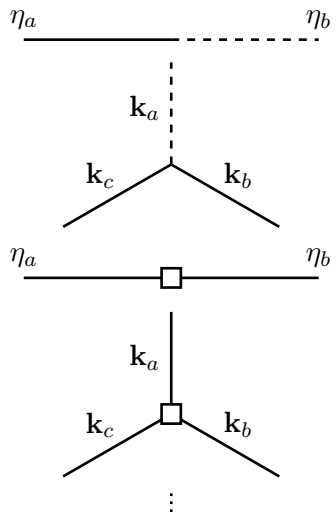

propagator: $-ig_{ab}(\eta_a, \eta_b)$

vertex: $-ie^{\eta}\gamma_{abc}(\mathbf{k}_a, \mathbf{k}_b, \mathbf{k}_c)$

power spectrum: $P^{\rm L}_{ab}(k; \eta_a, \eta_b)$

bispectrum: $B^{\rm L}_{abc}(\mathbf{k}_a, \mathbf{k}_b, \mathbf{k}_c; \eta_a, \eta_b, \eta_c)$

Figure 3.1: Fundamental building blocks of Feynman diagrams. The dashed lines represent the χ–field while the solid lines represent the ϕ–field. Time flows right to left in the propagator and the dots represent the series of higher order statistics.

We can also use functional derivatives to derive the full expression for Z from Z_0

$$Z\left[J_a, K_b; P^0\right] = \exp\left[-i\int \mathrm{d}\eta\; e^{\eta}\gamma_{abc}\left(\frac{-i\delta}{\delta K_a}\frac{-i\delta}{\delta J_b}\frac{-i\delta}{\delta J_c}\right)\right] Z_0\left[J_a, K_b; P^0\right] \tag{3.44}$$

This relation highlights the connection to perturbation theory where the interactions are taken into account order by order by expanding the exponential.

In [43] it has been shown that in the presence of initial non–Gaussianities the main results of this section (equations (3.40) and (3.43)) take the same form with equation (3.40) replaced by

$$\begin{aligned} Z_0[J_a, K_b; P^0, B^0, \cdots] = \exp\Bigg(&-\frac{1}{2}\int \mathrm{d}\eta_a \mathrm{d}\eta_b\; J_a(\mathbf{k}, \eta_a) P^{\rm L}_{ab}(k; \eta_a, \eta_b) J_b(-\mathbf{k}, \eta_b) \\ &-\frac{i}{6}\int \mathrm{d}\eta_a \mathrm{d}\eta_b \mathrm{d}\eta_c\; B^{\rm L}_{abc}(\mathbf{k}_1, \mathbf{k}_2, \mathbf{k}_3; \eta_a, \eta_b, \eta_c) J_a(\mathbf{k}_1, \eta_a) J_b(\mathbf{k}_2, \eta_b) J_c(\mathbf{k}_3, \eta_c) \\ &+ [T^{\rm L}] + \cdots - i\int \mathrm{d}\eta_a \mathrm{d}\eta_b\; J_a(\mathbf{k}, \eta_a) g_{ab}(\eta_a, \eta_b) K_b(-\mathbf{k}, \eta_b)\Bigg) \end{aligned} \tag{3.45}$$

where $B^{\rm L}_{abc}$ is the linearly evolved bispectrum, $[T^{\rm L}]$ represents a similar term with the linearly evolved trispectrum and the dots represent terms from higher order statistics. Equation (3.45) shows that differentiating Z_0 n times with respect to the source J_a will give

$$\frac{(-i)^n}{Z_0}\left.\frac{\delta^n Z_0}{\delta J_1(\mathbf{k}_1, \eta_1)\cdots\delta J_n(\mathbf{k}_n, \eta_n)}\right|_{J_a, K_b = 0} = \delta_D\left(\sum \mathbf{k}_i\right) S^{\rm L}_{a_1\cdots a_n}(\mathbf{k}_1, \cdots, \mathbf{k}_n; \eta_1, \cdots, \eta_n) \tag{3.46}$$

where $S^{\rm L}_{a_1\cdots a_n}$ represents the n'th order statistic linearly evolved in time. The linearly evolved statistics will constitute additional fundamental building blocks in the Feynman diagrams and will be represented by a box with the appropriate number of legs as shown in figure 3.1.

In equation (3.43) we can replace the first term in the exponential function by the infinite series

$$\begin{aligned}&-\frac{1}{2}\chi_a(\mathbf{k},0)P^0_{ab}(k)\chi_b(\mathbf{k},0)-\frac{i}{6}B^0_{abc}(\mathbf{k}_1,\mathbf{k}_2,\mathbf{k}_3)\chi_a(\mathbf{k}_1,0)\chi_b(\mathbf{k}_2,0)\chi_c(\mathbf{k}_3,0)\\&+\frac{1}{24}T^0_{abcd}(\mathbf{k}_1,\mathbf{k}_2,\mathbf{k}_3,\mathbf{k}_4)\chi_a(\mathbf{k}_1,0)\chi_b(\mathbf{k}_2,0)\chi_c(\mathbf{k}_3,0)\chi_d(\mathbf{k}_4,0)+\cdots\end{aligned} \tag{3.47}$$

including the initial bispectrum B^0_{abc}, trispectrum T^0_{abcd} and higher order statistics, all coupled to the χ–field. The fact that the initial statistics are coupled directly to the χ–field only tells us that the auxiliary field plays a crucial role in connecting the evolved ϕ–fields, $\phi(\eta)$, to the initial conditions.

Having defined all the fundamental building blocks of the Feynman diagrams we can in principle build all the non–linear results by taking the loop corrections into account order by order. Instead we will use the formalism of generating functionals to define resummed propagators and vertices that include loop corrections to all orders in perturbation theory.

3.5 Generating Functionals

We now define the generating functionals of connected diagrams W and one–particle irreducible (1PI) diagrams Γ as in Section 2.2

$$W[J_a,K_b]=-i\log Z[J_a,K_b] \tag{3.48}$$

and

$$\Gamma[\phi_a,\chi_b]=W[J_a,K_b]-\int \mathrm{d}\eta\mathrm{d}^3\mathbf{k}\,(J_a\phi_a+K_b\chi_b) \tag{3.49}$$

We will not distinguish between the fields ϕ_a and χ_b and their classical expectation values $\phi_{a,\rm cl}=\langle\phi_a\rangle$ and $\chi_{b,\rm cl}=\langle\chi_b\rangle$ in the presence of the sources. We only note that the physical situation with $J_a=K_b=0$ corresponds to $\phi_{a,\rm cl}=\chi_{b,\rm cl}=0$ because we are dealing with fluctuations away from the average of the density and velocity fields. As in Chapter 2 the classical fields in the presence of the sources are given by

$$\phi_a[J_a,K_b]=\frac{\delta W[J_a,K_b]}{\delta J_a}\quad,\quad \chi_b[J_a,K_b]=\frac{\delta W[J_a,K_b]}{\delta K_b} \tag{3.50}$$

The 1PI diagrams correspond to full vertices with any number of legs coming in from the right and going out to the left corresponding to differentiations of Γ with respect to ϕ and χ respectively[1] (see Section 3.6). The derivatives are always taken at $\langle\phi_a\rangle=\langle\chi_a\rangle=0$ to recover the physical situation. One can realize by considering the corresponding 1PI Feynman

[1]Notice the difference in notation as compared to [44] and [45] where Γ represents multi–point propagators.

diagrams that derivatives of Γ with respect to ϕ_a only, i.e. diagrams where every external line represents a ϕ–field, will vanish due to a closed loop of propagators. The second derivatives of Γ can then be written as

$$\begin{aligned}
\Gamma^{(2)}_{\phi_a\phi_b}(k;\eta_a,\eta_b) &= 0 \\
\Gamma^{(2)}_{\phi_a\chi_b}(k;\eta_a,\eta_b) &= g^{-1}_{ba}(\eta_a,\eta_b) - \Sigma_{\phi_a\chi_b}(k;\eta_a,\eta_b) \\
\Gamma^{(2)}_{\chi_a\phi_b}(k;\eta_a,\eta_b) &= g^{-1}_{ab}(\eta_a,\eta_b) - \Sigma_{\chi_a\phi_b}(k;\eta_a,\eta_b) \\
\Gamma^{(2)}_{\chi_a\chi_b}(k;\eta_a,\eta_b) &= iP^0_{ab}(k)\delta(\eta_a)\delta(\eta_b) + i\Phi_{ab}(k;\eta_a,\eta_b)
\end{aligned} \tag{3.51}$$

where the linear part can be read off of equation (3.43) and the Φ and Σ terms are the self–energies arising from non–linear interactions. The notation $\Gamma^{(2)}_{\phi_a\phi_b}$ represents the derivatives taken at $\phi_a = \chi_b = 0$ and includes a delta function in the momenta

$$\delta_D(\mathbf{k}+\mathbf{k}')\Gamma^{(2)}_{\phi_a\phi_b}(k;\eta_a,\eta_b) = \left.\frac{\delta^2\Gamma[\phi_a,\chi_b]}{\delta\phi_a(\mathbf{k},\eta_a)\delta\phi_b(\mathbf{k}',\eta_b)}\right|_{\phi_a,\chi_b=0} \tag{3.52}$$

Along the same lines as in equation (3.51) the full power spectrum and propagator can be defined in terms of the second derivatives of W with respect to the sources J and K

$$\begin{aligned}
W^{(2)}_{J_aJ_b}(\mathbf{k},\eta_a;\mathbf{k}',\eta_b) &= i\delta_D(\mathbf{k}+\mathbf{k}')P_{ab}(k;\eta_a,\eta_b) \\
W^{(2)}_{J_aK_b}(\mathbf{k},\eta_a;\mathbf{k}',\eta_b) &= -\delta_D(\mathbf{k}+\mathbf{k}')G_{ab}(k;\eta_a,\eta_b) \\
W^{(2)}_{K_aJ_b}(\mathbf{k},\eta_a;\mathbf{k}',\eta_b) &= -\delta_D(\mathbf{k}+\mathbf{k}')G_{ba}(k;\eta_a,\eta_b) \\
W^{(2)}_{K_aK_b}(\mathbf{k},\eta_a;\mathbf{k}',\eta_b) &= 0
\end{aligned} \tag{3.53}$$

The notation $W^{(2)}_{J_aJ_b}$ represents the derivatives taken at $J_a = K_b = 0$. The component $W^{(2)}_{K_aK_b}$ being zero is a consequence of the fact that the two sets of second derivatives in equations (3.51) and (3.53) constitute inverse matrices of each other. This can also be used to express the power spectrum as a sum of two contributions

$$P_{ab} = P^{\mathrm{I}}_{ab} + P^{\mathrm{II}}_{ab} \tag{3.54}$$

given by

$$\begin{aligned}
P^{\mathrm{I}}_{ab}(k;\eta_a,\eta_b) &= G_{ac}(k;\eta_a,0)G_{bd}(k;\eta_b,0)P^0_{cd}(k) \\
P^{\mathrm{II}}_{ab}(k;\eta_a,\eta_b) &= \int_0^{\eta_a} ds_1 \int_0^{\eta_b} ds_2\, G_{ac}(k;\eta_a,s_1)G_{bd}(k;\eta_b,s_2)\Phi_{cd}(k;s_1,s_2)
\end{aligned} \tag{3.55}$$

where P^{I} is the equivalent of the linearly evolved power spectrum using the full propagator, and P^{II} represents a new contribution from the interactions between the Fourier modes. It is clear from equation (3.55) that the full propagator and the self–energy Φ are key objects in this approach. Diagrammatically we will represent the full propagator with thick lines and Φ with a circle with two external χ–legs.

The full propagator, power spectrum and 1PI n–point functions appearing in equations (3.51) and (3.53) represent a generalization of the corresponding linear quantities in the sense that they include all loop corrections to the given quantity. Diagrammatically the full propagator can be written as

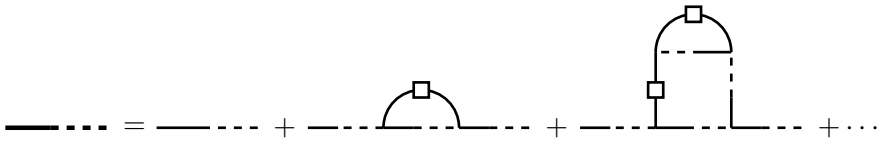

(3.56)

where the dots indicate all remaining two–loop diagrams and higher order loop contributions. With non–Gaussian initial conditions there will also be loop diagrams involving the higher order initial statistics. A Feynman diagram drawn with the full quantities will represent an infinite sum of diagrams in standard perturbation theory. The resummed quantities have been exploited in [27] and [28] to build a renormalized perturbation theory of cosmological structure formation.

The full bispectrum, trispectrum and higher order statistics can be obtained by taking higher order derivatives of W with respect to J, differentiating thrice for the bispectrum, four times for the trispectrum and so on.

3.6 Vertices

Similar to equation (3.51) we can identify the full vertex with derivatives of Γ

$$\begin{aligned}\Gamma^{(3)}_{\chi_a\phi_b\phi_c}(\mathbf{k},&s_1;-\mathbf{q},s_2;-\mathbf{k}+\mathbf{q},s_3)\\ &=-2\delta(s_1-s)\delta(s_2-s)\delta(s_3-s)e^s\gamma_{abc}(\mathbf{k},-\mathbf{q},-\mathbf{k}+\mathbf{q})\\ &\quad+\text{loop corrections}\end{aligned} \tag{3.57}$$

The factor of 2 comes from the ϕ^2 in equation (3.43) and the delta functions account for the fact that the tree level vertex is instantaneous, i.e. it has no time dependence. The full vertex will be represented by a filled circle in the Feynman diagrams so that the diagrammatic version of equation (3.57) reads

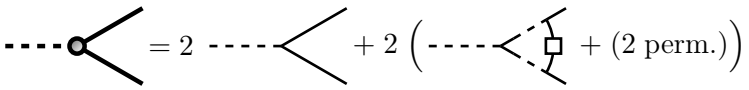

(3.58)

where I have suppressed the delta functions in the first term.

As mentioned in Section 3.5 this definition can be generalized to higher order vertices with any number of legs coming in from the right and going out to the left

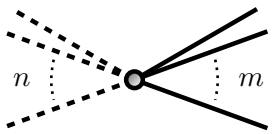

(3.59)

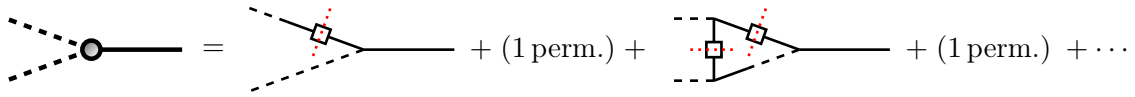

Figure 3.2: Decomposing a generalized vertex into n–point propagators. The red dotted lines indicate that the initial statistics work as couplings between individual vertices with just one outgoing χ–leg as described in the text.

with the constraint that the sum over momenta on each side must be equal and opposite, $\mathbf{k} = -\sum_{i=1}^{m} \mathbf{k}_i = \sum_{i=1}^{n} \mathbf{p}_i$. The vertices defined in this way express how a number of Fourier modes can interact and combine to create power on different scales than before. This is entirely a non–linear effect as the linear evolution will preserve the initial statistics.

Vertices with just one outgoing leg on the left side are the basis of the n–point propagators introduced by [44]. Their tree level expressions can be constructed using only the tree level vertex and the linear propagator, i.e. with no couplings to the initial conditions. On the other hand constructing diagrams with more than one outgoing leg requires the use of this kind of couplings. By considering the possible diagrams one can realize that in fact they are constructed by gluing together a number of vertices with just one outgoing leg by coupling them to the initial statistics. See figure 3.2 for an example.

The vertices constructed in this way are not fundamental objects in the renormalized perturbation theory of [44], but in the RG approach we will see that all the possible 1PI vertices will in principle play a role, so it is relevant to gain some insight into the general behaviour of these objects as well. Before turning to the RG approach I will clarify the connection between the formalism and notation presented here and that of [44] and [45].

3.7 From Vertices to Multi–Point Propagators

To get from the 1PI diagrams in Section 3.6 to the multi–point propagators equivalent to those in [44] we need to attach propagators to all the legs of the vertices so that the resulting diagrams describe how the initial Fourier modes at a time η_b evolve and affect each combination of Fourier modes at a later time η_a

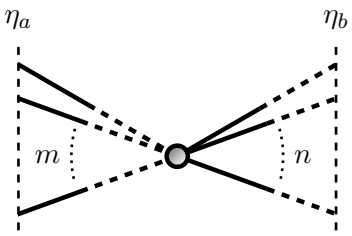

(3.60)

We will denote the multi–point propagators as $V^{(n,m)}_{a_1 \cdots a_m b_1 \cdots b_n}$ with n being the number of incoming legs and m the number of outgoing legs as shown in the diagram above. As an

example the formal expression for $V^{(2,1)}_{abc}$ in terms of full propagators and vertices will be

$$V^{(2,1)}_{abc}(\mathbf{k}_a,\eta_a;\mathbf{k}_b,\mathbf{k}_c,\eta_b) = \int_{\eta_b}^{\eta_a} \mathrm{d}s_1\mathrm{d}s_2\mathrm{d}s_3\; G_{ad}(k_a;\eta_a,s_1)\cdot \\ \Gamma^{(3)}_{\chi_d\phi_e\phi_f}(\mathbf{k}_a,s_1;\mathbf{k}_b,s_2;\mathbf{k}_c,s_3)G_{eb}(k_b;s_2,\eta_b)G_{fc}(k_c;s_3,\eta_b) \tag{3.61}$$

with the implicit requirement that $\mathbf{k}_a = -\mathbf{k}_b - \mathbf{k}_c$. In my work I will distinguish between n–point propagators that have $m = 1$ and multi–point propagators that have $m > 1$. This is in contrast to [44] and [45] where they only deal with the $m = 1$ case and the two terms are used interchangeably.

The n–point propagator $V^{(2,1)}_{abc}$ in this work is the equivalent of the three–point propagator $\Gamma^{(2)}_{abc}$ of [44]. Apart from the differences that arise due to the extra factor of $e^{-\eta}$ in equation (3.3) compared to the two–component field of [44], the two propagators describe the same overall evolution. Naturally this equivalence holds between all the n–point propagators $\Gamma^{(n-1)}$ of [44] and the corresponding $V^{(n-1,1)}$ of this work. It was shown in [44] for Gaussian initial conditions and in [45] for general initial conditions that the n–point propagators are connected to the integration kernels of equation (3.26) in such a way that the observable statistics at later times can be constructed directly from the n–point propagators. This is done in the same way as the vertices in Section 3.6 with more than one outgoing leg are constructed by gluing together n–point propagators via couplings to the initial statistics. A few of the contributions to the power spectrum will be

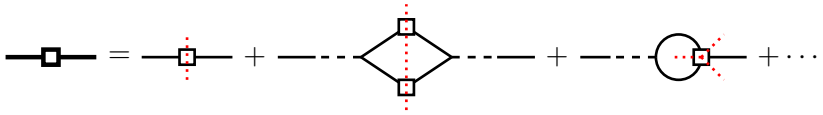

(3.62)

where the red dotted lines again indicate where the diagrams can be split into separate n–point propagators. It is clear from this direct approach where all the observables can be constructed from the n–point propagators, that there is no need to consider the multi–point propagators with $m > 1$ in their framework. As described in Section 3.6 this is not the case in our resummation scheme, so we will also consider the new class of multi–point propagators $V^{(n,m)}$ with $m > 1$.

We will conclude this section by studying the tree level expression for $V^{(2,1)}_{abc}$. The tree level version of equation (3.61) is obtained by replacing the full propagators with the linear ones and by use of the first term on the right hand side of equation (3.57)

$$V^{(2,1)}_{abc,\,\mathrm{tree}}(\mathbf{k},\eta_a;\mathbf{k}_1,\mathbf{k}_2,\eta_b) = -2\int_{\eta_b}^{\eta_a} \mathrm{d}s\; e^s g_{ad}(\eta_a,s)\gamma_{def}(\mathbf{k},\mathbf{k}_1,\mathbf{k}_2)g_{eb}(s,\eta_b)g_{fc}(s,\eta_b) \tag{3.63}$$

The factor of 2 expresses the two possible ways of contracting the vertex with the two last propagators and the overall minus sign is due to the sign convention adopted in equation (3.43).

To compare with [44] we will compute the component with $a = 1$ and growing mode initial conditions

$$V^{(2,1)}_{1bc,\,\mathrm{tree}}(\mathbf{k},\eta_a;\mathbf{k}_1,\mathbf{k}_2,\eta_b)u_b u_c = -2\Bigg[e^{\eta_a}\left(\frac{5}{7}+\frac{k_1 x}{2k_2}+\frac{k_2 x}{2k_1}+\frac{2x^2}{7}\right) \\ -e^{\eta_b}\left(\frac{3}{5}+\frac{k_1 x}{2k_2}+\frac{k_2 x}{2k_1}+\frac{2x^2}{5}\right)+e^{1/2(7\eta_b-5\eta_a)}\left(-\frac{4}{35}+\frac{4x^2}{35}\right)\Bigg] \tag{3.64}$$

where $x = (\mathbf{k}_1\cdot\mathbf{k}_2)/(k_1k_2)$. We see that setting η_b to zero and multiplying by a factor e^{η_a} will reproduce the tree level expression of [44] apart from the overall factor of -2 as expected.

3.8 Introducing a Cut–Off

To generate the renormalization group differential equations we need to introduce a cut–off that allows only the low–order loop corrections to contribute. A natural place to do this in the theory of structure formation is in the initial statistics. An initial power spectrum equal to zero for all k–values will correspond to a completely homogeneous universe where no structures will form, while raising the cut–off a little bit to include fluctuations at small k–values (or large scales) will correspond to a universe where all the initial fluctuations evolve linearly. Raising the cut–off further we begin to include smaller scales that will enter the weakly non–linear regime when they evolve with time. Thus a cut–off in the initial statistics will allow us to gradually include non–linearities in our theory as we let the cut–off go to infinity.

As in [33] we will use a step function to modify the initial conditions

$$\begin{aligned} P^0(k) &\to P^0_\lambda(k) = P^0(k)\theta_{\mathrm{H}}(\lambda-k) \\ B^0(\mathbf{k}_1,\mathbf{k}_2,\mathbf{k}_3) &\to B^0_\lambda(\mathbf{k}_1,\mathbf{k}_2,\mathbf{k}_3) = B^0(\mathbf{k}_1,\mathbf{k}_2,\mathbf{k}_3)\theta_{\mathrm{H}}(\lambda-(k_1+k_2+k_3)) \\ &\vdots \end{aligned} \tag{3.65}$$

The step function, θ_{H}, equals unity for $k < \lambda$ and zero for $k > \lambda$. For the higher order statistics there are no unique way to introduce the cut–off. Here I have used the sum of the magnitude of the wavenumbers to define the cut–off scale. Another possibility could be to use $\max\{k_i\}$. The choice of cut–off scale will affect the behaviour at low λ values, but as we take the limit $\lambda \to \infty$ there should be no difference between the choices.

Replacing the initial statistics with the λ–dependent ones in the generating functionals and differentiating with respect to λ will create the differential equations we are interested in. These can then be integrated from $\lambda = 0$ to $\lambda \to \infty$ to regain the full dynamics encoded in the initial conditions. We will denote the λ–dependent quantities by a lower case λ as in equation (3.65).

Because the cut–off appears only in connection with the initial statistics it is easy to calculate the λ–derivative of $Z_\lambda = Z[J_a, K_b; P^0_\lambda, B^0_\lambda, \cdots]$. Starting from equations (3.43) and

(3.47) in the presence of initial non–Gaussianities the result is

$$\begin{aligned}
\partial_\lambda Z_\lambda = &\int \mathcal{D}\phi_a \mathcal{D}\chi_b \, \exp(\cdots) \Bigg[-\frac{1}{2} \int \mathrm{d}\eta_{a,b} \mathrm{d}^3\mathbf{q} \; \delta(\eta_a)\delta(\eta_b)\chi_a\chi_b\delta(\lambda - q) P^0_{ab}(q) \\
&- \frac{i}{6} \int \mathrm{d}\eta_{a,b,c} \mathrm{d}^3\mathbf{q}_{1,2,3} \; \delta(\eta_a)\delta(\eta_b)\delta(\eta_c)\chi_a\chi_b\chi_c \, \delta\big(\lambda - \textstyle\sum q_i\big) B^0_{abc}(\mathbf{q}_1, \mathbf{q}_2, \mathbf{q}_3) \\
&+ \{T^0\} + \cdots \Bigg] \\
= &\frac{1}{2} \int \mathrm{d}\eta_{a,b} \mathrm{d}^3\mathbf{q} \; \delta(\lambda - q) P^0_{ab}(q) \delta(\eta_a)\delta(\eta_b) \frac{\delta^2 Z_\lambda}{\delta K_a \delta K_b} \\
&+ \frac{1}{6} \int \mathrm{d}\eta_{a,b,c} \mathrm{d}^3\mathbf{q}_{1,2,3} \; \delta\big(\lambda - \textstyle\sum q_i\big) B^0_{abc}(\mathbf{q}_1, \mathbf{q}_2, \mathbf{q}_3) \delta(\eta_a)\delta(\eta_b)\delta(\eta_c) \frac{\delta^3 Z_\lambda}{\delta K_a \delta K_b \delta K_c} \\
&+ \{T^0\} + \cdots
\end{aligned} \tag{3.66}$$

where we have introduced the compact notation $\mathrm{d}\eta_{a,b} = \mathrm{d}\eta_a \mathrm{d}\eta_b$ and $\mathrm{d}^3\mathbf{q}_{1,2,3} = \mathrm{d}^3\mathbf{q}_1 \mathrm{d}^3\mathbf{q}_2 \mathrm{d}^3\mathbf{q}_3$ and the argument of the exponential function in the first line can be read off of equations (3.43) and (3.47).

The RG equation for W can be obtained by taking the λ derivative of equation (3.48)

$$\partial_\lambda W_\lambda = -i \tfrac{1}{Z_\lambda} \partial_\lambda Z_\lambda \tag{3.67}$$

and combining with equation (3.66). The functional derivatives of Z_λ with respect to the source field K can be translated into functional derivatives of W_λ by use of the identities

$$\begin{aligned}
\frac{\delta^2 W_\lambda}{\delta K_a \delta K_b} = &- i \frac{1}{Z_\lambda} \frac{\delta^2 Z_\lambda}{\delta K_a \delta K_b} + i \frac{1}{Z_\lambda} \frac{\delta Z_\lambda}{\delta K_a} \frac{1}{Z_\lambda} \frac{\delta Z_\lambda}{\delta K_b} = -i \frac{1}{Z_\lambda} \frac{\delta^2 Z_\lambda}{\delta K_a \delta K_b} - i \chi_a \chi_b \\
\frac{\delta^3 W_\lambda}{\delta K_a \delta K_b \delta K_c} = &- i \frac{1}{Z_\lambda} \frac{\delta^3 Z_\lambda}{\delta K_a \delta K_b \delta K_c} + \chi_a\chi_b\chi_c \\
&- i \left(\chi_a \frac{\delta^2 W_\lambda}{\delta K_b \delta K_c} + \chi_b \frac{\delta^2 W_\lambda}{\delta K_a \delta K_c} + \chi_c \frac{\delta^2 W_\lambda}{\delta K_a \delta K_b} \right) \\
&\vdots
\end{aligned} \tag{3.68}$$

where we have used equation (3.50) to rewrite single derivatives of W with respect to K in terms of the χ–field. The terms that appear on the right hand side of the identities after the first term will be every combination of χ–fields and functional derivatives of W_λ of order 2 or higher that corresponds to the same number of differentiations as on the left hand side. The coefficient of the first term will always be $-i$ while the coefficients of the following terms are determined by an overall factor of i multiplied by an i for each χ field and each W_λ appearing

in the term. The end result for the RG equation for W_λ is

$$\begin{aligned}\partial_\lambda W_\lambda = &\frac{1}{2}\int \mathrm{d}\eta_{a,b}\mathrm{d}^3\mathbf{q}\;\delta(\lambda-q)P^0_{ab}(q)\delta(\eta_a)\delta(\eta_b)\left(i\chi_a\chi_b+\frac{\delta^2 W_\lambda}{\delta K_b\delta K_a}\right)\\ &+\frac{1}{6}\int \mathrm{d}\eta_{a,b,c}\mathrm{d}^3\mathbf{q}_{1,2,3}\;\delta\big(\lambda-\textstyle\sum q_i\big)B^0_{abc}(\mathbf{q}_1,\mathbf{q}_2,\mathbf{q}_3)\delta(\eta_a)\delta(\eta_b)\delta(\eta_c)\\ &\times\left(-\chi_a\chi_b\chi_c+i\left(\chi_a\frac{\delta^2 W_\lambda}{\delta K_b\delta K_c}+\chi_b\frac{\delta^2 W_\lambda}{\delta K_a\delta K_c}+\chi_c\frac{\delta^2 W_\lambda}{\delta K_a\delta K_b}\right)+\frac{\delta^3 W_\lambda}{\delta K_a\delta K_b\delta K_c}\right)\\ &+\{T^0\}+\cdots\end{aligned} \tag{3.69}$$

The main points to be drawn from this expression is that exactly one initial spectrum appears in each term on the right hand side and that all the functional derivatives of W_λ are with respect to K and not J. This last point ensures that the functional derivatives will not generate more couplings to the initial statistics than the ones already explicitly present in equation (3.69).

From equation (3.49) we see that $\partial_\lambda\Gamma_\lambda = \partial_\lambda W_\lambda$, so the RG equation for Γ_λ will be similar to equation (3.69) and we can use that equation to generate RG equations for any object of interest in the theory. We have not yet set the sources to zero to recover the physical situation so we keep all the terms in the parentheses on the right hand side even though they will vanish in the physical limit. For the rest of this chapter I will work with Gaussian initial conditions so that only the first line of equation (3.69) contributes.

3.9 The Full Propagator

The RG equation for the two–point propagator is obtained through the definition of G_{ab} in equation (3.53)

$$\begin{aligned}\partial_\lambda G_{ab,\lambda}(k,\eta_a,\eta_b) &= -\left.\frac{\delta^2(\partial_\lambda W_\lambda)}{\delta J_a(\mathbf{k},\eta_a)\delta K_b(-\mathbf{k},\eta_b)}\right|_{J_a,K_b=0}\\ &= -\frac{1}{2}\int \mathrm{d}\eta_c\mathrm{d}\eta_d\mathrm{d}^3\mathbf{q}\;\delta(\lambda-q)P^0_{cd}(q)\delta(\eta_c)\delta(\eta_d)W^{(4)}_{J_aK_bK_cK_d,\lambda}\end{aligned} \tag{3.70}$$

where the sources have now been set to zero. Performing the differentiations on W the result can be written in terms of full vertices and propagators

$$\begin{aligned}&W^{(4)}{}_{J_aK_bK_cK_d,\lambda}(\mathbf{k},\eta_a;-\mathbf{k},\eta_b;\mathbf{q},\eta_c;-\mathbf{q},\eta_d)\\ &=\int \mathrm{d}s_1\cdots\mathrm{d}s_4\;G_{ae,\lambda}(k;\eta_a,s_1)\,G_{fb,\lambda}(k;s_2,\eta_b)G_{gc,\lambda}(q;s_3,\eta_c)G_{hd,\lambda}(q;s_4,\eta_d)\\ &\quad\cdot\left[\Gamma^{(4)}_{\chi_e\phi_f\phi_g\phi_h,\lambda}(\mathbf{k},s_1;-\mathbf{k},s_2;\mathbf{q},s_3;-\mathbf{q},s_4)-2\int \mathrm{d}s_5\mathrm{d}s_6\;G_{li,\lambda}(|\mathbf{k}-\mathbf{q}|\,;s_5,s_6)\right.\\ &\quad\left.\cdot\;\Gamma^{(3)}_{\chi_e\phi_h\phi_l,\lambda}(\mathbf{k},s_1;-\mathbf{q},s_4;-\mathbf{k}+\mathbf{q},s_5)\Gamma^{(3)}_{\chi_i\phi_g\phi_f,\lambda}(\mathbf{k}-\mathbf{q},s_6;\mathbf{q},s_3;-\mathbf{k},s_2)\right]\end{aligned} \tag{3.71}$$

where the momentum and time dependence has been written out explicitly for clarity.

The combination $G_{gc,\lambda}(q;s_3,0)G_{hd,\lambda}(q;s_4,0)P^0_{cd}(q)\delta(\lambda-q)$ will arise naturally as the integration kernel in all RG equations. It is the λ–derivative of the $P^{\rm I}_{ab,\lambda}$ contribution to the full power spectrum in equation (3.55) taken by considering only the explicit λ–dependence in P^0_λ, so we will give it a diagrammatical representation as a crossed square with two legs. With this addition to the Feynman rules equation (3.70) has the diagrammatical form

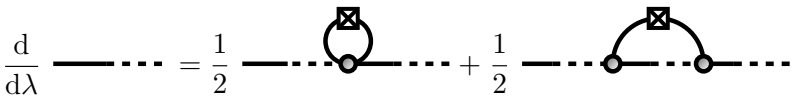

(3.72)

This equation represents a general rule for constructing RG equations in the case of Gaussian initial conditions, where only one–loop diagrams are present on the right hand side. This simple recipe arises from the fact mentioned in Section 3.8 that only one initial power spectrum appears on the right hand side of equation (3.69) and loops can only be constructed by use of couplings to the initial statistics.

The general rules as set up by [33] for generating the right hand side of the RG equation for a given quantity in the Gaussian case are

- Draw all one–loop corrections to the quantity using the full λ–dependent propagators, power spectra and vertices.

- Perform the λ–differentiation of the full expressions by considering only the explicit λ–dependence appearing in the $\theta_{\rm H}$ function of P^0_λ.

The RG equations constructed in this way represent exact differential equations for the full evolution of the quantity with λ including all loop corrections. As seen in equation (3.71) the evolution of the two–point propagator depends on the full λ dependent three–point and four–point vertices. These will in turn depend on higher order vertices creating a hierarchy of RG equations that will have to be truncated at some level to be solved. The obvious starting point will be to keep only the tree level expression for the vertex so that equation (3.70) is not coupled to the higher order equations. Integration of the RG equations will then include loop corrections to the propagator and power spectrum but not to the vertices. In the following subsections I will present the results obtained in this limit in [33].

3.9.1 One–loop results

Standard one–loop perturbation theory corresponds to keeping all quantities in equation (3.71) at tree level and integrating equation (3.70) from $\lambda=0$ to ∞. The tree level expression for the 1PI three–point function is the first term of equation (3.57) while the 1PI four–point function is zero in this approximation. The only dependence on λ remaining on the right hand side is

the delta function $\delta(\lambda - q)$, so the integration can easily be performed yielding

$$\begin{aligned} G^{\text{1–loop}}_{ab,\lambda\to\infty}(k;\eta_a,\eta_b) - G_{ab,\lambda=0}(k;\eta_a,\eta_b) &= G^{\text{1–loop}}_{ab}(k;\eta_a,\eta_b) - g_{ab}(\eta_a,\eta_b) \\ &= -\frac{1}{2}\int_0^\infty \mathrm{d}\lambda \int \mathrm{d}\eta_c \mathrm{d}\eta_d \mathrm{d}^3\mathbf{q}\ \delta(\lambda - q) P^0_{cd}(q)\delta(\eta_c)\delta(\eta_d) W^{(4),\text{1–loop}}_{J_a K_b K_c K_d} \\ &= 4\int \mathrm{d}s_1 \mathrm{d}s_2 \mathrm{d}^3\mathbf{q}\ e^{s_1+s_2} g_{ae}(\eta_a,s_1)\gamma_{ehl}(\mathbf{k},-\mathbf{q},-\mathbf{k}+\mathbf{q}) g_{hd}(s_1,0) \\ &\quad \times g_{gc}(s_2,0) P^0_{cd}(q) g_{li}(s_1,s_2)\gamma_{igf}(\mathbf{k}-\mathbf{q},\mathbf{q},-\mathbf{k}) g_{fb}(s_2,\eta_b) \end{aligned} \tag{3.73}$$

The final result is often expressed separately for the density propagator G_1 and the velocity propagator G_2 defined through $G_a = G_{ab}u_b = G_{a1} + G_{a2}$. With growing mode initial conditions, $P^0_{cd} = u_c u_d P^0$, the P^{I} contribution to the final power spectrum is given by $P^{\text{I}}_{ab} = G_a G_b P^0$ so that G_1 and G_2 contain the evolution of the density perturbations and velocity divergence, respectively. When contracting equation (3.73) with u_b, the linear propagator reduces to $g_{ab}u_b = u_a$, giving

$$\begin{aligned} G^{\text{1–loop}}_a = u_a + 4\int_{\eta_b}^{\eta_a} \mathrm{d}s_1 \int_{\eta_b}^{s_1} \mathrm{d}s_2 \int \mathrm{d}^3\mathbf{q}\ e^{s_1+s_2} P^0(q) g_{ae}(\eta_a,s_1)\gamma_{ehl}(\mathbf{k},-\mathbf{q},-\mathbf{k}+\mathbf{q}) u_h \\ \times\, g_{li}(s_1,s_2)\gamma_{igf}(\mathbf{k}-\mathbf{q},\mathbf{q},-\mathbf{k}) u_g u_f \end{aligned} \tag{3.74}$$

Standard perturbation theory follows only the dominant time dependence which in equation (3.74) corresponds to letting $\eta_b \to -\infty$. Performing the integrations over times and angles in this limit gives the final results

$$G^{\text{1–loop}}_a = u_a - 2\pi k^2 e^{2\eta} \int \mathrm{d}q\ P^0(q) M_a(q/k) \tag{3.75}$$

with

$$\begin{aligned} M_1(r) &= -\frac{1}{252 r^3}\left(r(6 - 79r^2 + 50r^4 - 21r^6) + \frac{3}{2}(1-r^2)^3(2+7r^2)\log\left|\frac{1-r}{1+r}\right|\right) \\ M_2(r) &= -\frac{1}{84 r^3}\left(r(6 - 41r^2 + 2r^4 - 3r^6) + \frac{3}{2}(1-r^2)^3(2+r^2)\log\left|\frac{1-r}{1+r}\right|\right) \end{aligned} \tag{3.76}$$

The sign convention in these equations emphasizes the fact that the one–loop correction is negative, i.e. the functions M_a are positive for all r. In the function M_1 we recognize the integrand of the one–loop correction to the matter power spectrum $P^{(1,3)}$ in standard perturbation theory and we can write

$$P^{(1,3)}(k,\eta) = 2\left(G^{\text{1–loop}}_1(k,\eta) - 1\right) P^0(k) \tag{3.77}$$

The one–loop result for G_1 obtained by integrating equation (3.75) with $P^0(q)$ given by the output of linear theory as calculated by CAMB [12] is plotted in figure 3.3. We see that at small scales G_1 becomes large and negative which is not a physical result, but signals the breakdown of perturbation theory.

3.9.2 Large–k results

The large–k regime is defined by $k\sigma_v \gg 1$ where σ_v^2 is the initial velocity dispersion

$$\sigma_v^2 = \frac{1}{3}\int \mathrm{d}^3\mathbf{q}\ \frac{P^0(q)}{q^2} \tag{3.78}$$

and k is the momentum running along the propagator. In this regime the integration kernel can be kept at linear order because the dominant q–values are low and taking the initial fields to be in the growing mode it reduces to

$$\approx g_{ac}(s_1,0)g_{bd}(s_2,0)u_c u_d P^0(q)\delta(\lambda-q) = u_a u_b \theta(s_1)\theta(s_2)P^0(q)\delta(\lambda-q) \tag{3.79}$$

where the step functions ensure that s_1,$s_2 > 0$.

Following [33] we take the one–loop RG equation for the propagator as a starting point to obtain an analytical expression in the large–k limit. For $k \gg q$ the vertices can be approximated by

$$\gamma_{def}(\mathbf{k},-\mathbf{q},-\mathbf{k}+\mathbf{q})u_e \approx \frac{\mathbf{k}\cdot\mathbf{q}}{2q^2}\delta_{df} \tag{3.80}$$

and repeated propagators can be contracted using

$$g_{ab}(s_1,s_2)g_{bc}(s_2,s_3) = g_{ac}(s_1,s_3)\theta(s_1-s_2)\theta(s_2-s_3) \tag{3.81}$$

where the step functions keep track of the time ordering. The end result for the RG equation is

$$\begin{aligned}\partial_\lambda G_{ab,\lambda}(k,\eta_a,\eta_b) &= -g_{ab}(\eta_a,\eta_b)\int_{\eta_b}^{\eta_a}\mathrm{d}s_1\int_{\eta_b}^{s_1}\mathrm{d}s_2\ e^{s_1+s_2}\int\mathrm{d}^3\mathbf{q}\ \delta(\lambda-q)P^0(q)\frac{(\mathbf{k}\cdot\mathbf{q})^2}{q^4}\\ &= -g_{ab}(\eta_a,\eta_b)k^2\frac{(e^{\eta_a}-e^{\eta_b})^2}{2}\frac{1}{3}\int\mathrm{d}^3\mathbf{q}\ \frac{P^0(q)}{q^2}\delta(\lambda-q)\end{aligned} \tag{3.82}$$

This is just the large–k limit of standard perturbation theory, so to go beyond this we will promote the linear propagator on the right hand side to the full λ–dependent one. The solution to the modified differential equation then becomes

$$G_{ab,\lambda\to\infty}(k;\eta_a,\eta_b) = g_{ab}(\eta_a,\eta_b)\exp\left(-k^2\sigma_v^2\frac{(e^{\eta_a}-e^{\eta_b})^2}{2}\right) \tag{3.83}$$

This result was first obtained in [28] by resumming an infinite series of loop diagrams in standard perturbation theory. It shows how the perturbative series gives a nice positive result if it is not truncated at any finite order. We saw in equation (3.55) that the propagator evolves the initial power spectrum through time to give the contribution P^I to the final power spectrum. This means that the exponential damping seen at large k values can be interpreted as a loss of memory of the initial conditions through the non–linear clustering of matter. We will see this more clearly in Section 3.10.

In Chapter 4 I will extend this result to multi–point propagators and non–Gaussian initial conditions.

3.9.3 Numerical solutions

The approximation $k \gg \lambda$ corresponds to $k \gg q$ in the vertex terms, so we can improve the result in equation (3.83) by including the full momentum dependency of the tree level vertex. The equation we wish to solve will then be

$$\begin{aligned}\partial_\lambda G_{ab,\lambda}(k;\eta_a,\eta_b) = & 4\int \mathrm{d}s_1\mathrm{d}s_2\; e^{s_1+s_2}\int \mathrm{d}^3\mathbf{q}\;\delta(\lambda-q)P^0(q)G_{ae,\lambda}(k;\eta_a,s_1)\\ & \times\gamma_{ehl}(\mathbf{k},-\mathbf{q},-\mathbf{k}+\mathbf{q})G_{hd,\lambda}(q;s_1,0)u_d G_{li,\lambda}(|\mathbf{k}-\mathbf{q}|\,;s_1,s_2)\\ & \times\gamma_{igf}(\mathbf{k}-\mathbf{q},\mathbf{q},-\mathbf{k})G_{gc,\lambda}(q;s_2,0)u_c G_{fb,\lambda}(k;s_2,\eta_b)\end{aligned} \tag{3.84}$$

The time dependence of the propagators on the right hand side makes a numerical solution to the full equation very time consuming, so we will use the large–k result to approximate the time dependence as

$$G_{ab,\lambda}(k;s_1,s_2) = H_{ab,\lambda}(k)\exp\left(-k^2\sigma_v^2\frac{(e^{s_1}-e^{s_2})^2}{2}\right) \tag{3.85}$$

where the functions $H_{ab,\lambda}(k)$ allow for an additional dependence on the momentum.

In [33] the additional assumption is made that the propagators and vertices can be contracted using

$$\begin{aligned}G_{ae,\lambda}(k;\eta_a,s_1)\gamma_{ehl}(\mathbf{k},-\mathbf{q},-\mathbf{k}+\mathbf{q})G_{li,\lambda}(|\mathbf{k}-\mathbf{q}|\,;s_1,s_2)\gamma_{igf}(\mathbf{k}-\mathbf{q},\mathbf{q},-\mathbf{k})G_{fb,\lambda}(k;s_2,\eta_b)&\\ = B_{ahgf}(\mathbf{k},\mathbf{q})G_{fb,\lambda}(k;\eta_a,\eta_b)\theta(\eta_a-s_1)\theta(s_1-s_2)\theta(s_2-\eta_b)&\end{aligned} \tag{3.86}$$

where the function $B_{ahgf}(\mathbf{k},\mathbf{q})$ holds the momentum dependence from one–loop perturbation theory. As we have seen in subsection 3.9.2 this assumption is correct in the $k \gg q$ limit where the vertex is approximated by equation (3.80), so that the momentum dependence is simply a factor $(\mathbf{k}\cdot\mathbf{q})^2/(4q^4)$. In fact it corresponds to a partial resummation of the tree level vertex along the same lines as the resummations I will present in Chapter 4 for the multi–point propagators. The assumption is that the contraction can also be used for small k where the full momentum dependence given in the functions M_a will be contained in the tensor B_{ahgf}.

We will concentrate on the density and velocity propagators $G_{ab,\lambda}u_b$ as we did in the one–loop case, so we define $h_{a,\lambda}(k) = H_{ab,\lambda}(k)u_b$. The RG equation for h_a can be written as

$$\partial_\lambda h_{a,\lambda}(k) = -4\pi k^2 S(\lambda;\eta_a,\eta_b)M_a(\lambda/k)P^0(\lambda)\bar{h}_\lambda^2(\lambda)\bar{h}_\lambda(k) \tag{3.87}$$

with the functions M_a given in equation (3.76) and the time integrals contained in

$$\begin{aligned}S(\lambda;\eta_a,\eta_b) &= \int_{\eta_b}^{\eta_a} ds_2\int_{\eta_b}^{s_2} ds_1\; e^{s_1+s_2}\exp\left(-\frac{\lambda^2\sigma_v^2}{2}\left((e^{s_1}-1)^2+(e^{s_2}-1)^2\right)\right)\\ &= \frac{\pi}{4\lambda^2\sigma_v^2}\left(\mathrm{erf}\left[\frac{\lambda\sigma_v(e^{\eta_a}-1)}{\sqrt{2}}\right]-\mathrm{erf}\left[\frac{\lambda\sigma_v(e^{\eta_b}-1)}{\sqrt{2}}\right]\right)^2\end{aligned} \tag{3.88}$$

The error function is defined as $\mathrm{erf}(x) = 2\pi^{-1/2}\int_0^x \mathrm{d}te^{-t^2}$.

On the right side $h_{a,\lambda}$ has been approximated by the average

$$h_{a,\lambda} \simeq u_a \bar{h}_\lambda = u_a \frac{h_{1,\lambda} + h_{2,\lambda}}{2} \tag{3.89}$$

and in the linear regime the initial value for h will be

$$h_{a,\lambda=0}(k) = u_a \exp\left(k^2\sigma_v^2 \frac{(e^{\eta_a} - e^{\eta_b})}{2}\right) \tag{3.90}$$

The one–loop result in equation (3.75) can be obtained by letting $\sigma_v \to 0$ and using $h_a = u_a$ so that $\bar{h}_\lambda = 1$ independent of k.

The results of a numerical integration of equation (3.87) for $G_1 = G_{11} + G_{12}$ can be seen in figure 3.3 where I have used $\Omega_\Lambda = 0.7$, $\Omega_\mathrm{m} = 0.3$, $\Omega_\mathrm{b} = 0.05$, $h = 0.7$, $n_\mathrm{s} = 1$ and $A_\mathrm{s} = 2.3 \times 10^{-9}$. The initial power spectrum has been taken from the output of CAMB at $z = 49$ making this the initial time in the definition of the time variable η. Thus η_b will be zero and η_a can be calculated from the linear growth factor at the given redshift divided by that at $z = 49$.

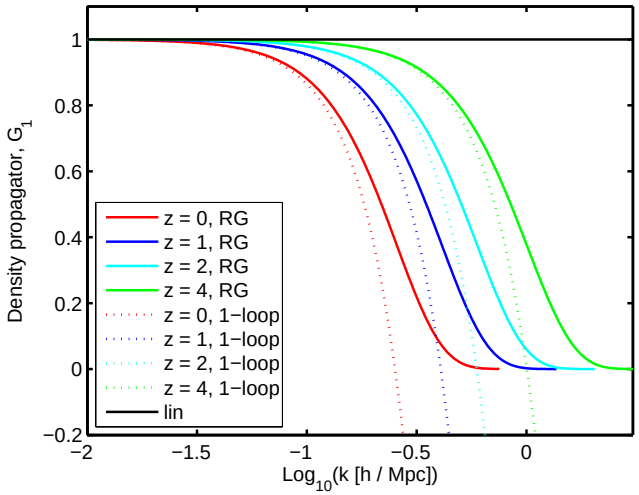

Figure 3.3: Full density propagators at $z = 0$, $z = 1$, $z = 2$ and $z = 4$ from left to right. The one-loop results are plotted as dotted lines and the black line is the linear result.

We see that the propagator still displays the damping at large k as seen in equation (3.83) and that the one–loop results on the other hand quickly become large and negative. It is also clear that the non–linear clustering causes the damping to start at lower k values as time goes by. As mentioned before this results in a loss of knowledge about the initial conditions on successively larger scales. The results closely resemble those obtained using renormalized perturbation theory in [28], where they were also compared to numerical simulations showing excellent agreement.

In figure 3.4 I compare the density and the velocity propagators G_1 and G_2 at $z = 0$. The difference between the two lies in the momentum functions M_a. The damping of the velocity propagator starts at earlier k values than that of the density propagator reflecting the fact that $M_2 > M_1$ for all r.

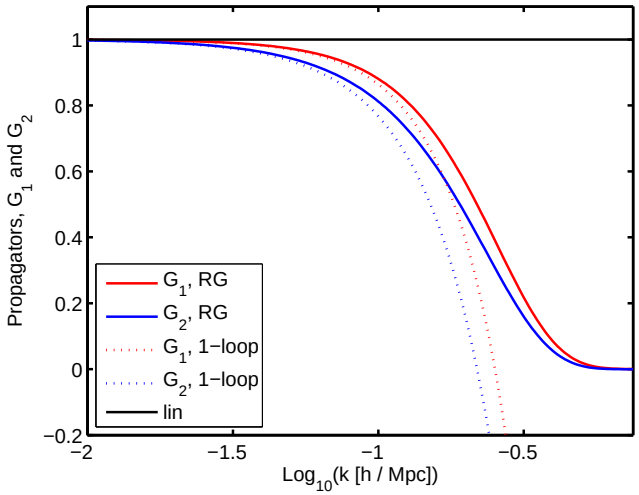

Figure 3.4: Comparison of the density and velocity propagators at $z = 0$. The one–loop results are plotted as dotted lines and the black line is the linear result.

3.10 The Power Spectrum

Having obtained the full propagators from the integration of equation (3.87) we can easily calculate the P^{I} contribution to the full power spectrum from equation (3.55) by evolving the initial power spectrum with the full propagators.

To calculate the P^{II} contribution we need to differentiate the expression in equation (3.55) with respect to λ, giving

$$\partial_\lambda P^{\mathrm{II}}_{ab,\lambda} = \int_0^{\eta_a} \mathrm{d}s_1 \int_0^{\eta_b} \mathrm{d}s_2 \left(\partial_\lambda \left(G_{ac,\lambda} \right) G_{bd,\lambda} \Phi_{cd,\lambda} + G_{ac,\lambda} \partial_\lambda \left(G_{bd,\lambda} \right) \Phi_{cd,\lambda} + G_{ac,\lambda} G_{bd,\lambda} \partial_\lambda \left(\Phi_{cd,\lambda} \right) \right) \tag{3.91}$$

where I have suppressed the arguments of the functions for simplicity. The RG equation for the propagators is given in equation (3.87) so we only need the RG equation for the self–energy Φ_{ab} to complete the calculation. Using the general approach outlined in Section 3.9 we get the diagrammatical RG equation for Φ by drawing the one–loop corrections

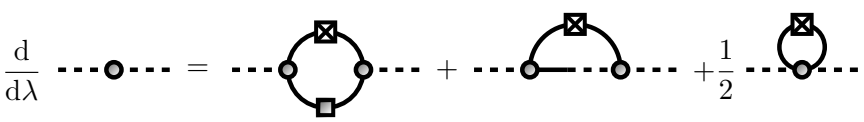

(3.92)

where the sum of the two contributions to the full power spectrum is represented by a gray square

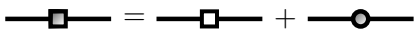

(3.93)

In the top part of the first two diagrams in equation (3.92) we have not included the P^{II} contribution to the power spectrum because the diagrams created by including this contribution would have no explicit λ–dependence.

We see in equation (3.92) that vertices with more than one χ–leg show up on the right hand side. To calculate the power spectrum we encounter vertices with up to two χ–legs, for the bispectrum we would have vertices with up to three χ–legs and so on. This is why it is relevant to generalize the n–point propagators of [44] to multi–point propagators with more than one outgoing leg in the RG formalism.

In the approximation where we keep the vertex at tree level only the first diagram will contribute because one of the 1PI 3–point functions in the second diagram includes two outgoing χ–fields which is beyond the tree level expression. The RG equation for Φ then becomes

$$\begin{aligned}\partial_\lambda \Phi_{ab,\lambda}(k;s_1,s_2) = 4e^{s_1+s_2}\int \mathrm{d}^3\mathbf{q}\;\delta(\lambda-q)P^{\mathrm{I}}_{cd,\lambda}(q;s_1,s_2)\\ \cdot P_{fe,\lambda}(|\mathbf{q}-\mathbf{k}|\,;s_1,s_2)\gamma_{adf}(\mathbf{k},-\mathbf{q},-\mathbf{k}+\mathbf{q})\gamma_{bce}(-\mathbf{k},\mathbf{q},\mathbf{k}-\mathbf{q})\end{aligned} \tag{3.94}$$

Again we need to make approximations for the time dependence of the power spectra on the right hand side. Using the approximations from Section 3.9, P^{I} will be approximated by

$$P^{\mathrm{I}}_{ab,\lambda}(q;s_1,s_2) \simeq u_a u_b \bar{h}^2_\lambda(q) P^0(q) \exp\left(-q^2\sigma_v^2\frac{(e^{s_1}-1)^2+(e^{s_2}-1)^2}{2}\right) \tag{3.95}$$

Inspired by this time dependence we will use a similar approximation for P^{II}

$$P^{\mathrm{II}}_{ab,\lambda}(q;\eta_a,\eta_b) \simeq P^{\mathrm{II}}_{ab,\lambda}(q;s_1,s_2) \exp\left(-q^2\sigma_v^2\frac{(e^{\eta_a}-e^{s_1})^2+(e^{\eta_b}-e^{s_2})^2}{2}\right) \tag{3.96}$$

The dependence of the end result for P^{II} on this ansatz was investigated in [33] showing little variations in the range of scales we are interested in. They compared the above ansatz to the very simple one $P^{\mathrm{II}}_{ab,\lambda}(q;\eta_a,\eta_b) \simeq P^{\mathrm{II}}_{ab,\lambda}(q;s_1,s_2)$. To ease the numerical integration further we will find the RG equation for the average power spectrum, $\bar{P}^{\mathrm{II}}_\lambda = \frac{1}{4}u_a u_b P^{\mathrm{II}}_{ab,\lambda}$.

Putting everything together we obtain the RG equation for P^{II}, which has been done in [33] for equal times, $\eta_a = \eta_b = \eta$

$$\begin{aligned}\partial_\lambda \bar{P}^{\mathrm{II}}_\lambda(k;\eta) = -4\pi k^2 \bar{h}^2_\lambda(\lambda)P^0(\lambda)\Bigg(&S(\lambda;\eta,0)u_a M_a(\lambda/k)\bar{P}^{\mathrm{II}}_\lambda(k;\eta)\\ &-\frac{1}{2k}\int_{|k-\lambda|}^{k+\lambda}\mathrm{d}p\,\Big[\theta(\lambda-p)\bar{h}^2_\lambda(p)U(\lambda^2,k^2,p^2;\eta)P^0(p)\\ &+U(k^2,\lambda^2,-p^2;\eta)\bar{P}^{\mathrm{II}}_\lambda(p;\eta)\Big]\frac{\left(3k^4-4(p^2-\lambda^2)^2+k^2(p^2+\lambda^2)\right)^2}{196k^2p^3\lambda^3}\Bigg)\end{aligned} \tag{3.97}$$

with the time dependence in the last two lines given by the function

$$U(\lambda^2, k^2, p^2; \eta) = \left[\int_0^\eta ds\, e^s \exp\left(-\frac{(\lambda^2 + p^2)\sigma_v^2}{2}(e^s - 1)^2 - \frac{k^2\sigma_v^2}{2}(e^\eta - e^s)^2 \right) \right]^2 \tag{3.98}$$

The first line on the right hand side of equation (3.97) comes from the RG equations for the propagators while the last two lines show the Φ–contribution. The initial condition at $\lambda = 0$ will be $P^{\rm II}_{ab,\lambda} = 0$. By rewriting a little we can recognize the standard one–loop momentum term from $P^{(2,2)}$ given in Section 3.3. The one–loop result can be reproduced in the $\sigma_v \to 0$ limit where $\bar{h}_\lambda = 1$ and $P^{\rm II}_{ab,\lambda} = 0$.

3.10.1 Numerical results

I solve the two equations (3.97) and (3.87) simultaneously to get the correct λ–dependence of $\bar{h}_\lambda$ in equation (3.97). In [40] it was pointed out that when comparing analytical approaches to N–body simulations it is important to choose the same initial time where the linear power spectrum is used as initial conditions in both calculations. The reason is that the non–linear evolution will generate non–Gaussianities and thereby alter the evolution of the power spectrum. I have chosen the initial time $z = 49$ to match the N–body results of [41] and use the cosmological parameters given in subsection 3.9.3.

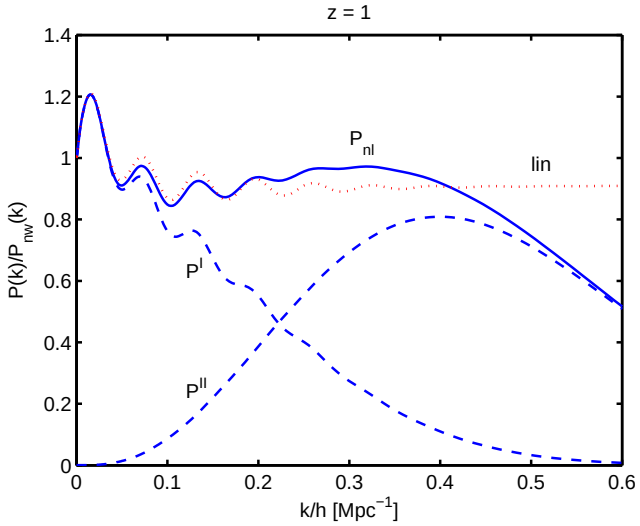

Figure 3.5: The two contributions to the power spectrum at $z = 1$.

In figure 3.5 I present the two contributions to the full power spectrum at $z = 1$. All spectra have been divided by a linearly evolved spectrum with no baryons to enhance the baryon acoustic oscillations. I have used the fitting formula of [42] to approximate this spectrum. The linear result is obtained by propagating P^0 with the linear propagators and multiplying by the factor of $e^{2\eta}$ as mentioned in Section 3.4. We see that $P^{\rm I}$ dominates in the linear regime and that this contribution contains all the effects from the BAO. The damping caused

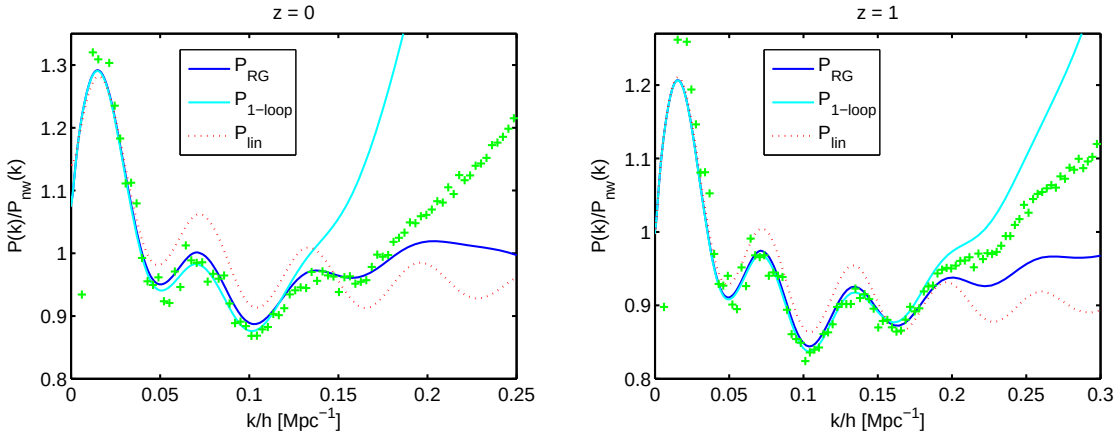

Figure 3.6: The power spectrum at $z = 0$ and $z = 1$ compared to the N-body results of [41] represented by plusses.

be the exponential decay of the full propagators make the BAO less prominent at larger k–values. In the non–linear regime P^{II} takes over and generates extra power as compared to the linear theory. In the regime from $k/h \sim 0.1\,\mathrm{Mpc}^{-1}$ to $0.3\,\mathrm{Mpc}^{-1}$ the decay of P^{I} is exactly compensated by the rise of P^{II} making the transition indistinguishable in the full power spectrum.

Figure 3.6 shows a comparison of my results at $z = 0$ and $z = 1$ to the N–body results of [41]. Also shown are the linear results and the standard one–loop results obtained from the RG equation. The RG results show very good agreement with the N–body results out to $k/h \sim 0.18\,\mathrm{Mpc}^{-1}$ at $z = 0$ and $k/h \sim 0.2\,\mathrm{Mpc}^{-1}$ at $z = 1$. At $z = 0$ the improvement over standard one–loop perturbation theory is clear at the scales $k/h \sim 0.13\,\mathrm{Mpc}^{-1}$ to $k/h \sim 0.2\,\mathrm{Mpc}^{-1}$, while at $z = 1$ both approaches start to deviate from the N–body results at $k/h \sim 0.2\,\mathrm{Mpc}^{-1}$.

The RG results sample a large portion of the BAO regime accurately predicting the size and position of the fluctuations and thus it complements the predictions from N–body simulations by giving a better physical understanding of the processes involved.

Chapter 4

Large–k Limit of Multi–Point Propagators

The multi–point propagators quantify the connection to the initial conditions by working as a direct link between the evolved spectra and the early ones. The large–k result obtained for the two–point propagator in subsection 3.9.2 showed that the memory of the initial distribution is erased at small scales. The results of this chapter show that the loss of memory is also present in the general higher order multi–point propagators.

We saw in Sections 3.9 and 3.10 that the large–k limit of the two–point propagator G_{ab} was a very useful result when dealing with the full RG equations. In a similar way the large–k limit of general multi–point propagators could be used in approximations including higher order vertices. It is also relevant to consider how the presence of initial non–Gaussianities will influence the exponential damping exhibited in the large–k result for the two–point propagator.

In [43] the two–point propagator was resummed in the large–k limit using the RG approach with non–Gaussian initial conditions. The large–k limit of the n–point propagators $V^{(n-1,1)}$ has been obtained both in the Gaussian [44] and the non-Gaussian case [45]. In this chapter I reproduce their results using the RG formalism and show that a similar large–k behaviour appears for the new class of multi–point propagators $V^{(n,m)}$, $m > 1$ introduced in Section 3.7. The results obtained here will be submitted to JCAP.

4.1 RG Equations for Multi–Point Propagators, Gaussian Initial Conditions

We start by considering the case of Gaussian initial conditions where only the first line of equation (3.69) contributes. In Section 3.9 I presented the results obtained for the two–point

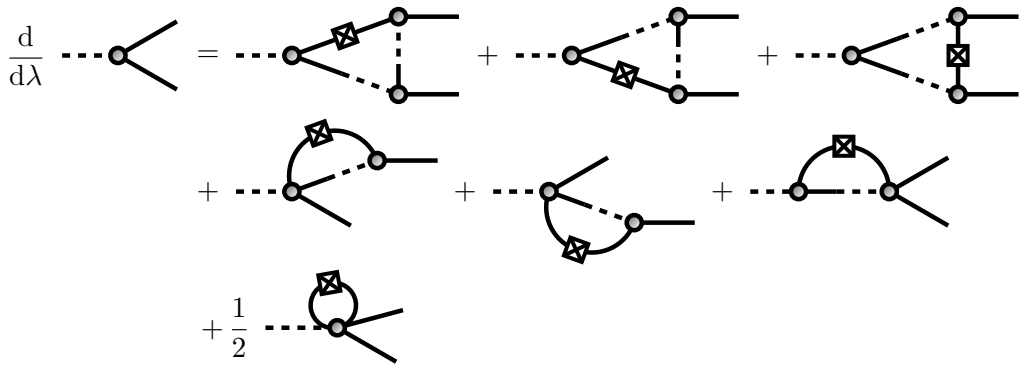

Figure 4.1: RG equation for the vertex $\Gamma^{(3)}_{\chi_a\phi_b\phi_c}$.

propagator G_{ab} in [33]. I will use the general rules set up there to generate RG equations for the multi–point propagators.

First we consider the multi–point propagator $V^{(2,1)}_{abc}(\mathbf{k},\eta_a;\mathbf{k}_1,\mathbf{k}_2,\eta_b)$. By taking the λ–derivative of equation (3.61) we see the general structure of the RG equations we will encounter

$$\begin{aligned}\partial_\lambda V^{(2,1)}_{abc,\lambda} = \int \mathrm{d}s_{1,2,3} \Big(&\partial_\lambda\left(G_{ad,\lambda}\right)\Gamma^{(3)}_{\chi_d\phi_e\phi_f,\lambda}G_{eb,\lambda}G_{fc} + G_{ad,\lambda}\Gamma^{(3)}_{\chi_d\phi_e\phi_f,\lambda}\partial_\lambda\left(G_{eb,\lambda}\right)G_{fc,\lambda}\\ &+ G_{ad,\lambda}\Gamma^{(3)}_{\chi_d\phi_e\phi_f,\lambda}G_{eb,\lambda}\partial_\lambda\left(G_{fc,\lambda}\right) + G_{ad,\lambda}\partial_\lambda\left(\Gamma^{(3)}_{\chi_d\phi_e\phi_f,\lambda}\right)G_{eb,\lambda}G_{fc,\lambda}\Big)\end{aligned} \tag{4.1}$$

The first three terms on the right hand side represent the RG corrections to each leg as already expressed in the RG equation for the propagator in equation (3.72). The last term represents the corrections that affect the vertex directly and using the rules from Section 3.9 we can express the vertex RG equation diagrammatically as seen in figure 4.1. The first diagram on the right hand side is the vertex correction that was included in the RG equation for the two–point propagator when using the assumption in equation (3.86).

The approach in equation (4.1) generalizes to higher order multi–point propagators in the sense that the RG equation can always be separated into one–loop diagrams that represent corrections to the two–point propagators in the legs and those that represent corrections to the vertex.

The right hand side of the RG equations for vertices with more than one χ–leg will in addition to the one–loop diagrams similar to those in figure 4.1 contain tree level diagrams of the form

(4.2)

Due to the delta functions $\delta(\lambda - q)$ from the integration kernel and $\delta(\mathbf{q} + \mathbf{k}_i)$ from the propagator these diagrams will only contribute in a single point $\lambda = k_i$ and will have no effect on the final solution of the differential equation. Thus we can safely ignore these deviations from the rules stated above.

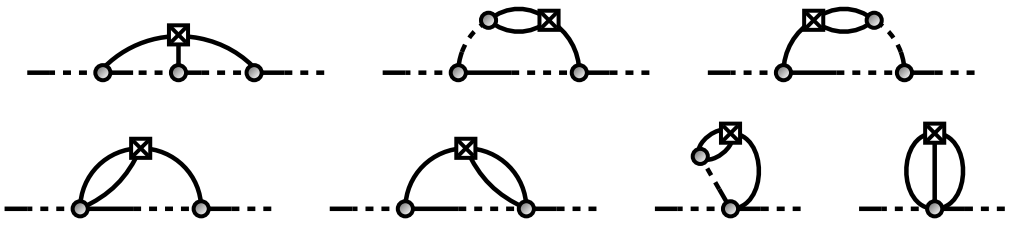

Figure 4.2: All loop diagrams derived from the second term of equation (3.69) for the two–point propagator.

As a final note we see that we can obtain the one–loop result from ordinary perturbation theory by keeping all quantities in the diagrams at tree level and integrate the resulting expression over λ. In this case only the first three diagrams on the right hand side of figure 4.1 will contribute due to there being higher order vertices in the last four.

4.2 RG Equations for Multi–Point Propagators, Non–Gaussian Initial Conditions

With the presence of initial non–Gaussianities the RG equations become more complicated. The first line in equation (3.69) will generate the same diagrams as presented in Section 4.1, but in addition to these the remaining terms will generate an infinite series of diagrams with up to two loops for the bispectrum, three for the trispectrum and so on. The integrations over $\mathbf{q}_i$ will give rise to higher order integration kernels of the form

$$G_{ad,\lambda}(q_1;s_1,0)G_{be,\lambda}(q_2;s_2,0)G_{cf,\lambda}(q_3;s_3,0)B^0_{def}(\mathbf{q}_1,\mathbf{q}_2,\mathbf{q}_3)\delta\left(\lambda-\sum q_i\right)\ ,[T^0]\ ,\ \cdots \qquad (4.3)$$

We will represent these diagrammatically as a crossed box with the appropriate number of legs for each order of the initial statistics. In accordance with the comments after equation (3.69) the general rule will be that only one coupling to the initial conditions in the form of the integration kernels will be present in each diagram. Thus the general rules from Section 3.9 for constructing the right hand side of the RG equation for a quantity can be reformulated in the non–Gaussian case as

- Draw all loop corrections to the quantity with exactly one crossed box using the full λ–dependent propagators, statistics and vertices.

The differentiation with respect to λ is already taken care of by including the crossed box. Figure 4.2 shows all the diagrams arising from the bispectrum integration kernel for the two–point propagator. As can be seen, all diagrams are two–loop corrections and similarly the trispectrum will only generate three–loop diagrams and so on. This will also be the case for the RG equations for vertices with just one χ leg.

For vertices with more than one χ leg there will be additional diagrams at lower order arising from each integration kernel, but the delta functions in the wavenumbers will limit

the range at which they contribute. For the vertex $\Gamma^{(3)}_{\chi_a\chi_b\phi_c}$ the bispectrum will generate 6 additional one–loop diagrams

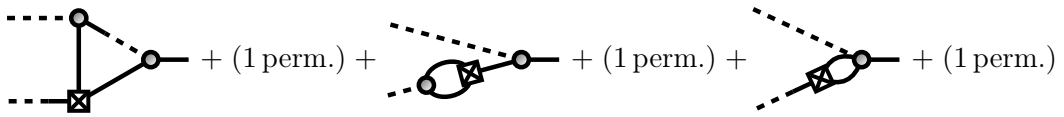

(4.4)

When performing two of the momentum integrations in equation (3.69) we get $\mathbf{q}_3 = -\mathbf{k}_1$ and $\mathbf{q}_2 = \mathbf{k}_1 - \mathbf{q}_1$, where $\mathbf{k}_1$ is the momentum associated with the lower leg to the left in the diagrams shown in equation (4.4). The delta function in equation (4.3) will then reduce to $\delta(\lambda - q_1 - k_1 - |\mathbf{k}_1 + \mathbf{q}_1|)$, so if k_1 is much larger than the scale at which the bispectrum has a significant amplitude, that is $k_1 \gg q_1$, the diagrams will only contribute in a very short range $2k_1 < \lambda < 2k_1 + 2q_1$. The same arguments apply to loop corrections from the higher order statistics, thus in the large–k limit that we will now turn to we can neglect the contribution from the diagrams at lower order in the perturbation series arising from each initial spectrum.

4.3 Large–k Limit with Gaussian Initial Conditions

In the Gaussian case the large–k regime is defined much like in subsection 3.9.2 by $k_i\sigma_v \gg 1$ where k_i are the momenta in each leg of the multi–point propagator. We use equation (3.79) for the integration kernel and take the standard one–loop expressions of the right hand side of the RG equations as our starting point. Here we will go through a detailed calculation for $V^{(2,1)}$ which will form the basis of the calculations for general multi–point propagators..

4.3.1 Large–k limit of $V^{(2,1)}$, the Gaussian case

Keeping the vertices at tree level means that only the last diagram in equation (3.72) and the first three diagrams in figure 4.1 will contribute. This gives a total of 6 diagrams to consider, one for each propagator and three for the vertex itself. We will go through the calculations of the first vertex correction as an example. The complete diagram is

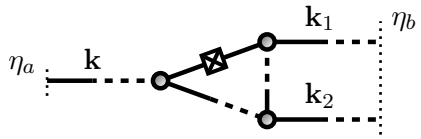

(4.5)

Keeping everything at tree level and using equation (3.79) for the integration kernel we get

$$\begin{aligned} -8\int \mathrm{d}^3\mathbf{q}\mathrm{d}s_{a,b,v}\; e^{s_a+s_b+s_v} P^0(q)\delta(\lambda-q)\theta(s_a)\theta(s_b) g_{ad}(\eta_a,s_a)\gamma_{def}(\mathbf{k},-\mathbf{q},-\mathbf{k}+\mathbf{q})u_e \\ \times g_{fg}(s_a,s_v)\gamma_{ghi}(\mathbf{k}-\mathbf{q},\mathbf{k}_1+\mathbf{q},\mathbf{k}_2)g_{ic}(s_v,\eta_b) \\ \times g_{hj}(s_v,s_b)\gamma_{jkl}(-\mathbf{k}_1-\mathbf{q},\mathbf{q},\mathbf{k}_1)u_k g_{lb}(s_b,\eta_b) \end{aligned} \tag{4.6}$$

where the intermediate times are restricted by $\eta_a > s_a > s_v > s_b > \eta_b$ via the theta functions in the linear propagators.

In the $k_i \gg q$ limit two of the vertices can be reduced further using the approximation in equation (3.80). The linear propagators can be contracted with the delta functions in the indices so that the dependence on s_a and s_b appears only in the exponential function in the first line of equation (4.6). Performing the two integrals over s_a and s_b then yields the large–k result

$$\begin{aligned} -2 \int \mathrm{d}s_v \, e^{s_v} g_{ag}(\eta_a, s_v) \gamma_{ghi}(\mathbf{k}, \mathbf{k}_1, \mathbf{k}_2) g_{ic}(s_v, \eta_b) g_{hb}(s_v, \eta_b) (e^{\eta_a} - e^{s_v})(e^{s_v} - e^{\eta_b}) \\ \times \int \mathrm{d}^3\mathbf{q} \, \frac{\mathbf{k} \cdot \mathbf{q}}{q^2} \frac{\mathbf{k}_1 \cdot \mathbf{q}}{q^2} P^0(q) \delta(\lambda - q) \end{aligned} \tag{4.7}$$

where the momentum integration in the last line can be rewritten as

$$(\mathbf{k} \cdot \mathbf{k}_1) \frac{1}{3} \int \mathrm{d}^3\mathbf{q} \, \frac{P^0(q)}{q^2} \delta(\lambda - q) \tag{4.8}$$

Going through a similar calculation for the other five diagrams will change only the momentum factor in front of the integral in equation (4.8) and the limits of integration over s_a and s_b. Adding all six contributions gives

$$\begin{aligned} \partial_\lambda V^{(2,1)}_{abc,\lambda} = \int \mathrm{d}s_v \, e^{s_v} g_{ag}(\eta_a, s_v) \gamma_{ghi}(\mathbf{k}, \mathbf{k}_1, \mathbf{k}_2) g_{ic}(s_v, \eta_b) g_{hb}(s_v, \eta_b) \\ \times \Big(k^2 \left(e^{\eta_a} - e^{s_v}\right)^2 + (k_1^2 + k_2^2 + 2\mathbf{k}_1 \cdot \mathbf{k}_2) \left(e^{s_v} - e^{\eta_b}\right)^2 \\ - 2\mathbf{k} \cdot (\mathbf{k}_1 + \mathbf{k}_2) \left(e^{\eta_a} - e^{s_v}\right) \left(e^{s_v} - e^{\eta_b}\right) \Big) \frac{1}{3} \int \mathrm{d}^3\mathbf{q} \, \frac{P^0(q)}{q^2} \delta(\lambda - q) \end{aligned} \tag{4.9}$$

Using the fact that $\mathbf{k} = -\mathbf{k}_1 - \mathbf{k}_2$ we can reduce the sum in the parentheses to $k^2 \left(e^{\eta_a} - e^{\eta_b}\right)^2$, and recognizing the tree level expression from equation (3.63). The end result for the large–k limit of the one–loop calculation of the RG equation for $V^{(2,1)}$ is

$$\partial_\lambda V^{(2,1)}_{abc,\lambda} = -V^{(2,1)}_{abc,\,\mathrm{tree}} k^2 \frac{\left(e^{\eta_a} - e^{\eta_b}\right)^2}{2} \frac{1}{3} \int \mathrm{d}^3\mathbf{q} \, \frac{P^0(q)}{q^2} \delta(\lambda - q) \tag{4.10}$$

We can now go beyond the usual one–loop result by promoting the tree level expression for the multi–point propagator on the right hand side to the full λ–dependent expression. The integration over λ is then straightforward and in the limit we are interested in, $\lambda \to \infty$, the result is

$$V^{(2,1)}_{abc,\lambda\to\infty} = V^{(2,1)}_{abc,\,\mathrm{tree}} \exp\left(-\frac{k^2 \sigma_v^2}{2} \left(e^{\eta_a} - e^{\eta_b}\right)^2 \right) \tag{4.11}$$

where we have used the initial condition $V^{(2,1)}_{abc,\lambda=0} = V^{(2,1)}_{abc,\,\mathrm{tree}}$ and σ_v has been defined in equation (3.78). This is the result obtained in [44] for the three–point propagator by resumming an infinite series of higher order loop diagrams in standard perturbation theory. The big advantage in the RG calculation is that we need only consider the explicit expressions of one–loop diagrams.

The result shows that in the large–k regime where standard perturbation theory is divergent at each order the full resummation of the dominant diagrams still gives a finite result with an exponential damping for large k–values.

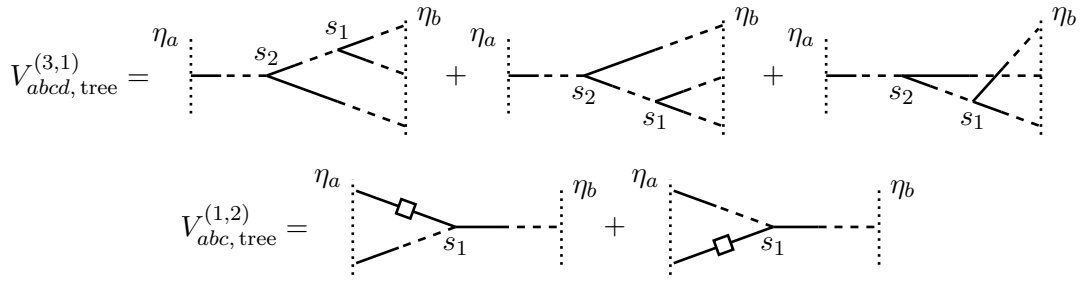

Figure 4.3: Tree level expressions for $V^{(3,1)}_{abcd}$ and $V^{(1,2)}_{abc}$.

4.3.2 Large–k limit of general multi–point propagators, the Gaussian case

For the general multi–point propagators there are two additional considerations that should be noted. First the tree level expressions for the diagrams will be a sum over a few different realizations that should be studied separately. Secondly the propagators with more than one outgoing ϕ–leg will have couplings to the initial power spectrum as part of their tree level expression. See figure 4.3 for two examples. We will now show that a calculation similar to that just presented can be performed for each of these tree level diagrams.

The lesson learned from the above calculation of one–loop diagrams is that in the large–k regime each loop diagram can be reduced to the tree level expression multiplied by a momentum factor and a time factor as in equation (4.7). The momentum factor can be rewritten as in equation (4.8) where the dot product in front of the integral is determined by the two legs in the tree level diagram that the loop is attached to. The time factor arises from the integration over $e^{s_a+s_b}$ where s_a and s_b are the two times of interaction where the loop hits the tree level diagram. The limits of the integrations can be read off from diagrams like those in figure 4.3 depending on which section of the tree level diagram the legs of the loop touch.

Let us start by considering a segment of a tree level diagram with a power spectrum. There will be three types of loop diagrams with both legs attached to such a segment

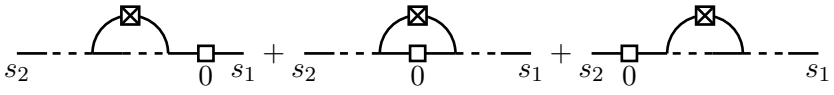

(4.12)

The momentum factor will be the same for all three diagrams while the time factors on the other hand are determined by integrations from the initial coupling to the power spectrum at time $t = 0$ to either s_1 or s_2 giving the sum

$$\frac{1}{2}\left(e^{s_2}-1\right)^2-\left(e^{s_2}-1\right)\left(e^{s_1}-1\right)+\frac{1}{2}\left(e^{s_1}-1\right)^2=\frac{1}{2}\left(e^{s_2}-e^{s_1}\right)^2 \tag{4.13}$$

Similarly any loop connected to the power spectrum segment with just one leg can be attached on either side of the square, but the sum of the two diagrams give a time factor of $(e^{s_2} - e^{s_1})$ times the common time factor associated with the other leg and the common momentum

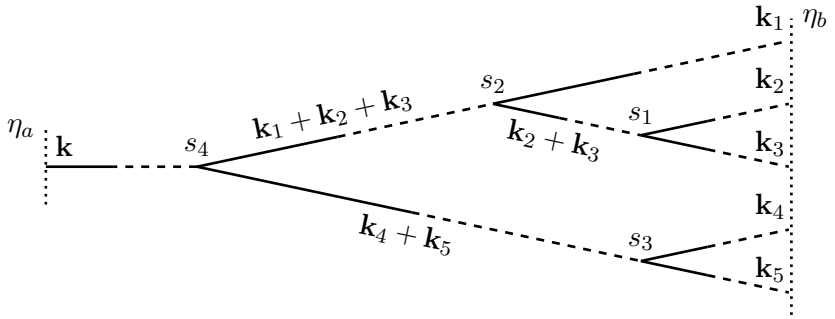

Figure 4.4: A tree level diagram for $V^{(5,1)}$.

factor. These considerations show that even though the segments with a power spectrum contribute with more loop diagrams than a propagator segment, the extra contributions add up to the same result as a propagator segment will give. Thus we can treat any appearance of the power spectrum in the tree level expressions in the same way as a regular two–point propagator when we sum over all one–loop corrections on the right hand side of the RG equations. The two tree level diagrams for $V^{(1,2)}$ in figure 4.3 can then be treated completely analogous to the $V^{(2,1)}$ calculation above. In general any tree level diagram for the multi–point propagator $V^{(n,1+m)}$ will be analogous to a tree level diagram for $V^{(n+m,1)}$, so we will now restrict our attention to the n–point propagators.

Each tree level diagram for the n–point propagator $V^{(n-1,1)}$ will contain $n-1$ mergings of legs on the right hand side of the diagram (see figure 4.4 for an example). The number of two–point propagators in such a diagram is $2n-1$ and the number of possible one–loop diagrams is $n(2n-1)$. We can treat all these one–loop corrections systematically by adding up diagrams with the loop connected to a certain segment of the tree level diagram separately.

If we consider a segment where two legs merge (as in the bottom part of the diagram in figure 4.4, where the legs with momenta $\mathbf{k}_4$ and $\mathbf{k}_5$ merge between the times η_b and s_4) we can use the calculation for $V^{(2,1)}$ to add all the loop diagrams with both legs on the same segment. The resulting momentum and time factor will be

$$|\mathbf{k}_i + \mathbf{k}_j|^2 \, (e^{s_l} - e^{\eta_b})^2 \tag{4.14}$$

where s_l is the time at which the next merging takes place and $\mathbf{k}_i$ and $\mathbf{k}_j$ are the momenta before the merging. Similarly there are three loops with just one leg attached to the segment and the other leg on a propagator with momentum $\mathbf{p}$ going between times s_{p_1} and s_{p_2}. These can be added to give the momentum and time factor

$$\begin{aligned} 2\mathbf{p} \cdot \big(\mathbf{k}_i \, (e^{s_m} - e^{\eta_b}) + \mathbf{k}_j \, (e^{s_m} - e^{\eta_b}) + (\mathbf{k}_i + \mathbf{k}_j) \, (e^{s_l} - e^{s_m}) \big) \, (e^{s_{p_2}} - e^{s_{p_1}}) \\ = 2\mathbf{p} \cdot (\mathbf{k}_i + \mathbf{k}_j) \, (e^{s_l} - e^{\eta_b}) \, (e^{s_{p_2}} - e^{s_{p_1}}) \end{aligned} \tag{4.15}$$

where we see that the time of merging, s_m, does not appear in the final result. This taken together with equation (4.14) shows that the segment can be treated as just one propagator with momentum $\mathbf{k}_i + \mathbf{k}_j$ between the times η_b and s_l when we sum over one–loop diagrams.

Using this approach iteratively for every merging of legs in the tree level expression under consideration we end up with just two legs merging at the final vertex where the result will depend only on the total momentum $\mathbf{k} = -\sum \mathbf{k}_i$ and the initial and final times η_a and η_b. The intermediate times will only appear in the explicit tree level expression that will be common to all the one–loop diagrams. As argued above the approach works also for tree level diagrams with more than one outgoing leg on the left hand side where there will be one or more legs with a power spectrum. The only difference being a change of sign in the momenta considered so that $\mathbf{k} = \sum \mathbf{p}_i = -\sum \mathbf{k}_j$ where $\mathbf{p}_i$ are the momenta on the left hand side and $\mathbf{k}_j$ the momenta on the right hand side.

When the sum over all one–loop corrections is taken the resulting momentum and time factors will be independent of which particular tree level realization we are considering so adding all possible one–loop diagrams for a given multi–point propagator will give

$$\partial_\lambda V^{(n,m)}_{a_1\cdots a_m b_1\cdots b_n,\lambda} = -k^2 \frac{(e^{\eta_a} - e^{\eta_b})^2}{2} \frac{1}{3} \int \mathrm{d}^3\mathbf{q}\, \frac{P^0(q)}{q^2} \delta(\lambda - q) \sum (\text{tree level diagrams}) \quad (4.16)$$

which is identical to equation (4.10). Promoting the tree level expression on the right hand side to the full λ–dependent one before integrating, we get the general large–k result

$$V^{(n,m)}_{a_1\cdots a_m b_1\cdots b_n,\lambda\to\infty} = V^{(n,m)}_{a_1\cdots a_m b_1\cdots b_n,\mathrm{tree}} \exp\left(-\frac{k^2\sigma_v^2}{2}(e^{\eta_a} - e^{\eta_b})^2\right) \quad (4.17)$$

This result has been obtained for $m = 1$ and $\eta_b = 0$ in [44]. The fact that it generalizes to $m > 1$ is not obvious from the construction of this class of multi–point propagators. As explained in Section 3.6 they can be constructed by combining two or more n–point propagators, $V^{(n-1,1)}$, via couplings to the initial statistics, but the result is not just a product of the $V^{(n-1,1)}$ results. There are additional couplings between the individual n–point propagators that modify the result.

Let us consider a specific diagram for $V^{(1,2)}$ to illustrate this point

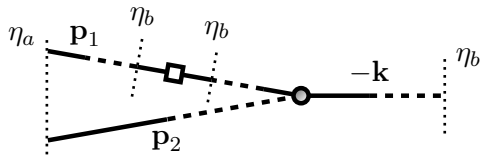

(4.18)

Here we have a two–point propagator $V^{(1,1)}_{ab} = G_{ab}$ running from η_b to η_a with momentum $\mathbf{p}_1$, and a three–point propagator $V^{(2,1)}_{def}$ running from η_b to η_a merging the two momenta $\mathbf{p}_1$ and $-\mathbf{k}$ into $\mathbf{p}_2$. The large–k results for these two have the damping factors

$$\exp\left(-\frac{p_1^2\sigma_v^2}{2}(e^{\eta_a} - e^{\eta_b})^2\right) \quad \text{and} \quad \exp\left(-\frac{p_2^2\sigma_v^2}{2}(e^{\eta_a} - e^{\eta_b})^2\right) \quad (4.19)$$

respectively while the combination in the diagram in equation (4.18) is damped by

$$\exp\left(-\frac{k^2\sigma_v^2}{2}(e^{\eta_a} - e^{\eta_b})^2\right) \quad (4.20)$$

where $\mathbf{k} = \mathbf{p}_1 + \mathbf{p}_2$. The additional couplings that arise in the combination of the two n–point propagators correspond to the term $2\mathbf{p}_1 \cdot \mathbf{p}_2$ in k^2.

This is analogous to bremsstrahlung processes in particle physics where couplings to an external potential leads to emissions or absorptions of particles. Here the initial conditions take the role of the external potential while each Fourier mode acts as an individual particle.

4.4 Large–k Limit with Non–Gaussian Initial Conditions

The large–k assumption of Section 4.3 is equivalent to assuming that the momenta $\mathbf{k}_i$ running along the legs of the tree level diagrams are much greater than the momentum $\mathbf{q}$ in the power spectrum integration kernel defined in subsection 3.9.2. We will also use this assumption in the case of initial non–Gaussianities so that the momenta $\mathbf{k}_i$ are always much greater than the loop momenta $\mathbf{q}_j$ in the integration kernels of equation (4.3).

As seen in equation (3.69) the right hand side of the RG equation can be split into separate contributions from each order of the initial statistics. The contribution from the power spectrum will not change due to the presence of initial non–Gaussianities so we can reuse the results from Section 4.3 directly. If we do not rewrite the momentum factors as in equation (4.8) the end result in equation (4.16) can be expressed as

$$\partial_\lambda V^{(n,m)}_{a_1\cdots a_m b_1\cdots b_n,\lambda} = -V^{(n,m)}_{a_1\cdots a_m b_1\cdots b_n,\lambda} \frac{\left(e^{\eta_a} - e^{\eta_b}\right)^2}{2} \int \mathrm{d}^3\mathbf{q}\, \frac{(\mathbf{k}\cdot\mathbf{q})^2}{q^4} P^0(q)\delta(\lambda - q) \tag{4.21}$$

where we have promoted the tree level expression to the full λ–dependent one.

Next we turn to the contribution from the bispectrum. As we argued in Section 4.2 we will only consider two–loop diagrams as the ones in figure 4.2. Out of these only the three in the first line will contribute at tree level, and the first one will have three vertices coupling directly to the large momentum in the tree level diagram as opposed to just two for the last two diagrams. We can see from the vertex coefficients α and β in equation (3.2) that these couplings introduce a hierarchy between the diagrams of the order

$$\frac{\mathbf{k}\cdot\mathbf{q}_1}{q_1^2}\frac{\mathbf{k}\cdot\mathbf{q}_2}{q_2^2}\frac{\mathbf{k}\cdot\mathbf{q}_3}{q_3^3} \gg \frac{\mathbf{k}\cdot\mathbf{q}_1}{q_1^2}\frac{\mathbf{k}\cdot(\mathbf{q}_2+\mathbf{q}_3)}{|\mathbf{q}_2+\mathbf{q}_3|^2}\frac{\mathbf{q}_2\cdot\mathbf{q}_3}{q_2^2} \tag{4.22}$$

so in the large–k regime we need only consider the first kind of diagrams where all legs are connected directly to the tree level diagram. This argument applies equally well to the case of higher order statistics.

Similar to equation (3.79) the bispectrum integration kernel reduces to

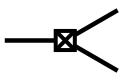

$$\approx u_a u_b u_c \theta(s_1)\theta(s_2)\theta(s_3) B^0(\mathbf{q}_1, \mathbf{q}_2, \mathbf{q}_3)\delta\left(\lambda - \textstyle\sum q_i\right) \tag{4.23}$$

when the initial fields are in the growing mode. This means that all three vertices that attach the bispectrum to the tree level diagram can be approximated using equation (3.80) and the delta function in the indices ensures that we are again left with just the tree level expression

times a momentum factor and a time factor as in equation (4.7). The momentum factor will be

$$\int \mathrm{d}^3\mathbf{q}_1\mathrm{d}^3\mathbf{q}_2\mathrm{d}^3\mathbf{q}_3 \; \frac{\mathbf{k}_1\cdot\mathbf{q}_1}{q_1^2}\frac{\mathbf{k}_2\cdot\mathbf{q}_2}{q_2^2}\frac{\mathbf{k}_3\cdot\mathbf{q}_3}{q_3^2}B^0(\mathbf{q}_1,\mathbf{q}_2,\mathbf{q}_3)\delta\left(\lambda-\sum q_i\right) \tag{4.24}$$

where $\mathbf{k}_i$ are the three momenta running along the segments of the tree level diagram where the loops are attached.

The time factor consists of the integral $\int \mathrm{d}s_1\mathrm{d}s_2\mathrm{d}s_3 \; e^{s_1+s_2+s_3}$ where s_i are the times of interaction with the loop momenta and the limits of integration depend on which segments the loops are attached to.

These observations generalize readily to higher order statistics, so the task is now to consider how these momentum and time factors add when we sum over all diagrams on the right hand side of the RG equations. We start by considering a segment with the merging of just two legs in the tree level diagram which is equivalent to the multi–point propagator $V^{(2,1)}$.

4.4.1 Large–k limit of $V^{(2,1)}$, the non–Gaussian case

For generality we will consider the nth order of the initial statistics. This means that there will be n loop legs that should be attached to the tree level diagram

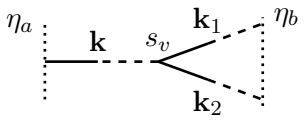

(4.25)

We will denote the momenta in the loop legs as $\mathbf{q}_1\cdots\mathbf{q}_n$ and the times when they interact as $s_1\cdots s_n$. It is not necessary to distinguish between the different loop legs since we integrate over both $\mathbf{q}_i$ and s_i and the initial statistics are symmetrized in their momentum dependence.

If there are m loop legs attached to a specific tree level leg in between times s_{v_1} and s_{v_2} the time factor from that leg is determined by the m integrals

$$\int_{s_{v_1}}^{s_{v_2}} \mathrm{d}s_m \; e^{s_m}\int_{s_{v_1}}^{s_m} \mathrm{d}s_{m-1} \; e^{s_{m-1}}\cdots\int_{s_{v_1}}^{s_2} \mathrm{d}s_1 \; e^{s_1} \tag{4.26}$$

which by induction can be shown to yield

$$\int_{s_{v_1}}^{s_{v_2}} \mathrm{d}s_m \; e^{s_m}\frac{1}{(m-1)!}\left(e^{s_m}-e^{s_{v_1}}\right)^{(m-1)} = \frac{1}{m!}\left(e^{s_{v_2}}-e^{s_{v_1}}\right)^m \tag{4.27}$$

Thus if we have m loop legs attached to the left leg in equation (4.25) they will contribute with a time and momentum factor given by

$$\frac{1}{m!}\left(e^{\eta_a}-e^{s_v}\right)^m\prod_{i=1}^{m}\frac{\mathbf{k}\cdot\mathbf{q}_i}{q_i^2} \tag{4.28}$$

The remaining $n-m$ legs should be attached to the two legs on the right hand side in equation (4.25). The resulting $n-m+1$ diagrams will have a common time factor of $(e^{s_v}-e^{\eta_b})^{n-m}$, but the fraction connected to the time factor (as in equation (4.27)) and the momentum factor will depend on exactly how many loop legs are connected to which tree level leg. With just one leg to attach we get two terms

$$-\mathbf{k}_1\cdot\mathbf{q}_i-\mathbf{k}_2\cdot\mathbf{q}_i=\mathbf{k}\cdot\mathbf{q}_i \tag{4.29}$$

where we have left out the factor of $1/q_i^2$. With two legs, one of the three terms can be rewritten using the invariance under $\mathbf{q}_i\leftrightarrow\mathbf{q}_j$ so that we get

$$\begin{aligned}&\frac{1}{2}(\mathbf{k}_1\cdot\mathbf{q}_i)(\mathbf{k}_1\cdot\mathbf{q}_j)+(\mathbf{k}_1\cdot\mathbf{q}_i)(\mathbf{k}_2\cdot\mathbf{q}_j)+\frac{1}{2}(\mathbf{k}_2\cdot\mathbf{q}_i)(\mathbf{k}_2\cdot\mathbf{q}_j)\\&\quad=\frac{1}{2}\left((\mathbf{k}_1\cdot\mathbf{q}_i)(\mathbf{k}_1\cdot\mathbf{q}_j)+(\mathbf{k}_1\cdot\mathbf{q}_i)(\mathbf{k}_2\cdot\mathbf{q}_j)+(\mathbf{k}_2\cdot\mathbf{q}_i)(\mathbf{k}_1\cdot\mathbf{q}_j)+(\mathbf{k}_2\cdot\mathbf{q}_i)(\mathbf{k}_2\cdot\mathbf{q}_j)\right)\\&\quad=\frac{1}{2}(\mathbf{k}\cdot\mathbf{q}_i)(\mathbf{k}\cdot\mathbf{q}_j)\end{aligned} \tag{4.30}$$

This result generalizes easily for $n-m$ legs yielding

$$\frac{1}{(n-m)!}\left(e^{s_v}-e^{\eta_b}\right)^{(n-m)}\prod_{i=m}^{n}\frac{\mathbf{k}\cdot\mathbf{q}_i}{q_i^2} \tag{4.31}$$

where we have reinstated the factors of $1/q_i^2$ and the common time factor.

Equation (4.31) taken together with equation (4.28) gives the total momentum and time factor obtained by adding all diagrams with m loop legs attached to the left leg in equation (4.25). Now adding all possible loop diagrams from the nth order initial statistic results in a sum over these factors from $m=0$ to $m=n$

$$\begin{aligned}&\sum_{m=0}^{n}\frac{1}{m!}\frac{1}{(n-m)!}\left(e^{\eta_a}-e^{s_v}\right)^m\left(e^{s_v}-e^{\eta_b}\right)^{(n-m)}\prod_{i=1}^{n}\frac{\mathbf{k}\cdot\mathbf{q}_i}{q_i^2}\\&=\frac{1}{n!}\prod_{i=1}^{n}\frac{\mathbf{k}\cdot\mathbf{q}_i}{q_i^2}\sum_{m=0}^{n}\binom{n}{m}\left(e^{\eta_a}-e^{s_v}\right)^m\left(e^{s_v}-e^{\eta_b}\right)^{(n-m)}=\frac{1}{n!}\left(e^{\eta_a}-e^{\eta_b}\right)^n\prod_{i=1}^{n}\frac{\mathbf{k}\cdot\mathbf{q}_i}{q_i^2}\end{aligned} \tag{4.32}$$

where we see that just as in the Gaussian case we have eliminated the dependence on the intermediate time s_v so that it will only appear in the explicit expression for the tree level diagram in equation (4.25).

The full result for the RG equation for $V^{(2,1)}$ after promoting the tree level expression to the full non–linear one is then

$$\begin{aligned}\partial_\lambda V^{(2,1)}_{abc,\lambda}=-V^{(2,1)}_{abc,\lambda}\Bigg(&\frac{\left(e^{\eta_a}-e^{\eta_b}\right)^2}{2!}\int\mathrm{d}^3\mathbf{q}\,\frac{(\mathbf{k}\cdot\mathbf{q})^2}{q^4}P^0(q)\delta(\lambda-q)\\&-\frac{\left(e^{\eta_a}-e^{\eta_b}\right)^3}{3!}\int\mathrm{d}^3\mathbf{q}_{1,2,3}\prod_{i=1}^{3}\frac{\mathbf{k}\cdot\mathbf{q}_i}{q_i^2}B^0(\mathbf{q}_1,\mathbf{q}_2,\mathbf{q}_3)\delta\left(\lambda-\textstyle\sum q_i\right)-\cdots\Bigg)\end{aligned} \tag{4.33}$$

We can express the initial statistics in terms of correlation functions of the initial density perturbation δ_0

$$\begin{aligned}\delta(\mathbf{q}_1+\mathbf{q}_2)P^0(q) &= \langle\delta_0(\mathbf{q}_1)\delta_0(\mathbf{q}_2)\rangle \\ \delta(\mathbf{q}_1+\mathbf{q}_2+\mathbf{q}_3)B^0(\mathbf{q}_1,\mathbf{q}_2,\mathbf{q}_3) &= \langle\delta_0(\mathbf{q}_1)\delta_0(\mathbf{q}_2)\delta_0(\mathbf{q}_3)\rangle \\ &\vdots\end{aligned} \tag{4.34}$$

This enables us to rewrite the parentheses in equation (4.33) more compactly so that the end result after integrating and letting $\lambda\to\infty$ is

$$V^{(2,1)}_{abc,\lambda\to\infty} = V^{(2,1)}_{abc,\mathrm{tree}}\exp\left(\sum_{n=2}^{\infty}\frac{(e^{\eta_a}-e^{\eta_b})^n}{n!}\left\langle\prod_{i=1}^{n}\int \mathrm{d}^3\mathbf{q}_i\,\frac{\mathbf{k}\cdot\mathbf{q}_i}{q_i^2}\delta_0(\mathbf{q}_i)\right\rangle\right) \tag{4.35}$$

The change in sign for the power spectrum term compared to equation (4.33) is due to the fact that the delta function $\delta(\mathbf{q}_1+\mathbf{q}_2)$ has not yet been enforced in this expression.

4.4.2 Large–k limit of general multi–point propagators, the non–Gaussian case

To generalize to all multi–point propagators we need to go through the same considerations as in subsection 4.3.2. For the n–point propagators $V^{(n-1,1)}$ with just one outgoing leg on the left hand side we can again use the calculation for $V^{(2,1)}$ above to show that every segment that merges two legs from the right can be treated as just one two–point propagator with the sum of the two initial momenta running along it. An iterative use of this gives the general result analogous to equation (4.35).

On the other hand the case of multi–point propagators with more than one outgoing leg on the left hand side is more complicated in the presence of initial non–Gaussianities. Apart from tree level segments that include an initial power spectrum there will also be segments that merge two or more legs by direct couplings to higher order initial statistics (see the first diagram in figure 4.5 for an example). We can split such diagrams into two parts by letting all the legs from the initial statistic go out to the time η_b before proceeding to the next interaction as seen in the second diagram of figure 4.5. Now any loop correction to such a tree level diagram that has a leg attached inside the center circle will not contribute to the RG equation when we sum over all diagrams, because the sum of the momenta coming from the initial statistic has to be zero. It is equivalent to the arguments leading up to equation (4.31) except with $\mathbf{k}=0$. This means that we can treat the diagram as separate multi–point propagators all going from η_b to η_a as shown in the last part of figure 4.5.

Each of these separate sections can again be reduced to a single two–point propagator carrying momentum $\mathbf{p}_i$ and calculating loop diagrams along the same lines as was done for $V^{(2,1)}$ we arrive at the same final result as seen in equation (4.35)

$$V^{(n,m)}_{a_1\cdots a_m b_1\cdots b_n,\lambda\to\infty} = V^{(n,m)}_{a_1\cdots a_m b_1\cdots b_n,\mathrm{tree}}\exp\left(\sum_{n=2}^{\infty}\frac{(e^{\eta_a}-e^{\eta_b})^n}{n!}\left\langle\prod_{i=1}^{n}\int \mathrm{d}^3\mathbf{q}_i\,\frac{\mathbf{k}\cdot\mathbf{q}_i}{q_i^2}\delta_0(\mathbf{q}_i)\right\rangle\right) \tag{4.36}$$

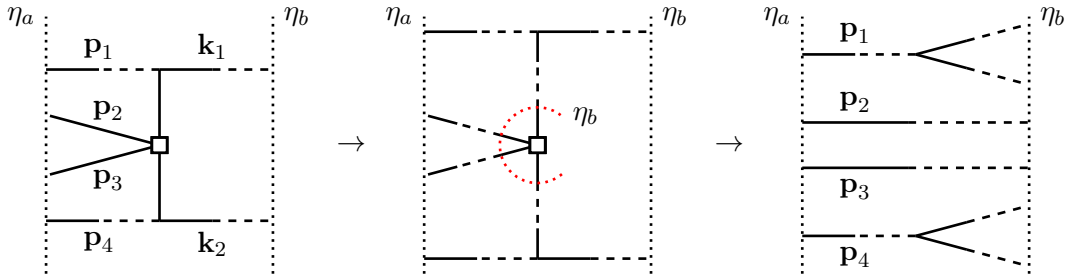

Figure 4.5: Example of a tree level diagram with a trispectrum merging 4 legs. The reasoning behind the last two diagrams is explained in the text.

This is the result obtained in [45] for the n–point propagators $V^{(n-1,1)}$, that we have shown also holds for the generalization $V^{(n,m)}$ with $m > 1$.

The multi–point propagators can be interpreted as a measure of how well the initial conditions are preserved at later times. The linear two–point propagator for instance tells us that the linear evolution preserves the initial statistics perfectly because it is normalized to 1 at all times. The full propagators on the other hand all show an exponential damping for large k–values meaning that the memory of the initial statistics is erased at small scales where the non–linear collapse of the matter density peaks has proceeded far beyond the regime where standard perturbation theory is valid.

The generalized results here show that even though the multi–point propagators $V^{(n,m)}$ with $m > 1$ are in a sense more connected to the initial conditions through their tree level expressions, they lose memory of the initial statistics at the same rate as the n–point propagators.

4.5 Comments

Assuming an isotropic background universe the terms in the exponential of equation (4.36) cannot depend on the direction of $\mathbf{k}$. We saw in the Gaussian case that the contribution from the power spectrum is proportional to k^2. Considering the term from the bispectrum the $\mathbf{k}$–dependence is contained in the factor

$$f(k) = \int \mathrm{d}^3\mathbf{q}_1 \mathrm{d}^3\mathbf{q}_2 \mathrm{d}^3\mathbf{q}_3 \, \frac{\mathbf{k}\cdot\mathbf{q}_1}{q_1^2} \frac{\mathbf{k}\cdot\mathbf{q}_2}{q_2^2} \frac{\mathbf{k}\cdot\mathbf{q}_3}{q_3^2} B^0(\mathbf{q}_1, \mathbf{q}_2, \mathbf{q}_3) \tag{4.37}$$

We can perform an explicit integration over the orientation of $\mathbf{k}$ yielding $4\pi f(k) = 0$, i.e. the bispectrum contribution vanishes. This will be the case for all the terms with uneven n in the sum. Only the even terms survive and the first correction to the Gaussian case comes from the trispectrum.

In [45] the correction from the trispectrum was computed in the case of local non–Gaussianities parametrized by the non–linearity parameters f_{NL} and g_{NL} introduced in Section 1.9. In their background cosmology with parameters $h = 0.7$, $\Omega_{\mathrm{m}} = 0.279$, $\Omega_{\mathrm{b}} = 0.0462$,

$n_{\rm s} = 0.96$ and $\sigma_8 \simeq 0.81$ the result for the two first non–zero terms in the exponential in equation (4.36) at $z = 0$ was

$$\frac{\left(e^{\eta_a}-1\right)^2}{2}\left\langle \int \mathrm{d}^3\mathbf{q}_1\mathrm{d}^3\mathbf{q}_2\, \frac{\mathbf{k}\cdot\mathbf{q}_1}{q_1^2}\frac{\mathbf{k}\cdot\mathbf{q}_2}{q_2^2}\delta_0(\mathbf{q}_1)\delta_0(\mathbf{q}_2)\right\rangle = -\sigma_v^2 k^2 = -18.06\, k^2 h^{-2}\mathrm{Mpc}^2 \quad (4.38)$$

and

$$\frac{\left(e^{\eta_a}-1\right)^4}{24}\left\langle \int \mathrm{d}^3\mathbf{q}_{1,2,3,4}\, \frac{\mathbf{k}\cdot\mathbf{q}_1}{q_1^2}\frac{\mathbf{k}\cdot\mathbf{q}_2}{q_2^2}\frac{\mathbf{k}\cdot\mathbf{q}_3}{q_3^2}\frac{\mathbf{k}\cdot\mathbf{q}_4}{q_4^2}\delta_0(\mathbf{q}_1)\delta_0(\mathbf{q}_2)\delta_0(\mathbf{q}_3)\delta_0(\mathbf{q}_4)\right\rangle$$
$$= 3.9\times 10^{-7}\left(f_{\rm NL}^{\rm loc}\right)^2 k^4 h^{-4}\mathrm{Mpc}^4 + 1.3\times 10^{-8}\, g_{\rm NL}^{\rm loc} k^4 h^{-4}\mathrm{Mpc}^4 \quad (4.39)$$

The contribution from the trispectrum is positive so the overall effect is to delay the exponential damping from the power spectrum. For the delay to be appreciable either $f_{\rm NL}^{\rm loc}$ or $g_{\rm NL}^{\rm loc}$ should be rather large.

The approach followed in the above calculations corresponds to resumming only loop diagrams where all the loop legs are attached directly to the multi–point propagator in standard perturbation theory. In [35] it was shown that in the Gaussian case it is possible to resum another class of diagrams in the large–k limit by essentially using a resummed power spectrum in the integration kernel of equation (3.79). It would be interesting to see if their result can be reproduced in the case of multi–point propagators.

Chapter 5

Conclusions and Outlook

The question of how the universe has evolved into its present state is still far from being answered. Many of the overall theories about the processes at work seem to be working well, but the details are not all in place. The subject of cosmological structure formation can provide many clues to both the initial state of the universe and the properties of the individual constituents that make up the energy content.

The focus of my work presented in this thesis has been the RG approach to non–linear structure formation. I have presented the general formalism and the main results obtained in a ΛCDM background cosmology with Gaussian initial statistics. The formalism can easily be generalized to other background cosmologies as long as the linear growth factor D^+ is independent of scale so that the reinterpretation of the time variable η can be implemented. It would be interesting to consider dark energy with a time varying equation of state parameter $w = w(\tau)$ or clustering quintessence characterized by a vanishing speed of sound as presented in [46].

In Chapter 4 I have investigated the large–k limit of multi–point propagators and shown that they all show the exponential damping that makes renormalized perturbation theory applicable further into the non–linear regime than standard perturbation theory. In [44] and [45] the large–k limit of the n–point propagators is used directly to construct the power spectrum and bispectrum at late times and on small scales. The result is then combined with standard one–loop perturbation theory on large scales by interpolating between the two regimes. In the RG approach the large–k limit of multi–point propagators could be used in a similar way as it has been for the two–point propagator in Sections 3.9 and 3.10. The large–k results represent a renormalization of the 1PI vertices so an implementation of the RG equations that go beyond the tree level approximation for the vertices might be possible.

Another possibility would be to calculate the power spectrum and bispectrum in the presence of initial non–Gaussianities. The framework to do this has been set up in Chapter 4, but the RG equations become more complicated when we are also interested in the behaviour

at small k–values. In this regime the kinds of diagrams in equations (4.2) and (4.4) that could be neglected in chapter 4 play an important role. In particular the power spectrum will get a new one–loop contribution from the initial bispectrum given by the diagram

(5.1)

It seems that including a diagram like this in the numerical calculations of P^{II} in subsection 3.10.1 should be possible. When it comes to the bispectrum the multi–point propagator $V^{(1,2)}$ provides us with the diagram

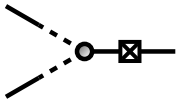

(5.2)

that might work as a first approximation to the renormalized bispectrum.

In conclusion there are many routes that could be followed from here using the work presented in this thesis as a starting point.

Acknowledgements

I would like to thank everyone who has in any way contributed to getting me and my thesis to where we are now. In particular I would like to thank:

My office mates Anna Sejersen Riis, Jan Hamann and Tina Lund. It has been been a great few years spent in your company. Special thanks to Anna for smiling the very first day at the university eight years ago and sharing my interests in both physics and everyday life ever since, and to Jan for proofreading and being able to answer all the questions I have had about cosmology.

My supervisor Steen Hannestad for discussions, ideas, advice and inspiration. Thomas Tram Bülow for many hours of discussions and help with the numerical work, and a general enthusiasm about all things related to physics. Jacob Brandbyge for always having N–body results ready and allowing me to use them. The whole cosmology group for many coffee breaks, dinners and visits to conferences. It has been an experience getting to know you all.

Massimo Pietroni for suggesting I should look at the large–k limit of multi–point propagators and many useful discussions while I was in Padova. The theoretical physics group in Padova for making me feel welcome.

Family and friends for always believing in me and for trying to understand what it is I have been working on all this time. My lovely boyfriend Dan Beltoft who has been an invaluable support through all of these years and who incidentally knows all there is to know about LaTeX. Thank you for always being so patient with me.

Bibliography

[1] B. Ryden, *Introduction to Cosmology* (Addison Wesley, 2003)

[2] D. J. Fixsen, *The Temperature of the Cosmic Microwave Background*, Astrophys. J. **707**, 916 (2009), [arXiv:0911.1955v2]

[3] A. G. Riess et al., *A 3% Solution: Determination of the Hubble Constant with the Hubble Space Telescope and Wide Field Camera 3*, Astrophys. J. **730**, 119 (2011), [arXiv:1103.2976v1]

[4] R. Amanullah et al., *Spectra and Light Curves of Six Type Ia Supernovae at* $0.511 < z < 1.12$ *and the Union2 Compilation*, Astrophys. J. **716**, 712 (2010), [arXiv:1004.1711v1]

[5] N. Jarosik et al., *Seven-Year Wilkinson Microwave Anisotropy Probe (WMAP) Observations: Sky Maps, Systematic Errors, and Basic Results*, Astrophys. J. Suppl. **192**, 14 (2011), [arXiv:1001.4744v1]

[6] W. J. Percival et al., *Baryon Acoustic Oscillations in the Sloan Digital Sky Survey Data Release 7 Galaxy Sample*, Mon. Not. Roy. Astron. Soc. **401**, 2148 (2010), [arXiv:0907.1660v3]

[7] S. Dodelson, *Modern Cosmology* (Academic Press, 2003)

[8] K. Nakamura et al. (Particle Data Group), J. Phys. G **37**, 075021 (2010)

[9] F. Bernardeau, S. Colombi, E. Gaztañaga, R. Scoccimarro, *Large-Scale Structure of the Universe and Cosmological Perturbation Theory*, Phys. Rept. **367**, 1 (2002), [arXiv:astro-ph/0112551v1]

[10] J. A. Peacock, *Cosmological Physics* (Cambridge University Press, 1999)

[11] A. Riotto, *Inflation and the Theory of Cosmological Perturbations*, (2002), [arXiv:hep-ph/0210162v1]

[12] A. Lewis, S.Bridle, *Cosmological parameters from CMB and other data: a Monte-Carlo approach*, Phys. Rev. D **66**, 103511 (2002), [arXiv:astro-ph/0205436v3]

[13] U. Seljak, M. Zaldarriaga, *A Line of Sight Approach to Cosmic Microwave Background Anisotropies*, Astrophys. J. **469**, 437 (1996), [arXiv:astro-ph/9603033v1]

[14] J. Lesgourgues, *The Cosmic Linear Anisotropy Solving System (CLASS) I: Overview*, (2011), [arXiv:1104.2932v2]

[15] R. Scoccimarro et al., *Non-Linear Evolution of the Bispectrum of Cosmological Perturbations*, Astrophys. J. **496**, 586 (1998), [arXiv:astro-ph/9704075v2]

[16] N. Bartolo et al. *Signatures of Primordial non-Gaussianities in the Matter Power-Spectrum and Bispectrum: the Time-RG Approach*, JCAP **1003**, 011 (2010), [arxiv:0912.4276v2]

[17] E. Komatsu et al., *Seven-Year Wilkinson Microwave Anisotropy Probe (WMAP) Observations: Cosmological Interpretation*, Astrophys. J. Suppl. **192**, 18 (2011), [arXiv:1001.4538v3]

[18] D. Larson et al., *Seven-Year Wilkinson Microwave Anisotropy Probe (WMAP) Observations: Power Spectra and WMAP-Derived Parameters*, Astrophys. J. Suppl. **192**, 16 (2011), [arXiv:1001.4635v2]

[19] M. E. Peskin, D. V. Schroeder, *An Introduction to Quantum Field Theory* (Westview Press, 1995)

[20] J. Ambjørn, J. L. Petersen, *Quantum Field Theory, Lecture Notes* (1998)

[21] R. Juszkiewicz, *On the evolution of cosmological adiabatic perturbations in the weakly non-linear regime*, Mon. Not. Roy. Astron. Soc. **197**, 931 (1981)

[22] E. T. Vishniac, *Why weakly non-linear effects are small in a zero-pressure cosmology*, Mon. Not. Roy. Astron. Soc. **203**, 345 (1983)

[23] J. N. Fry, *The Galaxy correlation hierarchy in perturbation theory*, Astrophys. J. **279**, 499 (1984)

[24] M. H. Goroff, B. Grinstein, S.-J. Rey, M. B. Wise, *Coupling of modes of cosmological mass density fluctuations*, Astrophys. J. **311**, 6 (1986)

[25] J. Carlson, M. White, N. Padmanabhan, *A critical look at cosmological perturbation theory techniques*, Phys. Rev. D **80**, 043531 (2009), [arXiv:0905.0479v1]

[26] R. Scoccimarro, *A New Angle on Gravitational Clustering*, (2000), [arXiv:astro-ph/0008277v1]

[27] M. Crocce, R. Scoccimarro, *Renormalized Cosmological Perturbation Theory*, Phys. Rev. D **73**, 063519 (2006), [arXiv:astro-ph/0509418v2]

[28] M. Crocce, R. Scoccimarro, *Memory of Initial Conditions in Gravitational Clustering*, Phys. Rev. D **73**, 063520 (2006), [arXiv:astro-ph/0509419v2]

[29] P. Valageas, *A new approach to gravitational clustering: a path-integral formalism and large-N expansions*, Astron. Astrophys. **421**, 23 (2004), [arXiv:astro-ph/0307008v3]

[30] P. Valageas, *Large-N expansions applied to gravitational clustering*, Astron. Astrophys. **465**, 725 (2007), [arXiv:astro-ph/0611849v2]

[31] P. McDonald, *Dark matter clustering: a simple renormalization group approach*, Phys. Rev. D **75**, 043514 (2007), [arXiv:astro-ph/0606028v3]

[32] S. Matarrese, M. Pietroni, *Baryonic Acoustic Oscillations via the Renormalization Group*, Mod. Phys. Lett. A **23**, 25 (2008), [arXiv:astro-ph/0702653v1]

[33] S. Matarrese, M. Pietroni, *Resumming Cosmic Perturbations*, JCAP **0706**, 026 (2007), [arXiv:astro-ph/0703563v2]

[34] M. Pietroni, *Flowing with Time: a New Approach to Nonlinear Cosmological Perturbations*, JCAP **0810**, 036 (2008), [arXiv:0806.0971v3]

[35] S. Anselmi, S. Matarrese, M. Pietroni, *Next-to-leading resummations in cosmological perturbation theory*, JCAP **1106**, 015 (2011), [arXiv:1011.4477v2]

[36] A. Taruya, T. Hiramatsu, *A Closure Theory for Non-linear Evolution of Cosmological Power Spectra*, (2007), [arXiv:0708.1367v2]

[37] T. Hiramatsu, A. Taruya, *Chasing the non-linear evolution of matter power spectrum with numerical resummation method: solution of closure equations*, Phys. Rev. D **79**, 103526 (2009), [arXiv:0902.3772v2]

[38] T. Matsubara, *Resumming Cosmological Perturbations via the Lagrangian Picture: One-loop Results in Real Space and in Redshift Space*, Phys. Rev. D **77**, 063530 (2008), [arXiv:0711.2521v3]

[39] P. Valageas, *Using the Zeldovich dynamics to test expansion schemes*, Astron. Astrophys. **476**, 31 (2007), [arXiv:0706.2593v2]

[40] B. Audren, J. Lesgourgues, *Efficient computation of the non-linear matter power spectrum of LambdaCDM*, (2011), [arXiv:1106.2607v1]

[41] J. Brandbyge, S. Hannestad, T. Haugboelle, Y. Y. Y. Wong, *Neutrinos in Non-linear Structure Formation - The Effect on Halo Properties*, JCAP **1009**, 014 (2010), [arXiv:1004.4105v1]

[42] D. J. Eisenstein, W. Hu, *Baryonic Features in the Matter Transfer Function*, Astrophys.J. **496**, 605 (1998), [arXiv:astro-ph/9709112v1]

[43] K. Izumi, J. Soda, *Renormalized Newtonian Cosmic Evolution with Primordial Non-Gaussianity*, Phys. Rev. D **76**, 083517 (2007) [arXiv:0706.1604v2]

[44] F. Bernardeau, M. Crocce, R. Scoccimarro, *Multi-Point Propagators in Cosmological Gravitational Instability*, Phys. Rev. D **78**, 103521 (2008), [arXiv:0806.2334v2]

[45] F. Bernardeau, M. Crocce, E. Sefusatti, *Multi-Point Propagators for Non-Gaussian initial conditions*, Phys. Rev. D **82**, 083507 (2010), [arXiv:1006.4656v1]

[46] E. Sefusatti, F. Vernizzi, *Cosmological structure formation with clustering quintessence*, JCAP **1103**, 047 (2011), [arXiv:1101.1026v3]